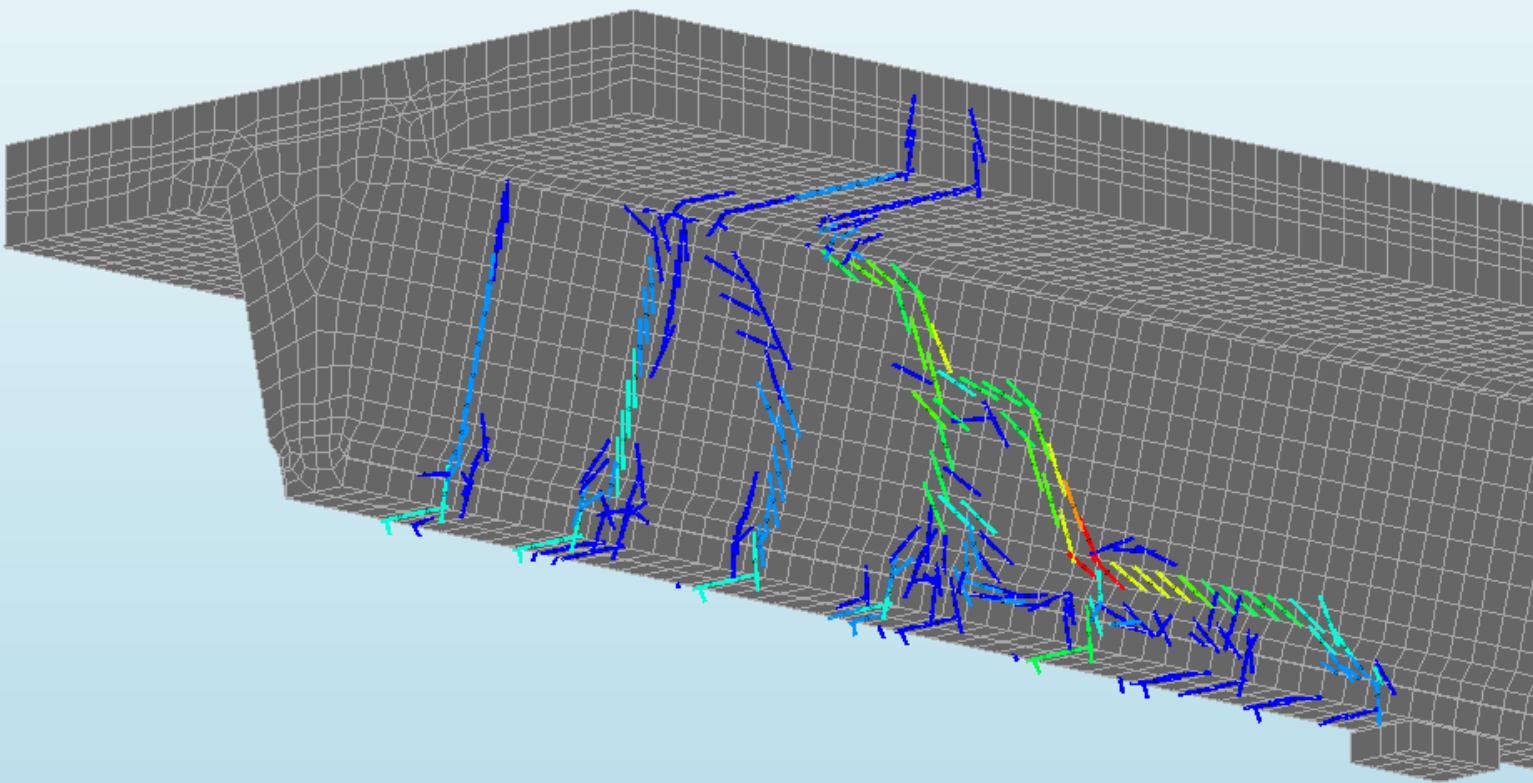


Transverse Shear Capacity of Deep Composite Slabs

Based on a Finite Element Analysis of ComFlor 210



Transverse Shear Capacity of Deep Composite Slabs

Based on a Finite Element Analysis of ComFlor 210

by

F.J. Stal

in partial fulfilment of the requirements for the degree of

Master of Science
in Civil Engineering

at the Delft University of Technology,
to be defended publicly on Thursday February 13, 2020 at 4:00 PM.

Supervisor:	Ir. J.M. Houben	TU Delft
Thesis committee:	Dr. ir. R. Abspoel	TU Delft
	Dr. ir. Y. Yang	TU Delft

Preface

Writing a thesis may be experienced as a period in life with a lot of ups and downs. At least, this was the case for me. After defining the subject, I found it very difficult to start. I read multiple papers and gathered a lot of information, but this only made me worried about how to make it to the end. As an advice to all my fellow graduation students: relax and take one step at a time. Sometimes, finite element software gives unexpected results. Other times, you may come up with questions even your supervisors don't have clear answers to. Be creative, self-reflective and discuss your problems. In the end, you'll find satisfaction.

First of all, I would like to thank Lambert Houben for taking over the role as supervisor from Dick Hordijk, as he retired from the TU Delft. I haven't experienced any adverse consequences of this change. Secondly, I would like to thank Paul Lagendijk for giving me the opportunity to graduate on this topic, since he came up with the subject from his daily work as structural engineer. The various meetings with him and Roland Abspoel really helped me getting through the process. Thank you both for all your valuable feedback. Since Paul also left the University, I would like to thank Yuguang Yang for taking over his role in the thesis committee and helping me finishing the project with his expertise on the transverse shear behaviour of concrete. Furthermore, I would like to thank Michele Longo for helping me with the questions that arose from finite element modelling. At last, special thanks go to:

- my parents, for the support and giving me their full trust in succeeding;
- my girlfriend, for dealing with my complaints every now and then;
- my father-in-law, for letting me borrow his desktop when my own laptop failed in computational power.

F.J. Stal
Dordrecht, February 2020

Contents

ABSTRACT	I
1. INTRODUCTION	1
1.1. STEEL-CONCRETE COMPOSITE ELEMENTS	1
1.2. OBJECTIVE.....	4
1.3. RESEARCH QUESTIONS.....	6
2. LITERATURE REVIEW	7
2.1. COMPOSITE SLABS IN GENERAL	7
2.1.1. <i>Materials</i>	7
2.1.2. <i>Origin</i>	8
2.1.3. <i>Production process</i>	8
2.1.4. <i>Types</i>	9
2.1.5. <i>Applications</i>	11
2.1.6. <i>Advantages</i>	11
2.1.7. <i>Disadvantages</i>	12
2.1.8. <i>Fire safety</i>	12
2.1.9. <i>Deep composite slabs: ComFlor 210 and ComFlor 225</i>	12
2.2. COMPOSITE BEHAVIOUR	14
2.3. FAILURE MECHANISMS OF COMPOSITE SLABS	18
2.4. LONGITUDINAL SHEAR RESISTANCE OF COMPOSITE SLABS ACCORDING TO EUROCODE 4.....	20
2.5. TRANSVERSE SHEAR RESISTANCE OF COMPOSITE SLABS ACCORDING TO EUROCODE 4 (REFERRING TO EUROCODE 2: CONCRETE STRUCTURES).....	23
2.6. TRANSVERSE SHEAR RESISTANCE OF STEEL DECKS ACCORDING TO EUROCODE 3.....	25
2.7. TRANSVERSE SHEAR RESISTANCE OF COMPOSITE SLABS ACCORDING TO LITERATURE	25
3. FINITE ELEMENT ANALYSIS	35
3.1. GEOMETRY AND LOADING CONDITIONS	35
3.2. FEA CONCRETE SECTION OF COMFLOR 210.....	38
3.2.1. <i>Material properties</i>	39
3.2.2. <i>Analysis procedure</i>	40
3.2.3. <i>Results and discussion</i>	42
3.3. FEA COMFLOR 210.....	47
3.3.1. <i>Material properties</i>	49
3.3.2. <i>Analysis procedure</i>	53
3.3.3. <i>Results and discussion</i>	54
3.4. FEA COMFLOR 210: A LOWER BOUND VALUE FOR THE TRANSVERSE SHEAR CAPACITY	61
3.4.1. <i>Material properties & analysis procedure</i>	62
3.4.2. <i>Results and discussion</i>	64
4. DISCUSSION	69
5. CONCLUSION	77
BIBLIOGRAPHY	79
APPENDIX A	81
APPENDIX B	84
APPENDIX C	85
APPENDIX D	87

Abstract

For calculation of the resistance of a composite slab against the transverse shear force, the Eurocode 4 (composite structures) simply refers to the calculation procedures of the Eurocode 2 (concrete structures). It is assumed that the composite slab consists out of a consecutive range of concrete ribs in its width direction, which are solely responsible for resisting the transverse shear force. To calculate the transverse shear capacity of these concrete ribs, an empirical formula is used that was originally derived for regular reinforced concrete beams (without stirrups). However, the concrete ribs of the composite slab are created by the profile of the steel deck, making that each concrete rib is accompanied by two steel webs on the sides. According to the Eurocode 3 (steel structures), these webs of the steel deck have their own transverse shear capacity, which is neglected by the current design approach defined in the Eurocode 4. Besides, the interaction between the steel deck and the concrete may lead to an even higher transverse shear capacity of the composite slab. In this thesis, the aforementioned two aspects, which are currently overlooked by the design principle of the Eurocode 4, are further studied by means of non-linear finite element modelling.

The validation of this empirical formula of the Eurocode 2 for calculating the transverse shear capacity of the concrete ribs is the first point of interest. From the finite element analysis (FEA) of the concrete section of ComFlor 210, it is concluded that the prediction of the transverse shear capacity by the Eurocode 2 is unnecessarily conservative. The study suggests to use the mean width of the concrete rib (b_0) in calculation, instead of the minimum width in the tensile area of the concrete rib (b_w), as an improvement to the method of the Eurocode 2.

In the next stage, the contribution of the steel deck to the transverse shear capacity of the composite slab is studied. The exact bonding properties between the steel deck and the concrete (at the interface) were not clear when the finite element model was developed, so some assumptions had to be made. When assuming that the steel deck can't separate from the concrete and the relative slip is restrained in longitudinal direction by the embossments, an increase of 131.6% in transverse shear capacity is found. Because of the assumed interface properties, the steel deck contributes to the total transverse shear capacity in the following ways: it resists a part of the transverse shear force in its webs; it acts as reinforcement to the concrete like a longitudinal rebar; it acts as reinforcement to the concrete like stirrups. However, whether this stirrup-functioning of the steel deck's webs is representative for the actual transverse shear behaviour of deep composite slabs is being questioned, because it relies on the assumption of no separation at the interface. Therefore, a second FEA of ComFlor 210 is executed in which the interaction between the steel deck and the concrete is neglectable. Still, an increase of 51.4% in transverse shear capacity is found, which can be considered as a lower bound value.

At last, from the FEA results of this thesis, it can indeed be concluded that the current Eurocode 4 provides a unnecessarily conservative calculation method for the transverse shear capacity of ComFlor 210. However, using a simple engineering model that adds up the partial resistances of the concrete ribs and the steel deck's webs, gives a better prediction while still being safe. For the partial resistance of the concrete ribs, the empirical formula of the Eurocode 2 is used, but this parameter b_w is substituted by b_0 as already mentioned in the foregoing. For the partial resistance of the steel deck's webs, the procedures of the Eurocode 3 are followed.

1. INTRODUCTION

As may have become clear from the title: this thesis is about the transverse shear capacity of deep composite slabs. A small introduction on composite elements is provided within this chapter, whereby it is explained why verification of the transverse shear capacity of deep composite slabs is the main point of interest. The research questions are formulated afterwards, which will be tried to be answered at the end of this thesis.

1.1. Steel-concrete composite elements

It is generally known that concrete needs reinforcement to restrain tensile stresses. This is traditionally taken care of by using steel rebars. This combination of steel and concrete is known as “reinforced concrete” and is globally used in designing structural safe buildings and bridges. However, other kinds of systems with the use of steel and concrete are also possible, e.g. circular steel tubes filled with concrete or steel girders connected to a concrete slab on top. These kinds of combinations are relatively new compared to the traditional reinforced concrete and are labelled differently as “steel-concrete composite elements” (or just “composite elements” as used in the sequel of this thesis).

Despite that steel and concrete are essentially two different materials, they still are completely compatible and complementary to each other[1]:

- One important aspect is that both materials have almost the same thermal expansion coefficient: $12 \cdot 10^{-6}/K$ for steel[30] and $10 \cdot 10^{-6}/K$ for concrete[24]. This means that internally generated stresses due to fluctuations in temperature are limited, because both materials expand and contract in good accordance;
- When the concrete (partly) envelops the steel section, it provides corrosion protection and increased fire resistance to the steel. This later can be an import aspect in the design of a building, because the strength and stiffness properties of steel easily reduce at strongly elevated temperatures;
- The concrete part can give increased resistance to common instability phenomena of steel sections, e.g. local buckling or lateral torsional buckling;
- The use of these two materials gives an ideal combination of strengths: concrete is the most efficient in compression, while steel is in tension.

Above-mentioned reasons have played a major part in the success of composite elements. However, a critical aspect is the connection between the different materials (especially for composite slabs and beams). To explain this, imagine two identical linear-elastic timber beams with dimensions $b \times h$ laying on top of each other. This is illustrated in Figure 1.1. When a load is applied on top and there is no interaction between the beams, both separate beams will experience positive and negative strains. This will give tensile and compressive stresses respectively. Additionally, a relative slip will be visible at the ends of the beams. Now, when the timber beams are connected to each other by gluing them together for instance, longitudinal shear stresses will develop at the interface. When these shear stresses won't be bigger than the capacity of the glue and the glue behaves very stiff, then this relative slip will not occur. The beams fully operate together, which gives an increase in the total section modulus of the “composite” beam.

$$W_{no\ interaction} = 2 \cdot \frac{1}{6} \cdot b \cdot h^2 = \frac{2}{6} \cdot b \cdot h^2$$

$$W_{full\ interaction} = \frac{1}{6} \cdot b \cdot (2h)^2 = \frac{4}{6} \cdot b \cdot h^2$$

$$\frac{W_{full\ interaction}}{W_{no\ interaction}} = \frac{\frac{4}{6} \cdot b \cdot h^2}{\frac{2}{6} \cdot b \cdot h^2} = 2$$

From these simple calculations, it may be established that the section modulus increases with a factor of 2 due to application of the glue as longitudinal shear connection. As a result, the stresses in the glued composite beam will also drop with a factor of 2 ($\sigma = M/W$). Not only the stresses will be lower, but also the deflection since the composite beam becomes much stiffer due to application of the glue. From Figure 1.1, it can be established that the bending stiffness EI is 4 times bigger in case of full interaction. Furthermore, it can also be seen that for full interaction, the top beam is completely in compression as the lower beam is in tension. Applying concrete on top and steel at the bottom would therefore be effective in this case. This explains in a very simple manner the power of composite elements.

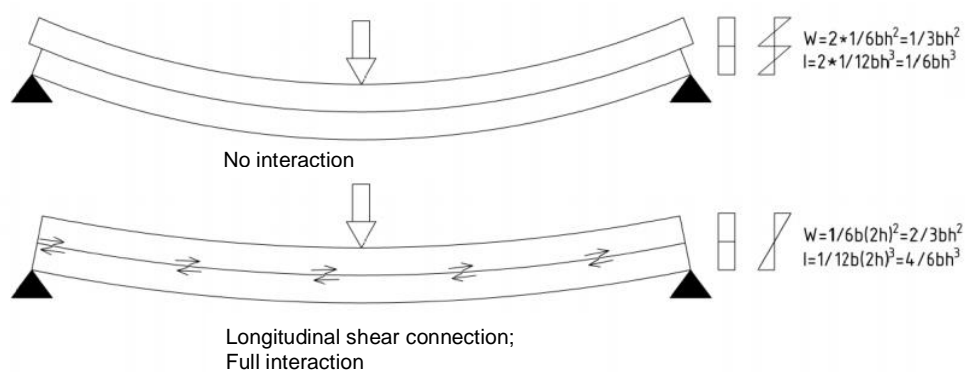


Figure 1.1 – The effect of longitudinal shear connections[31]

It may be concluded that it is of importance to ensure interaction between the separate elements. Sufficient longitudinal shear capacity should be provided at the interface. In case of steel-concrete composite beams, this is usually taken care of by applying mechanical shear connectors. A typical composite beam exists of a hot-rolled steel profile with a concrete slab on top (see Figure 1.2). Headed studs are often used as connectors, which are welded to the upper flange of the steel section after which the concrete is casted on top. The headed studs are surrounded with concrete after hardening, which provides a certain degree of longitudinal shear connection. Based on the former example (Figure 1.1), it may be established that this connection gives a significant improvement in bending stiffness of the total system. With the deflection criteria usually being normative for the steel section, it makes that less steel is necessary to support the concrete slab. This reduction in steel weight can overcome the additional costs for application of the headed studs. Furthermore, an important aspect of the connection is that it has a ductile behaviour. A brittle connection can lead to a total loss of composite behaviour at early stage of overloading, which is not desired. Figure 1.3 shows a typical test of headed studs as used in composite beams. It is obvious to see that the use of headed studs provides a ductile longitudinal shear connection.

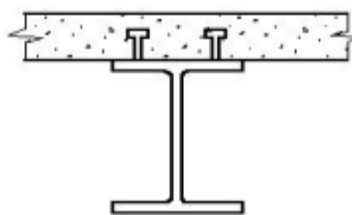


Figure 1.2 – Typical composite beam: steel section connected to a concrete slab on top by headed studs[1]

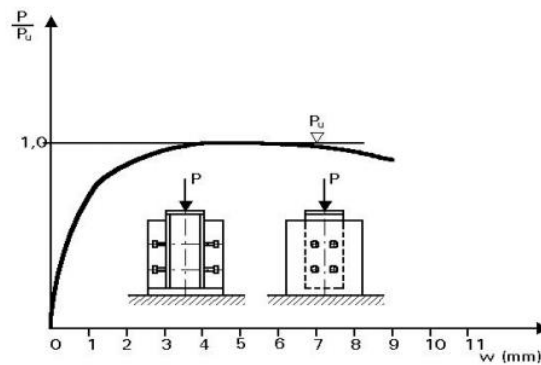


Figure 1.3 – Shear test on headed studs[1]

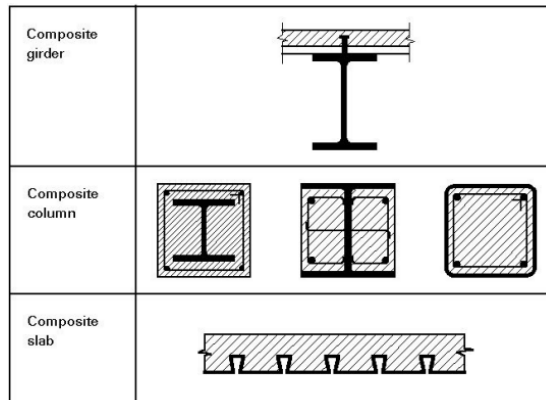


Figure 1.4 – Main categories of composite elements[1]

Composite elements can be divided into 3 categories: beams (or girders), columns and slabs. Examples of these kinds of elements are shown in Figure 1.4. Composite beams and columns are outside the scope of this thesis: the focus lays on the structural behaviour of composite slabs. In general, composite beams and slabs do have the most agreement on structural behaviour, since they are both mainly subjected to bending and shear. Therefore, not only for composite beams, but also for composite slabs it is of importance that the steel deck and the concrete topping act together. This can only be achieved by ensuring the development of longitudinal shear stresses at the interface between the elements. In composite slabs this is generally taken care of by applying embossments in the steel deck. These embossments improve the longitudinal shear capacity at the interface due to mechanical interlock between the steel deck and the concrete.



Figure 1.5 – Steel decking (ComFlor 210) is put in position between supporting beams[37]

Composite slabs are generally applied as floor systems. It has turned out to be a safe way of building in which the speed of construction is greatly improved[2]. It owes its performance to the smart way of

utilizing the intrinsic properties of steel and concrete in the same way as for composite beams. Profiled steel decking is put in position between the supporting beams and columns (Figure 1.5), whereby it serves as formwork on which the concrete can be cast. After hardening of the concrete, both components act together in carrying the load. This construction method makes that in case of sagging bending moments, the concrete is mainly in compression and the steel deck in tension. Both materials have good strength properties for these types of stresses, which makes that the load can be carried with a minimum use of materials. Since the concrete is spread on the steel deck, no external formwork is needed, and it offers a possibility for unproped construction. On basis of this description of composite floor systems, it may be concluded that the construction method is mainly developed for the best way of carrying the bending moment. It is the curvature, generated by the load, that causes the concrete to be in compression and the steel in tension. This distribution of stresses mostly leads to shallow designed slabs. Application of deep composite slabs can be necessary when the load or span becomes big. A composite slab is labelled as deep when its steel deck is over 200 mm high[9].

1.2. Objective

Looking at the Eurocode 4 for verification of composite slabs on structural safety, it can be established that the calculation procedures for the bending moment capacity and longitudinal shear capacity are well described. The bending moment capacity of a composite slab is its resistance against the tensile and compressive stresses caused by the bending (Figure 1.6). With the longitudinal shear capacity it is meant to what extent the composite slab is able to prevent extensive slipping at the interface between the concrete and the steel deck (Figure 1.7). However, for calculation of the transverse shear capacity of a composite slab, which is the resistance against the transverse shear force (Figure 1.8), the Eurocode 4 (composite structures) simply refers to the Eurocode 2 (concrete structures) without providing additional information. The transverse shear capacity of a composite slab is therefore totally assigned to its concrete part. Figure 1.9 shows the transverse shear failure of a reinforced concrete beam, with its distinctive inclined cracks from support to loading point. For reinforced concrete members, this type of failure is normally referred to as shear failure. But for composite slabs, a distinction is made between longitudinal shear failure and transverse shear failure (or vertical shear failure as used in other literature[17][18][21]).

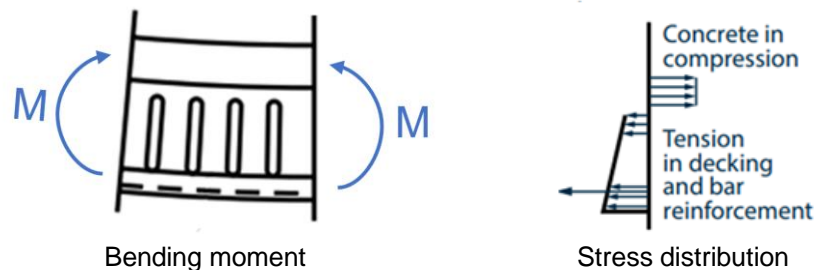


Figure 1.6 – Bending of a composite slab[23]

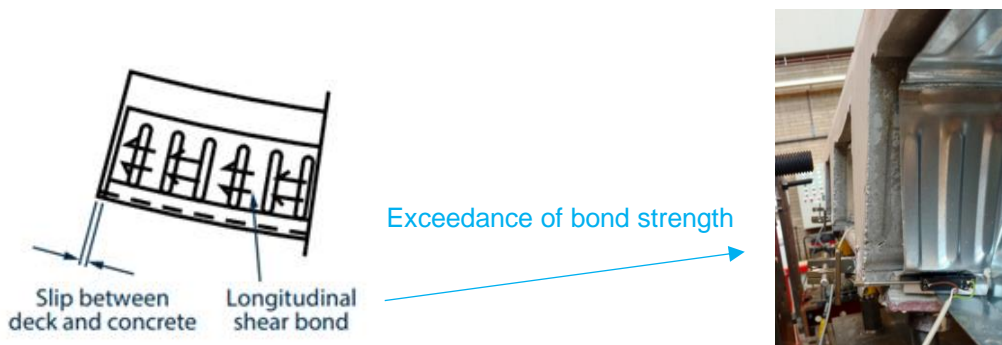


Figure 1.7 – Longitudinal shear failure[23][16]



Figure 1.8 – Transverse shear force[23]



Figure 1.9 – Transverse shear failure of a reinforced concrete beam[33]

With the Eurocode 4 referring to Eurocode 2, it makes that the transverse shear capacity of a composite slab is based on empirical formulas that were derived for reinforced concrete members. The Eurocode 4 lacks in information about the influence of the steel deck on the total transverse shear resistance and therefore it is supposed that this causes the current calculation method to be unnecessarily conservative. So, there are formulas to predict the transverse shear capacity of the concrete section (Eurocode 2); there are formulas to predict the transverse shear capacity of the steel deck (Eurocode 3), but there is no good prediction method for the combined resistance (Eurocode 4). In this thesis, it is tried to review the current standard and find a more realistic calculation method for the transverse shear capacity of deep composite slabs.

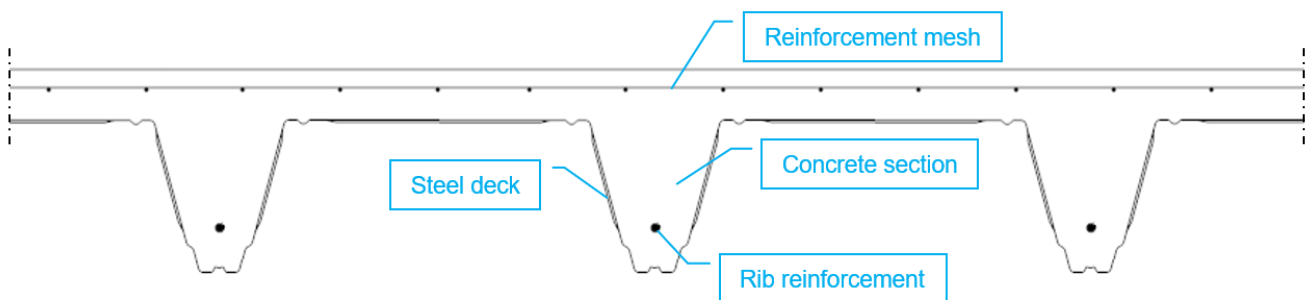


Figure 1.10 – Typical cross-section deep composite slab (ComFlor 210)[32]

It has been chosen to focus on deep composite slabs in this thesis. A typical cross-section of a deep composite slab is shown in Figure 1.10. The following elements can be distinguished: a thin steel deck at the bottom with concrete casted on top (concrete section); additional rebars in the concrete ribs and a reinforcement mesh in the top layer. Due to the shape of the steel deck, the deep composite slab consists out of concrete ribs which are positioned at a relatively large mutual distance (600 mm for ComFlor 210). As will become clear in the next chapter, these concrete ribs provide the transverse shear resistance of the composite slab according to the Eurocode 4. Therefore, it may be expected that deep composite slabs are generally more vulnerable to transverse shear compared to shallow composite slabs, in which the concrete ribs are spaced at a much smaller mutual distance. Furthermore, it can be seen in Figure 1.10 that the steel deck contains large webs, which are oriented nearly vertically.

These webs provide the transverse shear resistance of the steel deck according to the Eurocode 3, but this resistance is totally neglected in calculation of the total transverse shear capacity of the composite slab. Therefore, it is expected that considerably more transverse shear capacity is present than currently predicted. It should be noticed that due to the high web slenderness of the steel deck, it is expected to be more susceptible to local buckling, which reduces its capacity.

1.3. Research questions

The objective of this thesis (as described in the former section) is translated into short research questions, which will be tried to be answered at the end of this thesis. The sub-questions are meant to help answering the main question.

Main question

- How to calculate the transverse shear capacity of deep composite slabs?

Sub-questions

- How big is the transverse shear capacity of the concrete section and how does this relate to the current Eurocode 2: Concrete structures (EN 1992)?
- What is the influence of the steel deck on the transverse shear capacity and how does this relate to the current Eurocode 4: Composite structures (EN 1994)?

In order to give answers to these questions, the thesis will be started with a review of current literature. More in-depth knowledge of composite slabs will be provided. After the literature review, the results of the Finite Element Analysis will be discussed. These results will be used to answer the research questions and make a conclusion. The structure of the thesis is illustrated in Figure 1.11.

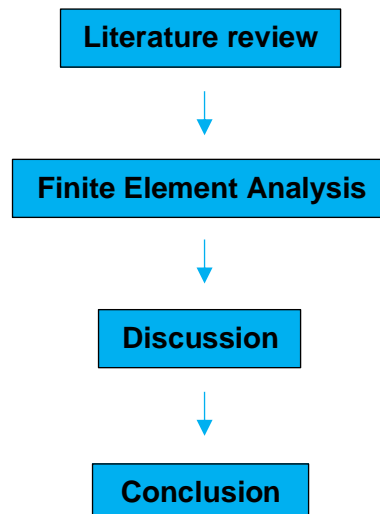


Figure 1.11 – Structure of the thesis

2. LITERATURE REVIEW

This chapter presents a review of literature which will help to get more insight into the subject. It is started with some general aspects about (deep) composite slabs and their structural behaviour. After distinguishing the different failure modes of composite slabs, this chapter will mainly focus on the transverse shear capacity. Calculation procedures according to standards and literature will be discussed at the end of this chapter.

2.1. Composite slabs in general

To give this thesis a proper basis, some general aspects of composite slabs are being discussed in this section. It is explained where it is made of, where it originates from and which variants are used in current building techniques. Furthermore, the production process is explained, different types of applications are provided and advantages/disadvantages are mentioned. At last, information is given on the fire safety of composite slabs and two variants of deep composite slabs are shown that are mainly used in the Netherlands[4] and the United Kingdom[23].

2.1.1. Materials

A composite slab is a structural element that is composed out of different materials. Steel-concrete composite slabs are discussed in this thesis. As clarified by the name: it is a combination of (cold-formed) steel and concrete.

Cold-formed steel

The profiled metal deck at the bottom of the slab is made of thin-walled cold-formed steel. This deck serves as both formwork and reinforcement to the concrete. The steel deck is characterized by its average yield strength and is the most effective in tension. This especially holds for thin-walled steel, where compressive stresses can easily lead to local buckling. Commonly used steel grades are S280 and S350[4]. Higher grades rarely give significant advantages due to stiffness limitations[10]. The steel deck is usually fabricated from hot-dipped galvanized plates with protective zinc layers (approximately 0.02 mm on each surface)[6]. This is normally sufficient to protect the steel from hazards when applied as internal floors in non-aggressive environments[6].

Concrete

Concrete is a non-homogeneous material that in its most standard form is composed out of aggregates, cement and water. The combination of cement and water glues the aggregates together due to a hydration process. Aggregates are ranged from fine to coarse in the concrete to prevent the inclusion of big areas of cement only. Concrete is characterized by its compressive strength, because this is its most outstanding property. The tensile strength of concrete is only about 10% of its compressive strength, so for most of its applications reinforcement is needed to resist the tensile stresses. In composite slabs, the concrete is applied as topping on the profiled steel deck. This steel deck acts as reinforcement to the concrete. Concrete can have multiple additives/adjustments to improve its characteristics. In the United Kingdom, a frequently applied variant in composite slabs is lightweight concrete to reduce the self-weight of the slab[9].

2.1.2. Origin

As mentioned in literature[5], Loucks and Gillet (1926) firstly patented a structural solution in which a steel deck was used in combination with concrete. The resistance of this “composite” slab was only obtained by the load-carrying capacity of the steel deck. The function of the concrete was mainly to protect for possible fire and to level the decking for functionality. Some decades later, Granco Steel Products Company (1950) marketed the first steel deck for composite slabs, called Cofar. This deck was provided with transverse wires welded to the top of profile to ensure composite behaviour. Freiberg (1954) investigated the Cofar’s resistance and published an important article on the design of composite slabs. Later in 1967, the so-called Hibond was introduced. This contained a new trapezoidal profile with embossments and re-entrant parts, and was the precursor of currently used steel decks in composite slabs.

2.1.3. Production process

The production of a composite slab starts with the manufacturing of the profiled steel deck. This deck is made in a process of cold forming. The process starts with the production of raw steel in a Basic Oxygen Furnace (BOF) or an Electric Arc Furnace (EAF). The steel is poured into a slab and then reduced into thinner strips of steel (so-called “hot band”)[7]. In the finishing process, the hot band is further reduced into thin “cold rolled steel” [7]. Protective zinc layers are added through a galvanization process and the sheet is coiled. This coil with steel is the start-product for the second process to produce the desired cold-formed section. This process is shown in Figure 2.1. First, the coil is unwound, after which the plate goes through a flattener to remove possible imperfections. These imperfections can be caused by transportation of the coil for instance. After the plate has been flattened, embossments are pushed into the plate (if demanded). The steel plate is now put into the desired shape by means of roll forming: the plate is drawn through a series of rollers, which bend the plate into the desired profile. No heat is required in this process (so the name cold forming) and the shape can therefore only be maintained by plastic deformation of the steel. In the end, the profile is cut into the desired length and collected for transportation. The profile of the steel deck is generally such that it is completely nestable to make one stack. The steel decks are therefore effectively transported to the building site, as it takes little space to transport a lot of decks.

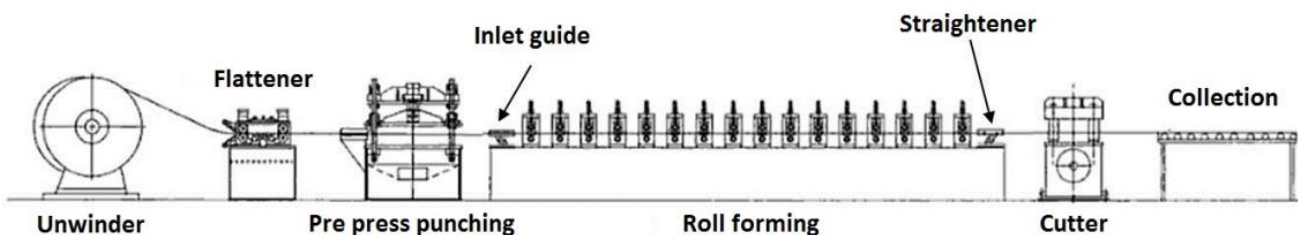


Figure 2.1 – Production process of cold-formed steel[16]

Once arrived at the building site, the steel decks are put in position by the construction workers by hand. This is possible due to the low self-weight. The last step is to lay down additional reinforcement on the steel deck, after which the concrete is casted on top. The steel deck has to carry the wet concrete in the beginning, but the composite slab is obtained after hardening of the concrete.

Effects of cold forming

Since the plate is bent at room temperature, plastic strains will develop in the corners of the profile. Cold forming therefore involves strain hardening effects which locally influence the yield stress, the ultimate strength and the ductility[8]. The degree of influence is dependent on the radius of curvature,

the thickness of the plate, the type of steel and the forming process[8]. Figure 2.2 shows an example of the influence on the yield stress. The yield stress has become substantially higher near the corners due to strain hardening. The average yield stress of the section has also become higher.

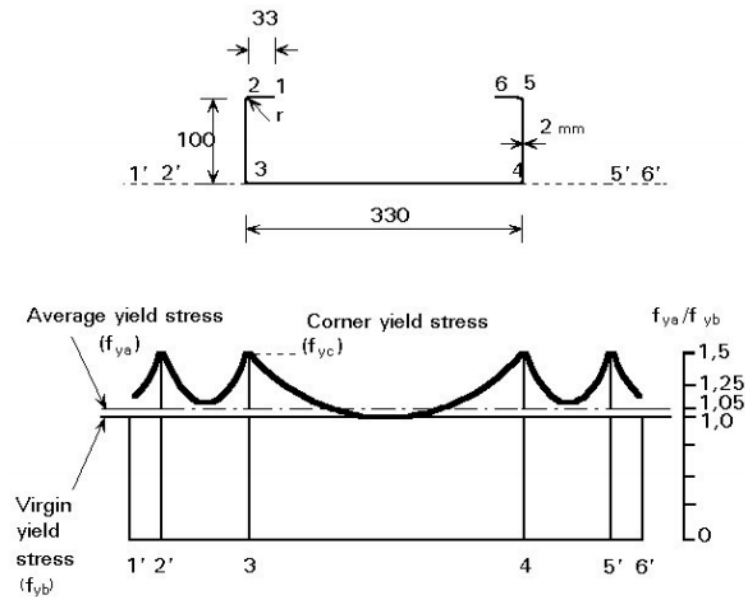


Figure 2.2 – Effect of cold forming on the yield stress[8]

2.1.4. Types

Composite slabs can roughly be divided into two categories based on the profile of the decking. This is shown in Figure 2.3. A distinction is made between the re-entrant profile (left) and the trapezoidal profile (right). In the Netherlands, the steel deck usually has a height in the range from 46 to 225 mm, with a sheet thickness varying from 0.9 to 1.25 mm[4]. For shallow steel decks (height < 200 mm), typical total slab thicknesses vary in the range from 100 mm to 250 mm[9]. For deep steel decks (height > 200 mm), this is in the range from 280 mm to 320 mm[9].

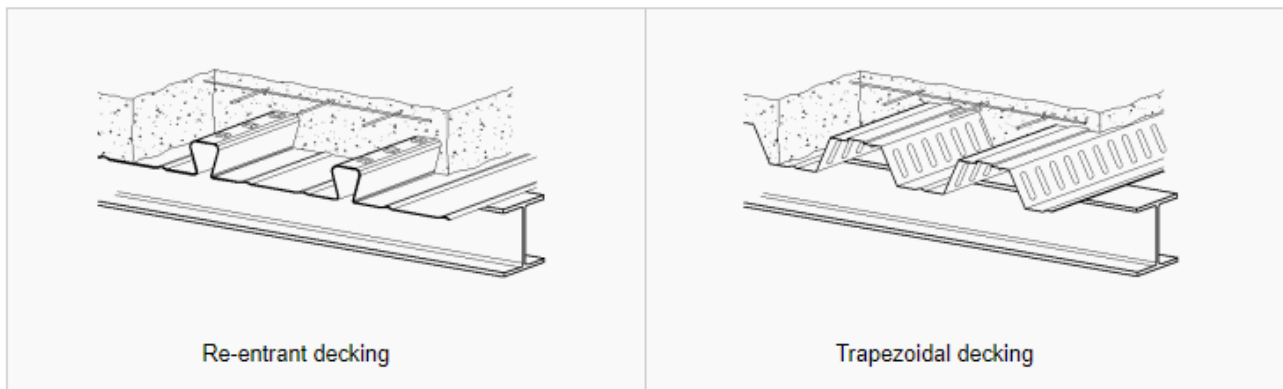


Figure 2.3 – Two types of profiled steel decks in composite slabs[2]

The choice of the profile is strongly dependent on the span and construction method. Short span composite slabs are generally constructed in an unpropped way, meaning that the steel deck has to carry the weight of the wet concrete and other construction loads. This phase controls the design of the steel deck. Due to the short span, the stresses in the composite slab after hardening of the concrete are generally low. For such slabs, trapezoidal profiled steel decks are most often used with limited longitudinal shear resistance[6]. This is because they have the lowest self-weight per square metre of floor area[6]. If the span becomes big (e.g. > 6m), props can be necessary to support the steel deck.

After hardening of the concrete, the composite slab is more highly stressed due to the longer span. This final stage may become governing in design, whereby a good longitudinal shear resistance will be required between the concrete and steel for transfer of the stresses. Re-entrant profiles are often used leading to greater self-weights per square metre of floor area[6].

The profiled steel deck at the bottom of the composite slab can be labelled as very thin. Local buckling can therefore become a critical aspect. During the construction phase, the wet concrete doesn't fulfil any role in carrying the load. This makes that the steel deck is not only loaded in tension, but also in compression. Local buckling due to these compressive stresses must be resisted, which makes that stiffeners are applied in the profile as shown in Figure 2.4. In the upper flange, a re-entrant form has been applied which improves the resistance for local buckling. The same holds for the embossments in the webs, which also play an important role in improvement of the longitudinal shear resistance of the composite slab.

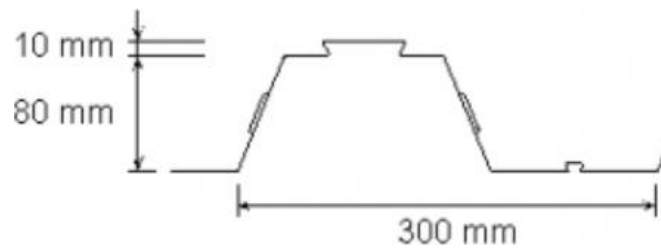
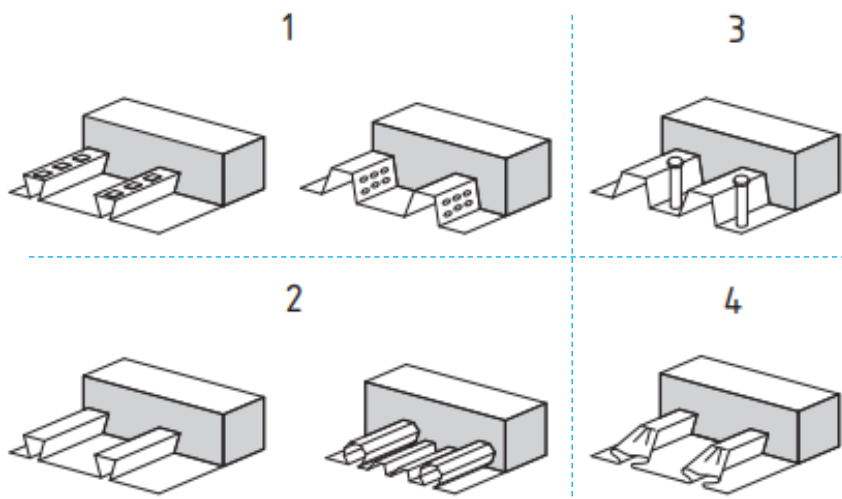


Figure 2.4 - Typical 80 mm trapezoidal steel deck with stiffeners[2]

For composite slabs it holds that the slip at the interface must be prevented partly or completely, as well as the vertical separation between the steel and concrete. The importance of this has been explained in section 1.1. In composite beams, this is most often assured by making use of headed studs. In composite slabs, there are more ways to ensure the composite behaviour. These are illustrated in Figure 2.5 (provided in EN 1994-1-1[3]).



1. mechanical interlock due to deformations in the steel deck;
2. frictional interlock for re-entrant steel profiles;
3. end anchorage by welded studs (only in combination with 1 or 2);
4. end anchorage by deformation of the ribs at the end of the deck (only in combination with 2).

Figure 2.5 – Options to ensure bonding between the steel deck and the concrete [3]

2.1.5. Applications

Composite slabs are frequently applied as floors in steel-framed buildings. These buildings often have one of the following applications[9]:

- Office
- Industrial building
- Warehouse
- Leisure building
- Stadium
- Hospital
- School
- Cinema
- Housing

Furthermore, composite slabs offer a good solution in refurbishments projects, due to the reduced weight compared to regular concrete slabs. The steel deck can easily be brought inside the building and can get modified into the desired shape.

2.1.6. Advantages

Composite slabs contain a lot of advantages which are listed below[9].

- **Speed of construction**

Bundles of steel decks can be lifted to desired position by one crane movement which makes the crane time minimal. The individual sheets can be installed by hand due to the low self-weight. The use of the steel deck as formwork and working platform speeds up the construction process for the next phases. For most of the cases minimal additional reinforcement is required and large areas of flooring can be poured with concrete quickly.

- **Safe method**

The steel decks provide a safe platform for the construction workers to perform their activities. It also offers a protection for falling objects.

- **Better use of material properties**

In ordinary concrete slabs, the concrete outside the compressive zone has low contribution to the strength of the slab due to the low tensile resistance of the concrete. In composite slabs, due to the shape of the steel deck, the concrete outside the compressive zone is reduced which makes it more effective in material use.

- **Lightweight and shallower construction**

Due to the effectiveness of composite slabs, the weight and size of the primary structure can be reduced significantly. Consequently, the costs and size of the foundation can also be reduced.

- **Structural stability**

The composite slab can act as a lateral restraint for the supporting beams, when it is sufficiently connected to these members.

- **Sustainable**

Due to savings in transport and trying to minimize the use of concrete, composite slabs are generally more sustainable than many other solutions. Furthermore, the steel in composite slabs can be recycled repeatedly without reducing its inherent properties.

- **Easy installation of services**

Pipes and cables for services like electricity, telephone and other network cabling can easily be hung to the bottom of the composite slab. This is done by making use of special equipment that can be attached to the steel deck due to its particular shape.

2.1.7. Disadvantages

Composite slabs also contain some disadvantages as listed below.

- **Less effective for hogging bending moments**

Composite slabs are less effective for hogging bending moments, since in this case the concrete is in tension and the steel deck is in compression. Necessarily, reinforcement has to be applied in the top layer of the concrete section and local buckling of the thin steel deck should be avoided.

- **One-way span**

Due to the shape of the composite slab with ribs in one direction, the load-carrying capacity in transverse direction is much lower.

2.1.8. Fire safety

Fire safety generally is an important aspect in the design of structural elements. The influence of fire safety on the design process is mainly dependent on the application of the building: a fire resistance of 30, 60, 90 or 120 minutes can be required. When composite slabs are applied as floors in buildings, special attention should be paid to guarantee the required fire resistance. This is because of the steel deck at the bottom of the composite slab, which can easily be heated in case of fire. Steel loses much of its strength and stiffness at strongly elevated temperatures, so this becomes very critical when there is nothing present in the concrete to carry the tensile stresses. Therefore, additional reinforcement is often needed and rebars are positioned in concrete ribs (called rib reinforcement in this thesis). These rebars can take over the tensile stresses in case of fire, whereby they are protected by the surrounding concrete.

2.1.9. Deep composite slabs: ComFlor 210 and ComFlor 225

In the Netherlands and United Kingdom (UK), composite floor systems are generally known by the tradename “ComFlor®”. The main supplier of these floor systems in the Netherlands is Dutch Engineering[4]. They offer composite floors in the range from ComFlor 46 up to ComFlor 225, in which the number indicates the height of the steel deck. As shown earlier in section 2.1.4, the steel deck can have a trapezoidal or re-entrant profile. ComFlor 210 and 225 are labelled as deep composite floors/slabs and both these types contain a trapezoidal profiled steel deck (see Figure 2.6). The steel decks are made of grade S280GD (minimum yield strength of 280 MPa) and are provided with protective zinc layers of a total mass of 275 g/m² (approx. 0.02 mm on each surface)[4]. The total sheet thickness of ComFlor 210 can be 1.0 mm or 1.25 mm, while ComFlor 225 is only offered with a 1.25 mm sheet thickness[4]. It should be noticed that there are some inconsistencies in the use of the name “ComFlor®” between the Netherlands and the UK. For example, ComFlor 75 in the Netherlands refers to ComFlor 60 in the UK. Furthermore, differences in applied steel grades can also be found, e.g. deep composite slabs in the UK are normally offered with a steel grade of S350GD[23].

For composite slabs with a shallow steel profile (e.g. ComFlor 46), the steel deck is normally put on top of the supporting beams. It is connected to these beams with headed studs, after which the composite slab and supporting beams also act compositely. The composite slab is continuously supported over the beams (shown in Figure 2.3). In contrast, ComFlor 210 and 225 are usually supported within the beam depth, e.g. on the bottom flanges of the supporting beams as shown in Figure 2.7. This provides a very shallow floor zone. The steel deck is simply supported, but the concrete topping is still continuous over the supporting beams. As also shown in Figure 2.7, the steel decks are provided with end diaphragms. These diaphragms are of importance for the structural integrity of the deck and to ensure that the concrete doesn't flow away when it is poured. Typical spans for deep composite slabs extending up to 5.6 metres and 9 metres for unpropped and propped construction respectively[4].

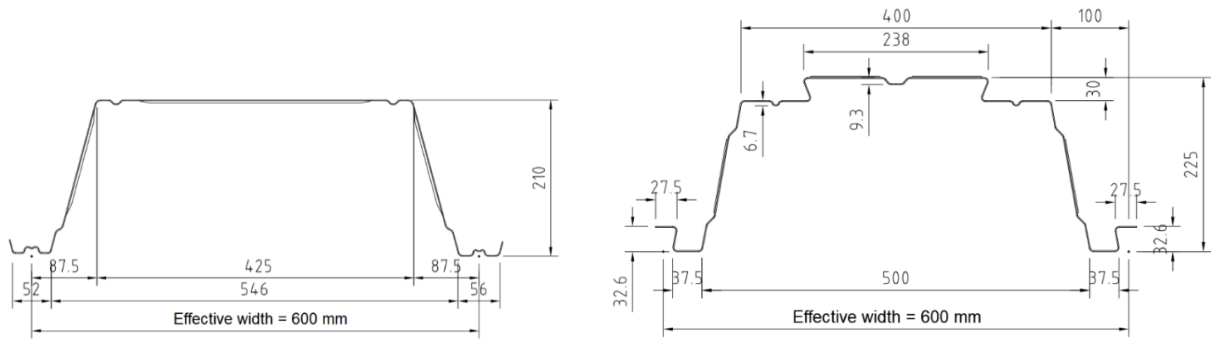


Figure 2.6 – Steel profile for deep decks: ComFlor 210 (left) and ComFlor 225 (right)[4]

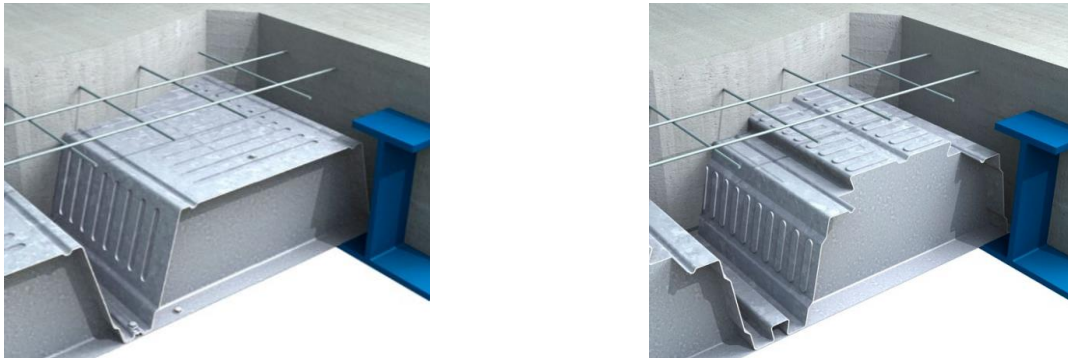


Figure 2.7 – Composite slabs supported on lower flange: ComFlor 210 (left) and ComFlor 225 (right)[23]

Minimal mesh reinforcement is always applied in the top layer of the slab to reduce the crack width due to shrinkage[4]. This reinforcement also distributes the effects of localised loads and provides a certain hogging moment capacity. Mainly based on this later two aspects, it can be necessary to increase the applied reinforcement in the top layer by using additional reinforcement bars. This especially holds for the regions at the supports in case of hogging moment conditions. Furthermore, for deep composite slabs, the resistance is always increased by using additional rib reinforcement[4]. This rib reinforcement is positioned at the bottom of the slab (with some concrete cover) and is necessary in case of fire. However, the benefit of this reinforcement is considered for both normal (room temperature) and fire conditions. Figure 2.8 shows the way this rib reinforcement is put in position. Furthermore, from this figure it may also be observed that the steel deck has an overlap at the bottom of the ribs, caused by the assemblance of the separate parts of the steel deck. The sheet thickness is therefore two times bigger at the bottom of the ribs. Connectors are applied with some mutual distance over the full length of this bottom flange. These connectors consist out of “shear clips” and self-drilling screws (which go through these clips and the separate plates of the bottom flange)[4].

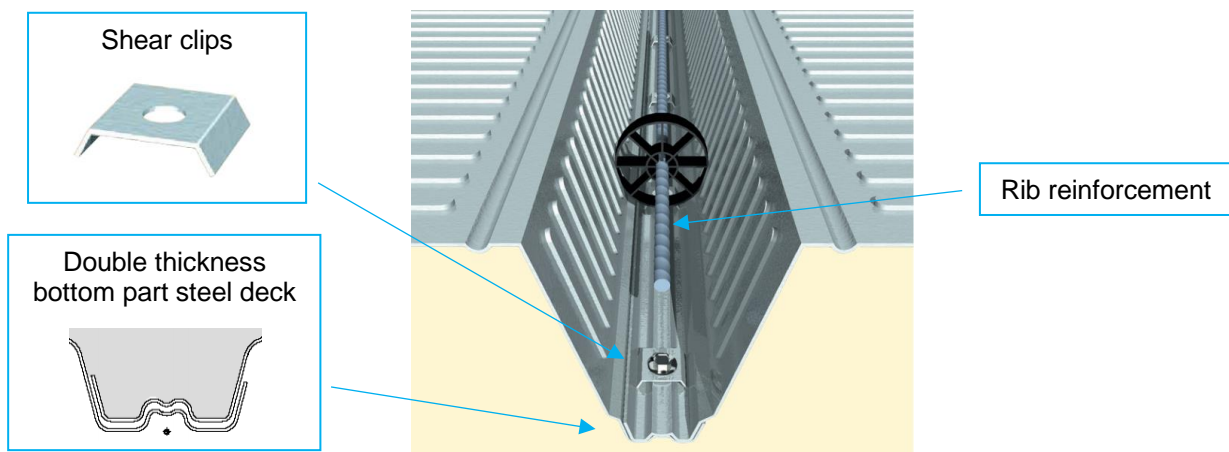


Figure 2.8 – Positioning of rib reinforcement in ComFlor 210[4]

It needs to be noticed that the considered deep composite slabs of this thesis aren't officially covered by the Eurocode 4. This is because they don't meet the requirement on narrowly spaced webs as prescribed in clause 9.1.1 of EN 1994-1-1[3]. This requirement is defined by an upper limit of 0.6 for the ratio b_r/b_s . Figure 2.9 shows the definitions of these parameters b_r and b_s . For ComFlor 210, the ratio is equal to $425/600 = 0.71$. For ComFlor 225, the ratio is equal to $400/600 = 0.67$. As may be established, both profiles don't meet the requirement since these values are bigger than 0.6.

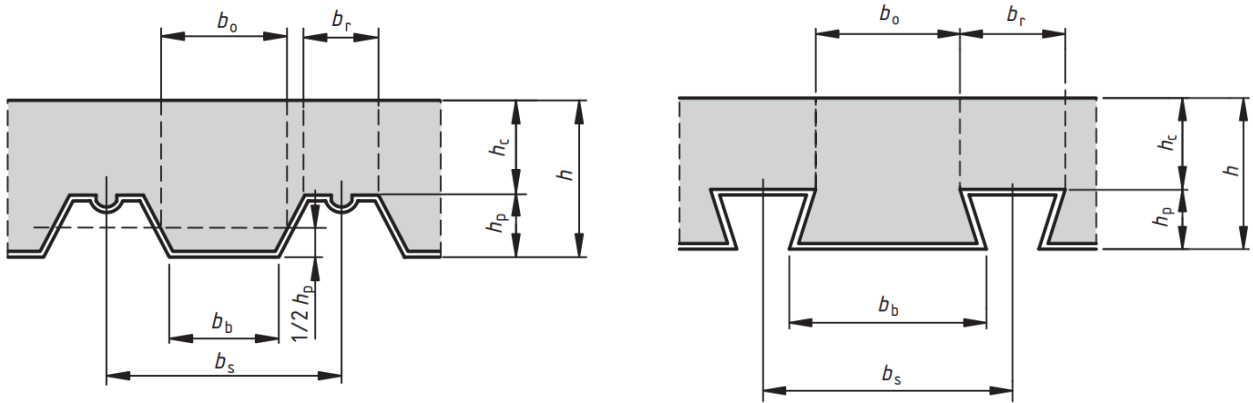


Figure 2.9 – Definition of different parameters for trapezoidal (left) and re-entrant (right) steel decks[3]

2.2. Composite behaviour

The structural behaviour of a composite slab depends on the properties of the separate materials and the connection between them. Figure 2.10 shows the distribution of forces and stresses in a deep composite slab due to a distributed load. At midspan, the stress distribution is such that the concrete top layer is in compression, while the steel is in tension. Concrete in tension is neglected due to its weak tensile properties. The transverse shear force is zero at midspan where the bending moment is at its maximum. At the support this is visa-versa, making that the shear stresses are significantly higher at this location. This holds for both the longitudinal and transversal shear stresses. Longitudinal shear stresses are generated between the steel deck and the concrete section (bonding). Slip is likely to occur due to the non-rigidity of this connection. The bond capacity is improved by the embossments in the steel deck due to mechanical interlock. The shape of the steel deck is also of importance: a re-entrant profile has better connection properties than a trapezoidal profile, because it offers more resistance against vertical separation between the steel and concrete (opening of the interface).

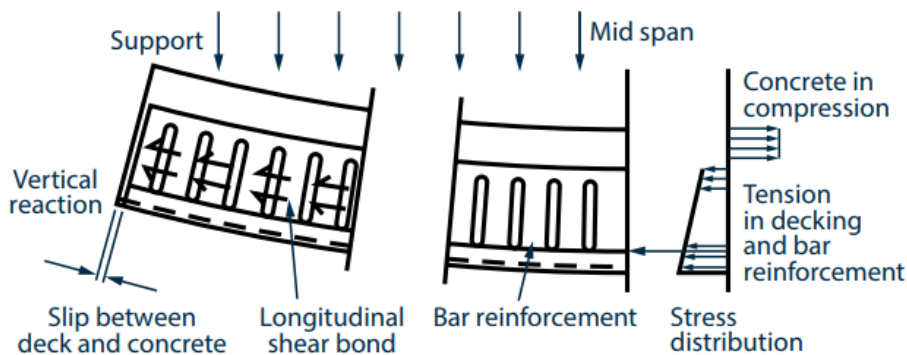


Figure 2.10 – Stresses in a deep composite slab[23]

As also described by Schuurman[12], the three main important aspects of the interface are its strength, stiffness and ductility. This distinction in properties is quite straight-forward, as these aspects are generally important for structural elements. The meaning of these properties can be related to the stress-slip diagram of Figure 2.11. The strength of the interface is the maximum shear stress τ_u that

can be reached, the ductility is the maximum slip $\delta_{//,u}$ that can be reached and the stiffness E_{int} is the tangent to the diagram. Two ultimate cases of interaction can be distinguished: full and no interaction. For no interaction, the longitudinal shear stress is zero for every value of slip. For full interaction, there is no slip for every value of longitudinal shear stress (below τ_u). Cases in between can be referred to as partial interaction. The influence of the mentioned properties on the composite behaviour will now be discussed.

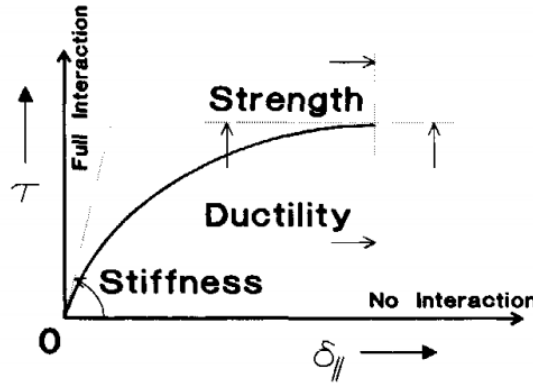


Figure 2.11 – Qualitative shear-slip curve[12]

Strength of the interface

Consider the simplistic composite beam model as shown in the introduction of this thesis in Figure 1.1. A part of this composite beam is also shown in Figure 2.12. For each separate beam ($h \times b$) at the top and bottom, it holds that its stress distribution can be replaced by a normal force N and a bending moment M_p^* . The total bending moment capacity of the composite beam $M_{R,comp}$ equals the summation of these bending moments and the product of the normal force N times the internal lever arm z (equation 2.1). The longitudinal shear stresses at the interface will result in a shear force T (equation 2.2). This longitudinal shear force T (acting over a length x from the left support) is in equilibrium with normal force N at the considered cross-section. When there is no interaction between the beams, T equals zero, meaning that the normal force N also has to be zero. Assuming elasto-plastic behaviour, both separate beams can now be loaded to their full plastic capacities M_p as shown in Figure 2.12 (above the y -axis). When there is interaction between the beams, T doesn't equal to zero, resulting in a normal force N in each beam. Due to the presence of the normal forces, the separate beams can't be loaded to their full plastic capacities, but only to a reduced bending moment capacity M_p^* (equation 2.3). When the normal force N equals its plastic capacity N_p , the ultimate bending moment capacity $M_{Ru,comp}$ of the composite beam is reached.

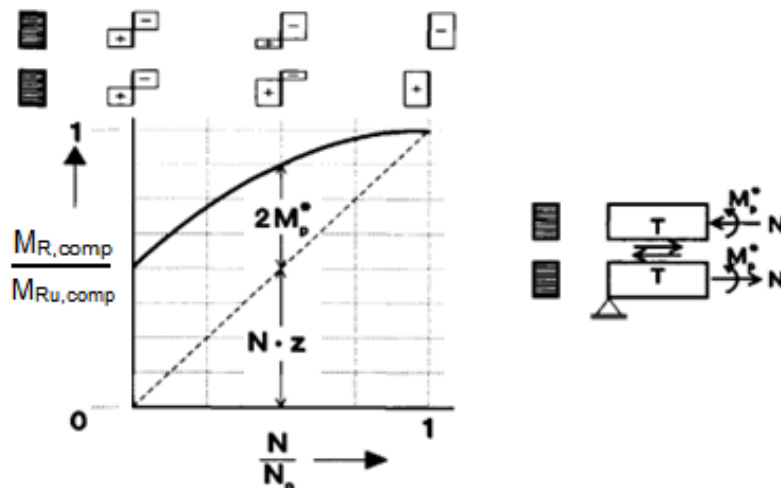


Figure 2.12 – Development of the ultimate moment capacity due to composite behaviour ($N = T$)[12]

$$M_{R,comp} = 2 * M_p^* + N * z \quad 2.1$$

$$T = b \int_0^x \tau dx \quad 2.2$$

$$M_p^* = M_p * \left(1 - \left(\frac{N}{N_p}\right)^2\right), \text{ with } M_p = \frac{b \cdot h^2}{4} \cdot f_y \text{ and } N_p = b \cdot h \cdot f_y \quad 2.3$$

What may be concluded from the former is that the strength of the interface is of importance for development of the ultimate capacity of the composite element. As shown, the greatest benefit in bending moment capacity $M_{R,comp}$ is when both separate parts can be loaded to their full plastic normal capacities. This can only be reached when the interface is strong enough to carry the corresponding longitudinal shear force T . This is not only dependent on the ultimate value for the longitudinal shear stress τ_u , but also on the distance x from the support as the value of T is also dependent on this later variable. The value of τ_u therefore determines at which distance from the support the ultimate capacity $M_{R,comp}$ of the composite beam can be reached. A higher longitudinal shear strength leads to a lower distance from the support. This length is called L_{SF} and can be calculated with equation 2.4.

$$L_{SF} = \frac{N_p}{\tau_u} \quad 2.4$$

Composite slabs are much more complex than the fictitious composite beam as used in above's explanation, but still it can be established that the strength of the longitudinal shear connection is an important factor for the capacity of the composite slab.

Stiffness of the interface

The stiffness of the connection E_{int} influences the bending stiffness of the composite slab and its load-carrying capacity. This can be explained with the help of Figure 2.13, in which again the same composite beam is shown. The situation on the left of the figure corresponds to no interaction, which means that the stiffness of the connection equals to zero (x-axis in Figure 2.11). This results in a relatively large slip and a discontinuity in strains/stresses at the location of the interface. The situation on the right corresponds to full interaction as a result of an infinite stiffness (y-axis in Figure 2.11), leading to no slip at the interface. Both normal stresses and transverse shear stresses are now continuous over the height of the composite beam. Formulas are provided below to compare both ultimate cases of interaction. From these formulas it may be concluded that the moment of inertia increases with a factor of 4 ($I_2 = 4I_1$) when the stiffness of the connection is increased from zero to infinity. As a result, the total deformation reduces proportionally ($\delta_2 \sim EI_2^{-1}$). This directly shows how the bending stiffness of the composite beam is affected by the stiffness of the connection. Furthermore, it can also be seen that the normal stresses reduce with a factor of 2, which means that a two times larger force is needed to cause the same stress level.

$$I_1 = 2 \cdot \frac{1}{12} bh^3 = \frac{2}{12} bh^3$$

$$\delta_1 = \frac{FL^3}{48EI_1} = \frac{FL^3}{8Ebh^3}$$

$$\sigma_{1,max} = \frac{M \frac{h}{2}}{I_1} = \frac{\frac{1}{4} FL \cdot \frac{h}{2}}{\frac{2}{12} bh^3} = \frac{3FL}{4bh^2}$$

$$\tau_{1,max} = \frac{VS}{bI_1} = \frac{\frac{F}{2} \cdot \frac{bh^2}{8}}{b \cdot \frac{2}{12} bh^3} = \frac{3F}{8bh}$$

$$I_2 = \frac{1}{12} b(2h)^3 = \frac{8}{12} bh^3 = 4I_1$$

$$\delta_2 = \frac{FL^3}{48EI_2} = \frac{FL^3}{32Ebh^3} = \frac{\delta_1}{4}$$

$$\sigma_{2,max} = \frac{M \frac{2h}{2}}{I_2} = \frac{\frac{1}{4} FL \cdot \frac{2h}{2}}{\frac{8}{12} bh^3} = \frac{3FL}{8bh^2} = \frac{\sigma_{1,max}}{2}$$

$$\tau_{2,max} = \frac{VS}{bI_2} = \frac{\frac{F}{2} \cdot \frac{b(2h)^2}{8}}{b \cdot \frac{8}{12} bh^3} = \frac{3F}{8bh} = \tau_{1,max}$$

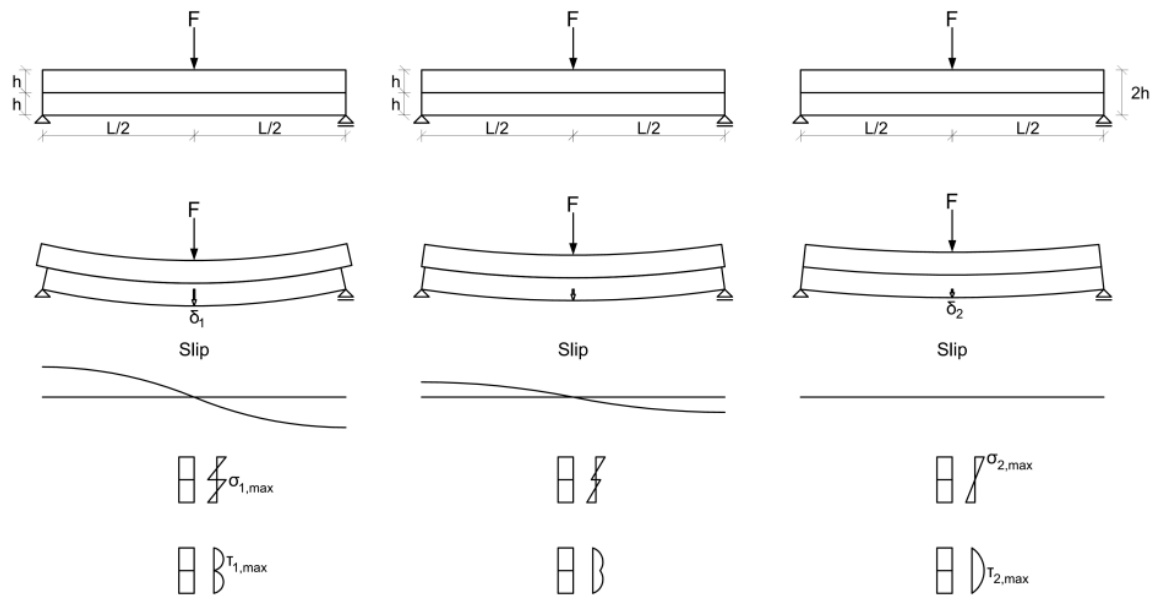


Figure 2.13 – Comparison between no, partial and full interaction in a composite beam[16]

Ductility

Ductile behaviour of the interface is an important aspect in preventing brittle failure of the whole composite element. This has been well explained by Schuurman[12], who described three types of longitudinal shear connections in a composite beam. Figure 2.14 shows the properties of these connections (A, B and C) together with the boundary conditions of the composite beam. Connection A and B both have an infinite stiffness, with B having a ductile behaviour in contrast to A. Connection C has a ductile behaviour and a finite stiffness. The composite beam is made of a linear-elastic material with an infinite strength.

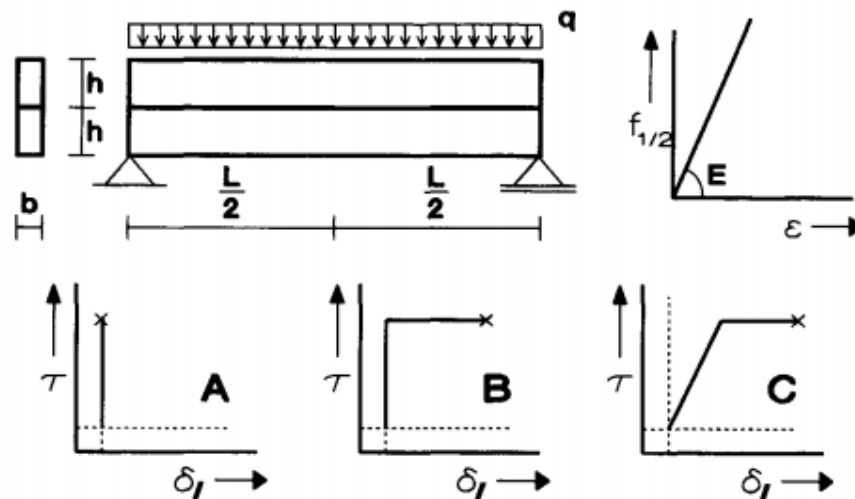


Figure 2.14 – Three types of longitudinal shear connections: A) brittle and infinite stiffness, B) ductile and infinite stiffness, C) ductile and finite stiffness.[12]

From classical mechanics it is known that the transverse shear force in the composite beam is at its maximum near the supports in case of a distributed loading. With an infinite stiffness of the interface as in connection A and B, full interaction is obtained leading to a maximum shear stress at the location of the interface (shown in Figure 2.13). This holds for both the transversal and longitudinal shear stress.

When the load on the composite beam increases, the longitudinal shear stress τ increases, reaching its maximum first at the location of the supports. In case of connection A, after reaching the strength of the connection τ_u , it fails in a very brittle way. The stress release causes the whole interface to fail progressively like a zipper, without additional increase of the load [12]. With this happening, the bending stiffness of the composite beam reduces with a factor of 4 (from EI_2 to EI_1 , see Figure 2.13). In other words, the composite beam quickly changes from full interaction to no interaction. This also causes that the normal stresses will increase with a factor of 2, which could lead to total failure of the beam when the material contains a finite strength. Since no strength is specified in this example, additional loading is possible and will be carried by the two separate beams.

For connection B and C, it holds that after reaching τ_u at the supports, the longitudinal shear stress doesn't drop to zero, but stays at a constant level. This introduces some slip, causing the bending stiffness to reduce at these locations. This reduction in bending stiffness only propagates towards the midspan when the load on the composite beam is increased. By doing so, τ_u will be reached at more locations of the interface. In the end, τ_u is reached over the full length of the interface and the bending stiffness of the total composite beam is also reduced with a factor of 4. The end-situation is thus the same as for connection A. The only difference is that additional loading is needed to cause this end-situation for connection B and C.

Introducing a finite stiffness as in connection C makes that the slip at the interface is introduced before reaching the strength of the interface τ_u . This causes the bending stiffness to drop quicker for connection C than B, resulting in a bigger deflection at the same load level. In the ultimate phase, when τ_u is reached over the full length of the interface, every case (A, B and C) contains the same bending stiffness EI_1 . Figure 2.15 gives an overview of the load-displacement behaviour for all three different connections. The marked points with index 1 indicate the occasions when τ_u is reached at the supports, while the points with index 2 indicate the occasions when τ_u is reached over the full interface.

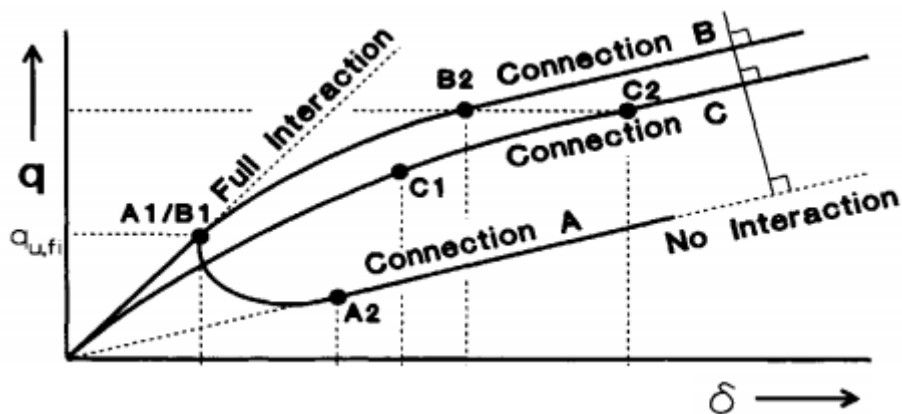


Figure 2.15 – Load-displacement curves for three different types of longitudinal shear connections [12]

2.3. Failure mechanisms of composite slabs

Composite slabs are susceptible to three possible failure mechanisms [12]:

1. Flexural failure
2. Longitudinal shear failure
3. Transverse shear failure (or vertical shear failure)

Figure 2.16a gives indications for the locations of these failure mechanisms in case of a four-point bending test. The index of the location corresponds to the index of the failure mechanism as given above. Flexural failure occurs when the bending moment capacity of the composite slab is exceeded.

This failure mechanism is characterised by yielding of the steel deck (and rib reinforcement), with the concrete on top in compression. This failure mechanism is most often ductile and frequently occurs in the middle region of the span (between the localized loads caused by force W in Figure 2.16a). In order to utilize the bending moment capacity of the slab, it is needed to provide enough bonding between the concrete and steel at the interface. Longitudinal shear failure is therefore a secondly common noticed failure mechanism in composite slabs. This failure mode is limited by the shear capacity of the connection (τ_u , see Figure 2.11) and is characterized by excessive slip between the steel and concrete. Diagonal cracks near the loading point are also often visible[13]. Most research in composite slabs has been conducted to this failure mechanism in order to characterize its corresponding resistance. To date, it is still not possible to determine it barely with design formulas. The longitudinal shear capacity is therefore provided by the supplier and determined by testing. At last, transverse shear failure is a third possible failure mechanism which mainly occurs closely to the supports. This mechanism is known by its brittle character and should be avoided. The failure mode is generally characterised by opening of the cracks in the concrete which are oriented diagonally from the support to the loading point.

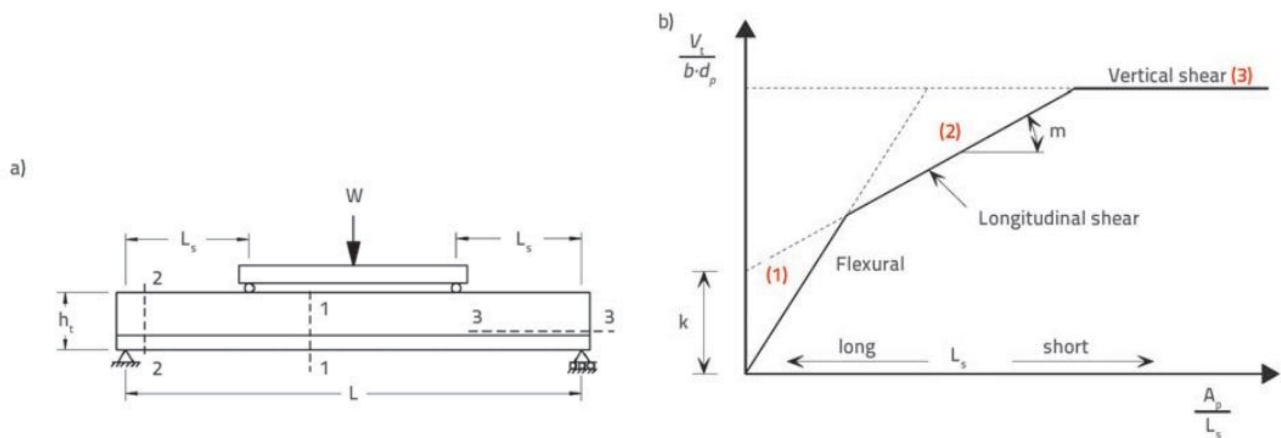


Figure 2.16 – a) Four-point bending test of composite slab with locations for failure modes; b) Failure load V_t (local load at the end of L_s) as a function of the inversed shear span (L_s^{-1})[13]

The governing failure mode in a composite slab is influenced by the shear span L_s . The shear span is defined as the distance between the local load and the support, as also visible in Figure 2.16a. The dependency of the failure mode on this shear span is shown in Figure 2.16b. In this figure, the failure load V_t is qualitatively plotted against the inversed shear span L_s^{-1} . Keep in mind that this inversion causes long spans to be close to zero. The quantities are normalized by constants b , d_p and A_p , which are respectively the width of the slab, the effective depth of the slab and the cross-sectional area of the steel deck.

What can be seen in Figure 2.16b is that the load-carrying capacity for flexural failure increases for shorter shear spans. A short shear span makes that the bending moment in the composite slab is lower compared to a large shear span loaded by the same force W . Therefore, for large shear spans the ultimate bending moment capacity is reached at a lower load-level than for short shear spans. For that reason, flexural failure mainly occurs when the shear span is large and especially for slender slabs having a relatively low bending moment capacity.

Furthermore, it can be seen in Figure 2.16b that the load-carrying capacity for transverse shear failure is independent of the shear span. The four-point bending test causes the shear force to be constant within the shear span L_s . Assuming that the composite slab has an equal transverse shear resistance over its whole length, indeed leads to the fact that the failure load for transverse shear is independent of the shear span. Increasing or decreasing the shear span only leads to movement of the point loads,

but this movement doesn't increase the shear force in the slab. It should be noticed that this is off course a purely theoretical way of thinking, as research has shown that the transverse shear capacity of concrete sections is dependent on the shear span[28].

Assuming a short shear span and neglecting longitudinal shear failure, the load can be increased until the transverse shear capacity of the slab is reached. When this failure load is now kept constant, but moved towards the midspan, makes that the transverse shear force in the slab remains the same while the bending moment increases. At a critical value for the shear span, not the transverse shear capacity, but the bending moment capacity will become governing and the slab fails in bending. This is also visible in Figure 2.16b as the intersection of the dashed lines for flexural and transverse shear failure.

Due to the presence of the interface, longitudinal shear failure should be considered. The interface should be strong enough in order to reach the ultimate bending moment capacity of the composite slab. This has been explained in section 2.2, in which it was shown that the longitudinal shear force T needs to be big enough to reach the ultimate moment capacity of the composite beam (as also for slabs). This force T is dependent on the strength of the connection τ_u and the length x from the support (see equation 2.2). This length x equals the shear span L_s , since the longitudinal shear stresses only develop within this part of the composite slab. Let's assume that flexural failure is the governing mode for a given (long) shear span and this shear span will be reduced. At some critical point, the longitudinal shear force T becomes too big in order to maintain the ultimate bending moment capacity, because the shear span L_s (or distance x) becomes too short. In this case it is demanded that the connection provides a shear stress above its ultimate strength τ_u , but since this is not possible, longitudinal shear failure occurs. This transition from flexural failure to longitudinal shear failure is visible in Figure 2.16b as the intersection of the corresponding lines. The resistance of a composite slab against longitudinal shear failure (as expressed in Figure 2.16b) can be determined by testing with the so-called $m-k$ method. The meanings of these symbols are also visible in the figure. It can be seen that the resistance against longitudinal shear failure increases for shorter shear spans. This may seem contradictory, as it is expected that longitudinal shear failure occurs at an earlier stage when the shear span (= length which can carry the longitudinal shear stresses) is reduced. However, the load-carrying capacity should be related to the load that shall cause flexural failure for the same shear span L_s . When this is done and the diagram for longitudinal shear failure is assessed with respect to the diagram for flexural failure, it can be established that the difference between the two diagram gets bigger when the shear span is reduced. This indeed confirms the expectation that longitudinal shear failure occurs at an earlier stage for shorter shear spans.

This thesis focusses on the transverse shear failure of deep composite slabs. What can be concluded from the former is that transverse shear failure is the closest related to longitudinal shear failure according to the theory. Therefore, both corresponding resistances are further explained in the following sections.

2.4. Longitudinal shear resistance of composite slabs according to Eurocode 4

NEN 1994-1-1[3] specifies two methods for determining the resistance against longitudinal shear failure, namely the $m-k$ method and the partial shear method. This later method may only be applied to composite slabs with a ductile longitudinal shear behaviour. The behaviour may be considered as ductile if the failure load for longitudinal shear exceeds the load that causes a relative end slip of 0.1 mm by more than 10%. If this failure load is reached at a midspan deflection of more than $L/50$, the failure load should be taken as the load that causes this deflection of $L/50$.

Ductile behaviour isn't a requirement for application of the m - k method and can therefore be used for every composite slab that is governed by EN 1994-1-1[3]. With this method, m and k are empirical constants which have to be determined by testing as shown in Figure 2.17. The composite slabs are brought to failure in a four-point bending test (with line loads). Before this procedure, the slab is first cyclically loaded between 20% and 60% of the expected failure load. With this cyclic load it is intended to represent the load over a period of time and to minimize the influence of chemical/adhesive bonding between the steel and concrete[15]. Typically, two sets of three tests (or three sets of two tests) are carried out, in which each set has a different shear span L_s . The shear span for each set is chosen such that it is as long or short as possible (not less than $3h_t$) for every tested slab to still fail in longitudinal shear. After gathering the test results, m and k are obtained by drawing a linear line at a specific distance below the lowest failure load in each set (to allow for scatter in the test results). The distance between this line and the test results is prescribed by the Eurocode 4.

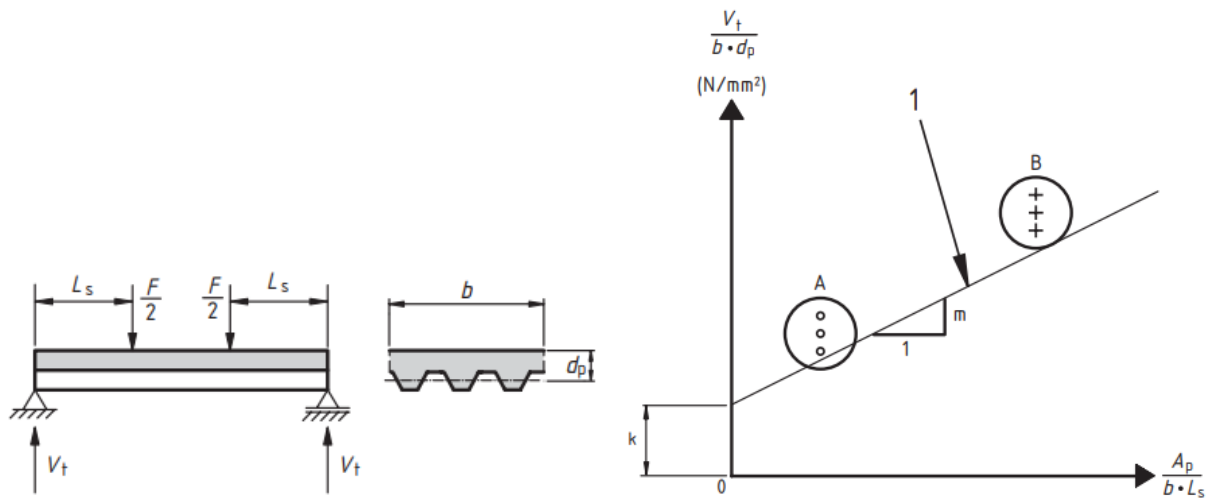


Figure 2.17 – Test method to determine the values for m and k [3]

As can be seen in Figure 2.17, m relates to the slope of the line and k relates to the offset of the line at the y -axis. They are used in equation 2.5 to determine the resistance of the composite slab against longitudinal shear failure $V_{l,Rd}$. As explicitly mentioned in clause 9.7.3 of EN 1994-1-1[3], the nominal cross-sectional area A_p of the steel deck is used in equation 2.5, as it is normally used in the test evaluations to determine m and k . To be consistent, d_p is therefore defined as the distance between the top fibre of the slab and the centroidal axis of this nominal cross-section A_p of the steel deck. When the effective cross-section A_{pe} is used, d_p should be related to the centroidal axis of this effective cross-section. The effective cross-section A_{pe} is obtained by reducing the nominal cross-section A_p with the area that includes the embossments (according to Eurocode 4).

$$V_{l,Rd} = V_t = \frac{b d_p}{\gamma_{vs}} \left(\frac{m A_p}{b L_s} + k \right) \quad 2.5$$

With:

- b width of the slab [mm];
- d_p effective depth of the slab [mm];
- γ_{vs} safety factor for the ultimate limit state [-];
- A_p nominal cross-section of the steel deck [mm²];
- L_s shear span [mm];
- m, k empirical factors [MPa]

Because of full-scale testing, the m - k method is a time-consuming and costly process. When a new type of steel deck is developed, the values for constants m and k in principal have to be determined for every thickness, coating and grade of the steel deck; for every total slab depth to be used and for a range of concrete strengths and densities[3][15]. To reduce the number of tests, some simplifications for these requirements are given in EN 1994-1-1[3].

The partial shear method may only be applied to composite slabs with ductile longitudinal shear behaviour, because it is based on a simple engineering model with rigid stress-blocks for the steel and concrete. This is shown in Figure 2.18. With this method it is possible to determine the longitudinal shear resistance τ_u of the connection between the concrete and steel. The longitudinal shear stress is assumed to be equally distributed within the shear span. At least four tests have to be carried out, in which for three tests the shear span has to be as long as possible while still providing longitudinal shear failure. In the other test, the shear span must be as short as possible (not less than $3h_t$) with also providing longitudinal shear failure. This later test is to confirm the ductility requirement for the partial shear method. In each test, the bending moment M_{test} at longitudinal shear failure should be divided by the calculated bending moment capacity $M_{p,Rm}$ based on a full shear connection (stress distribution on the top-right of the diagram in Figure 2.18). With this ratio, a horizontal line from A to B can be drawn, after which the degree of shear connection η_{test} can be determined at point C. Subsequently, the shear resistance τ_u for every test can be determined with the help of equation 2.6.

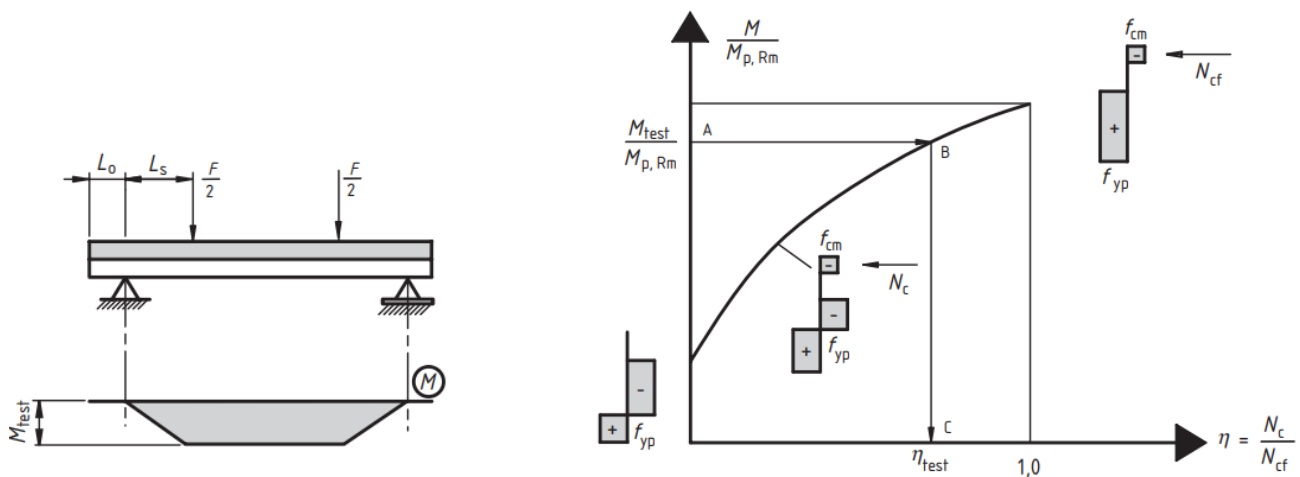


Figure 2.18 – Partial shear method[3]

$$\tau_u = \frac{\eta N_{cf}}{b (L_s + L_0)}$$

2.6

With:

- η degree of shear connection [-];
- N_{cf} compressive force in concrete for full shear connection [N];
- b width of the slab [mm];
- L_s shear span [mm];
- L_0 length of the overhang [mm].

As discussed in section 2.1.9, EN 1994-1-1[3] doesn't cover ComFlor 210 ($b_r/b_s > 0.6$). Despite this, Van Erp[16] recently determined the longitudinal shear resistance of this composite slab with the methods provided in EN 1994-1-1[3]. In his thesis, he tested multiple ComFlor 210 type of composite slabs with a total height of 280 mm. The slabs contained $\varnothing 12$ mm longitudinal rebars as rib

reinforcement and a $\varnothing 8$ -150 mm mesh in the top layer; both made of steel with a minimal strength of 500 MPa. The thickness of the steel deck was 1 mm and had a minimal strength of 350 MPa. The concrete had an expected nominal strength of 20 MPa. He found values of $m = 154.3$ MPa and $k = 0.0369$ MPa. In the determination of these constants he used an (effective) cross-section A_p of 1140.5 mm²/m for the steel deck. Furthermore, he found an average value of $\tau_u = 0.103$ MPa, with corresponding characteristic value $\tau_{u,Rk} = 0.0716$ MPa and design value $\tau_{u,Rd} = 0.0573$ MPa. In the determination of these values, he assumed an effectiveness of 12.5% for the parts of the embossments. This means that for calculation, the effective thickness of the steel deck at these locations is assumed to be 0.125 mm instead of 1 mm.

2.5. Transverse shear resistance of composite slabs according to Eurocode 4 (referring to Eurocode 2: concrete structures)

Transverse shear failure is most likely to occur for highly concentrated loads near the supports and in general for composite slabs with a low L/h_t ratio (i.e. span/depth)[15]. The resistance of a composite slab against transverse shear failure ($V_{t,Rd}$) is prescribed in clause 9.7.5 of EN 1994-1-1[3] (Eurocode 4), which simply refers to clause 6.2.2 of EN 1992-1-1[24] (Eurocode 2). This later is about the transverse shear capacity of concrete members without shear reinforcement (stirrups). From this, it may be established that the transverse shear resistance of a composite slab according to the Eurocode 4 is completely based on its concrete part (i.e. concrete ribs of the composite slab). The standard indirectly suggests that the steel deck doesn't give any additional resistance to the composite slab in case of transverse shear failure. Equation 2.7 can be used to calculate the transverse shear resistance $V_{t,Rd}$ of a composite slab per rib in accordance with Eurocode 4 and 2 (see also Figure 2.20). The effective width b_w has to be taken as the smallest width of the concrete rib in the tensile area according to EN 1992-1-1[24]. In the old Dutch code NVN-ENV 1994-1-1[26], the effective width is specified differently as b_0 (see Figure 2.19). In case of a trapezoidal profiled deck, b_0 equals the mean width of the concrete rib; for a re-entrant deck, b_0 is equal to the minimum width at the top of the trough of the steel deck. The use of this parameter b_0 instead of b_w can also be found in other literature[15][17][18].

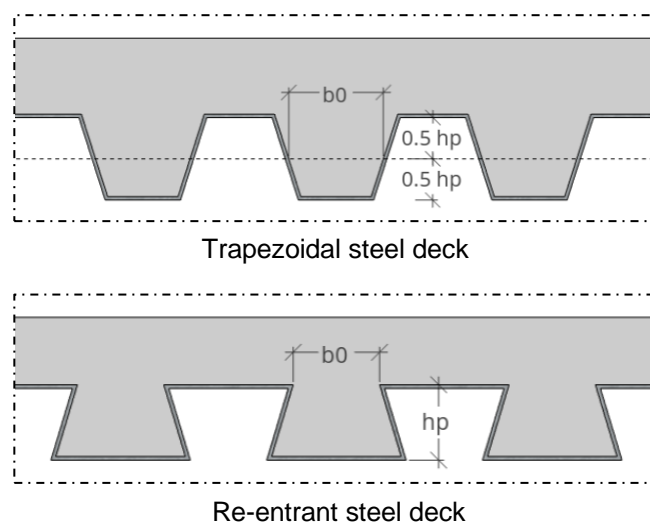


Figure 2.19 – Definition parameter b_0 in composite slabs

Furthermore, it may be concluded that there are some ambiguities in this calculation method, caused by the fact that Eurocode 4 simply refers to Eurocode 2 without providing additional information. For example, it is not perfectly clear whether it is allowed to take into account the area of the steel deck in calculation of the longitudinal reinforcement ratio ρ_l , which positively contributes to the transverse shear

resistance according to the formula. Since the steel deck acts as tensile reinforcement in almost the same way as ordinary rebars (ULS: plastic stress distribution), the author tends to assert that this is allowed. On the contrast, since equation 2.7 is empirically determined for reinforced concrete members, it is simply not known how the area of the steel deck can be implemented into this formula for calculation of the composite slab's resistance. Furthermore, no guidance is given on how to take the effective depth of the composite slab in case of presence of rib reinforcement. To comply with both norms EN 1992-1-1[24] and EN 1994-1-1[3], the following is recommended by the author and applied in this thesis:

- No rib reinforcement → Effective depth d is taken as the distance between the top fibre of the slab and the centroidal axis of the effective steel deck (i.e. d_p in EN 1994-1-1[3]); reinforcement ratio ρ_l is set to zero.
- Including rib reinforcement → Effective depth d is taken as the distance between the top fibre of the slab and the centroidal axis of the longitudinal rebar; reinforcement ratio ρ_l is based on the tensile area of the rebar.

$$V_{t,Rd} = V_{Rd,c} = C_{Rd,c} k (100 \rho_l f_{ck})^{\frac{1}{3}} b_w d \geq 0.035 k^{3/2} f_{ck}^{1/2} b_w d \quad 2.7$$

With:

- $V_{t,Rd}$ transverse shear resistance of the composite slab per rib [N];
- $V_{Rd,c}$ transverse shear resistance of the concrete part per rib [N];
- $C_{Rd,c}$ empirical coefficient [-];
- $k = 1 + \sqrt{\frac{200}{d}} \leq 2.0$, with d in mm [-];
- $\rho_l = \frac{A_{sl}}{b_w d} \leq 0.02$ [-];
- A_{sl} total area of the tensile reinforcement, that is minimally anchored with a length of $(l_{bd} + d)$ beyond the cross-section considered [mm²];
- l_{bd} design anchorage length [mm];
- f_{ck} characteristic concrete compressive strength [MPa];
- b_w smallest width of the cross-section in the tensile area [mm];
- d effective depth composite slab [mm].

The general mission of the Eurocode is to ensure structural safety with efficiently making use of materials. Prediction of the strength should therefore be as close as possible to reality, but literature[17][18][21] suggests that EN 1994-1-1[3] gives too conservative results when it comes to the transverse shear resistance of a composite slab. The most obvious clarification is that the influence of the steel deck is not considered.

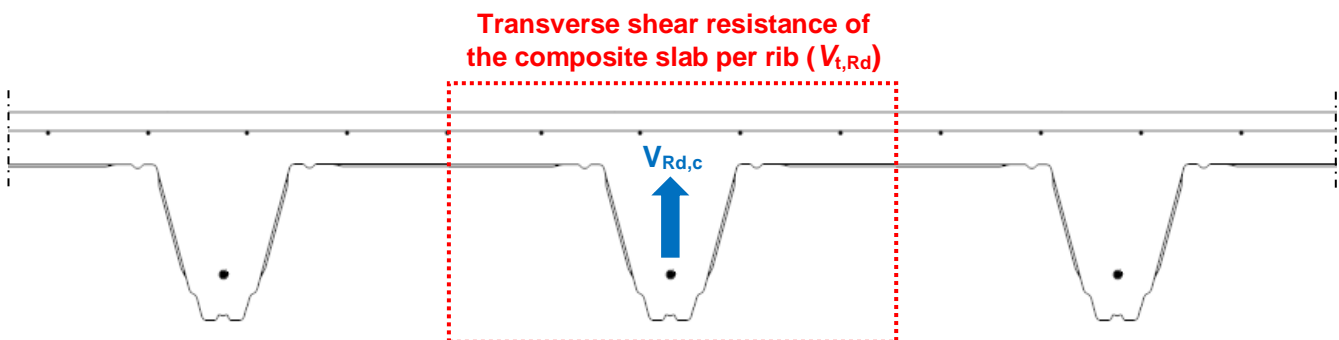


Figure 2.20 – Transverse shear resistance of a composite slab per rib ($V_{t,Rd}$) according to Eurocode 4: it is totally based on the capacity of the concrete section ($V_{Rd,c}$)

2.6. Transverse shear resistance of steel decks according to Eurocode 3

During construction of a composite slab, the steel deck has to carry the wet concrete and other construction loads in an often unpropped way as explained in section 2.1.3. As a result, transverse shear stresses will develop in the webs of the steel deck. These stresses must be resisted to guarantee safety. The transverse shear resistance $V_{b,Rd}$ of a steel deck is prescribed in clause 6.1.5 of EN 1993-1-3[25] and can be calculated with equation 2.8. It has been chosen to express the transverse shear resistance of the steel deck in Newtons for one “rib” (see Figure 2.21). This has been done to comply with the former section about the transverse shear capacity of a composite slab and to be consistent throughout the whole thesis. One rib contains two webs, which clarifies the factor of 2 in equation 2.8.

$$V_{b,Rd} = 2 \cdot \frac{\frac{h_w}{\sin(\varphi)} t f_{bv}}{\gamma_{M0}} \quad 2.8$$

With:

$V_{b,Rd}$	transverse shear capacity of a steel deck (expressed per “rib”) [N];
f_{bv}	shear strength considering buckling [MPa];
h_w	height of the web between the centrelines of the flanges, measured perpendicularly to these flanges (Figure 2.24) [mm];
t	thickness of the web (excluding coatings) [mm];
φ	angle of the web relative to the horizontal axis [rad];
γ_{M0}	material factor for the ULS [-].

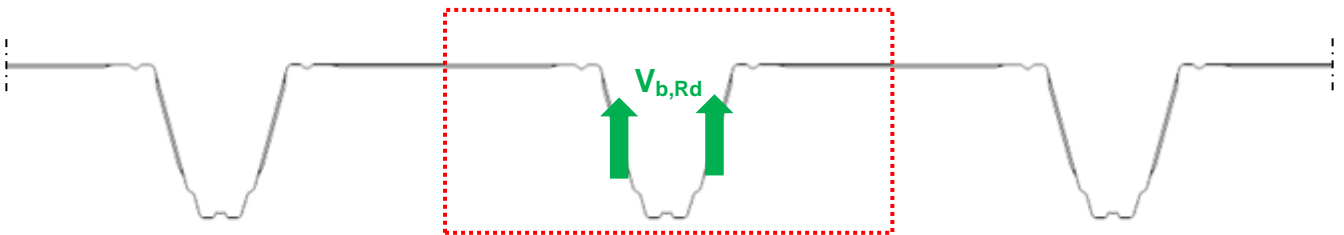


Figure 2.21 – Transverse shear resistance steel deck $V_{b,Rd}$ per “rib” (bounded by red dashed lines)

Since the steel deck might be sensitive to local buckling due to its high plate slenderness, shear buckling is considered by introducing a shear buckling strength f_{bv} in equation 2.8. Normally the shear strength of steel is taken as $f_y/\sqrt{3}$, but depending on the web slenderness the value for f_{bv} may be below this shear strength. More information is provided in Appendix A.

2.7. Transverse shear resistance of composite slabs according to literature

In section 2.5 it has been explained that the transverse shear resistance of a composite slab is only depended on the resistance of its concrete ribs according to Eurocode 4. The contribution of the steel deck to this resistance is totally neglected. Someone may use the tensile area of the steel deck in calculation of the longitudinal reinforcement ratio ρ_l , but it is doubted if this is allowed since the Eurocode 4 doesn't specifically mention this. Suppose it is allowed, then it would still be remarkable that the contribution of the steel deck to the transverse shear resistance is based on its area rather than its shape[17]. The webs of the steel deck ensure that this profile has a significant transverse shear resistance on its own as explained in section 2.6 (according to Eurocode 3). Therefore, it may be contradictory to neglect the resistance of these webs in calculation of the transverse shear resistance of the composite slab.

Stark[18] tried to validate a new design model for the transverse shear resistance of composite slabs. He distinguished three potential contributions to this resistance as shown in Figure 2.22. These contributions can be described as follows:

- I. Transverse shear resistance of the concrete ribs;
- II. Transverse shear resistance of the steel deck;
- III. Additional transverse shear resistance from the concrete above the flanges of the steel deck.

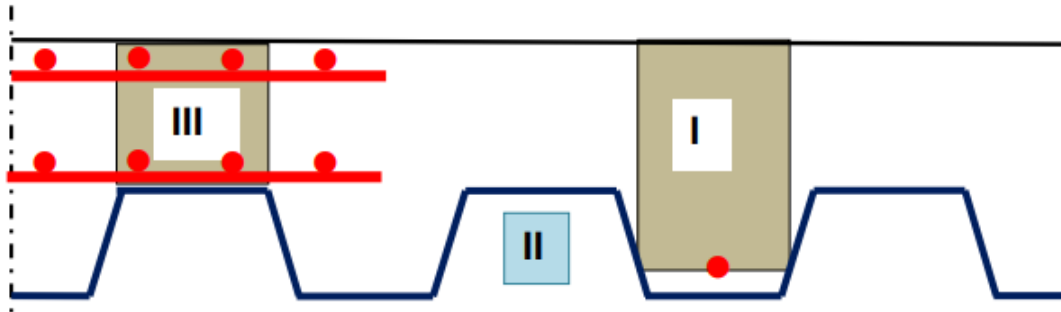


Figure 2.22 – Potential contributions to the transverse shear resistance of a composite slab[18]

The first contribution to the transverse shear resistance of a composite slab has been well explained in section 2.5. According to Stark[18], the effective depth d has to be taken as the distance between the top fibre of the slab and the centroidal axis of the rib reinforcement. Furthermore, the mean width of the concrete rib b_0 has to be used in calculation as the effective width of the concrete rib (instead of b_w). The rebars are assumed to be fully anchored, while the contribution of the steel deck to the longitudinal reinforcement ratio is conservatively neglected.

The contribution of the steel deck (II) is based on the assumption that each separate web provides a transverse shear resistance equal to the vertical component of the shear yield capacity V_{lu} of that web (see Figure 2.23). This shear yield capacity V_{lu} can be calculated with equation 2.9, by which the transverse shear resistance $V_{Rd,p}$ of the steel deck can be calculated with equation 2.10. It can be established that Stark’s model is in great agreement with Eurocode 3 (see section 2.6), although there are some differences:

- no reduced shear strength is used to consider shear buckling;
- the height of the web is taken as the part between the radii to the flanges (h_l , see Figure 2.24).

$$V_{lu} = h_l \cdot t \cdot \frac{f_y}{\sqrt{3}} \tag{2.9}$$

$$V_{Rd,p} = 2 \cdot \frac{\cos(\alpha) \cdot V_{lu}}{\gamma_{M0}} \tag{2.10}$$

With:

- $V_{Rd,p}$ contribution of the steel deck to the transverse shear resistance of a composite slab for one rib (according to Stark[18])[N];
- V_{lu} shear yield capacity of a steel deck’s web [N];
- h_l height of the web, specified as the distance between the radii to the flanges (Figure 2.24) [mm];
- t thickness of the web (excluding coatings) [mm];
- f_y yield strength [MPa];
- α angle of the web with respect to the vertical axis [rad].

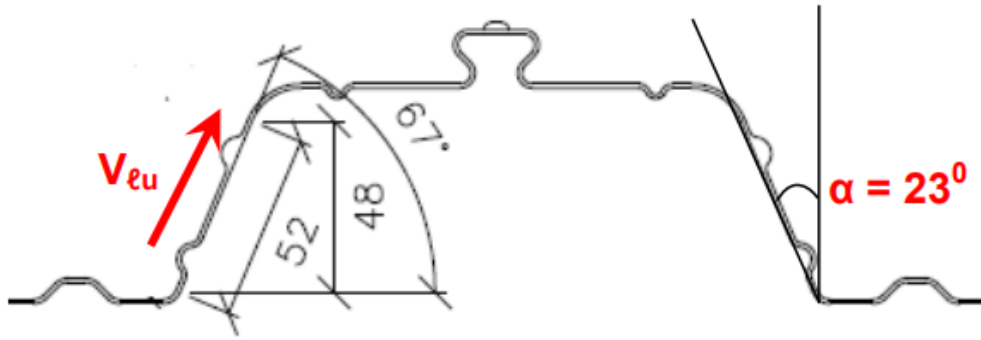


Figure 2.23 – Transverse shear resistance of the web V_u (example for ComFlor 60(UK))[18]

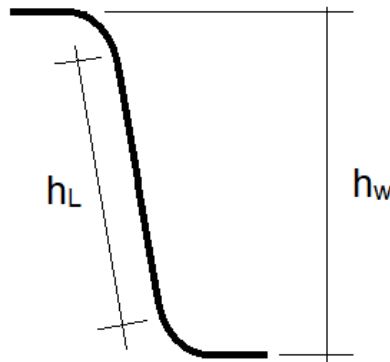


Figure 2.24 – Definition of h_w and h_l

The contribution of the concrete part above the flanges (III) is based on the same principles as for the contribution of the concrete ribs (I). Prerequisite for this contribution is that a double reinforcement mesh is present in the upper part of the composite slab as also can be seen in Figure 2.22[18]. The transverse shear resistance $V_{Rd,c2}$ of this concrete part can be calculated with equation 2.11. Visualization of the model is given in Figure 2.25.

$$V_{Rd,c2} = C_{Rd,c} k (100 \rho_l f_{ck})^{\frac{1}{3}} b_{w2} d_2 \geq 0.035 k^{\frac{3}{2}} f_{ck}^{\frac{1}{2}} b_{w2} d_2 \quad 2.11$$

With:

- $V_{Rd,c2}$ contribution of the concrete part above the flanges according to Stark[18] [N];
- $C_{Rd,c}$ empirical coefficient [-];
- $k = 1 + \sqrt{\frac{200}{d_2}} \leq 2.0$ with d_2 in mm [-];
- $\rho_l = \frac{A_{sl}}{b_{w2} d_2} \leq 0.02$ [-];
- A_{sl} cross-sectional area of the lower reinforcement mesh in the concrete part above the flange [mm²];
- f_{ck} characteristic concrete compressive strength [MPa];
- $b_{w2} = b_s - b_0$ [mm];
- b_s centre-to-centre distance concrete ribs [mm];
- b_0 mean width of the concrete rib [mm];
- d_2 effective depth of the concrete part above the flange [mm];

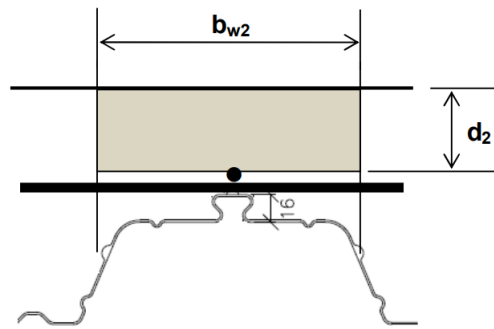


Figure 2.25 – Area of the concrete part above the flange that contributes to the transverse shear resistance of the composite slab[18]

According to the model of Stark[18], the total transverse shear resistance of the composite slab is obtained by simply adding the contributions of the three different parts. In order to validate the model, series of experiments were conducted by Popo-Ola[19] on ComFlor 60(UK) type of composite slabs. The tested specimens were 600 mm wide and contained two complete concrete ribs. The steel deck was made of S350. Different parameters were varied in the tests: the concrete strength, the total slab height, the reinforcement mesh, the sheet thickness and the rib reinforcement. Based on comparison of test results with calculated values, it has been concluded by Stark[18] that the model provides safe values for all tests: the maximum ratio of calculated resistance to corresponding test result is equal to 0.86. For calculation of the transverse shear resistance, the contribution of the concrete ribs (I) has only been considered when rib reinforcement was present in the corresponding test. The same holds for the contribution of concrete parts above the flanges (III) with respect to the double reinforcement mesh in the top layer of the composite slab. This is based on the observation in tests without rib reinforcement, that after crack initiation in the concrete ribs, the load was transferred to the steel deck which carried almost all of the load[18]. This led to a considerable uplift of the concrete part with respect the steel deck (vertical separation)[18]. Most important conclusion of the experiments and corresponding report is that the steel deck considerably contributes to the transverse shear resistance of the composite slab. For almost all tests this contribution could be calculated with equation 2.10 according to Stark[18].

Since the use of a double reinforcement mesh is not very common in practice, the contribution of the concrete part above the flange (III) may be neglected in the calculation of the total transverse shear resistance $V_{t,Rd}$. This leads to the proposed calculation method as shown in equation 2.12, in which the transverse shear resistance of the composite slab equals the summation of the capacity of the concrete rib ($V_{Rd,c}$) and the capacity of the steel deck ($V_{Rd,p}$). This is illustrated in Figure 2.26.

$$V_{t,Rd} = V_{Rd,c} + V_{Rd,p} = \max\left(C_{Rd,c} k (100\rho_l f_{ck})^{\frac{1}{3}} b_0 d ; 0.035 k^{\frac{3}{2}} f_{ck}^{\frac{1}{2}} b_0 d\right) + 2 \cdot \cos(\alpha) \cdot h_t \cdot t \cdot \frac{f_y}{\gamma_{M0}} \quad 2.12$$

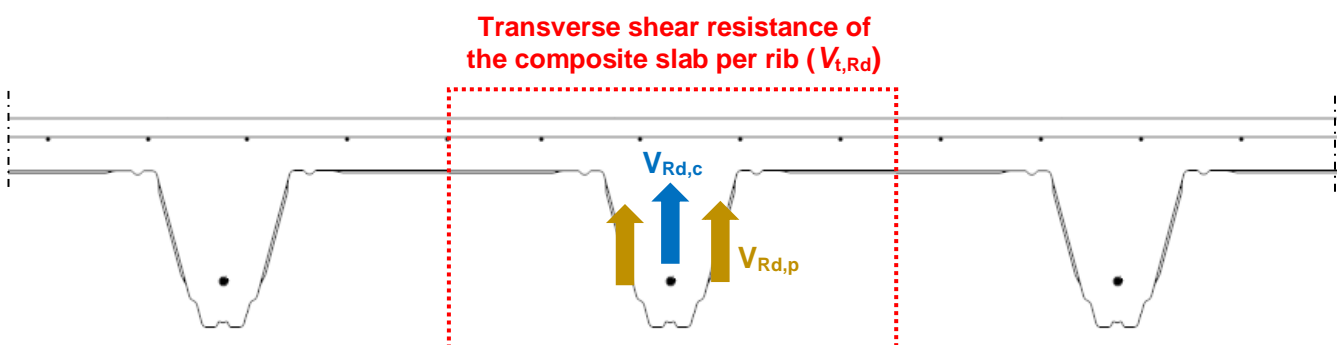


Figure 2.26 – Transverse shear resistance of composite slab per rib according to Stark[18]

Summing-up the partial resistances of the concrete rib and the steel deck for the total transverse shear resistance of the composite slab is in great accordance with the Brazilian standard (clause Q.3.1.3.1 of ABNT NBR 8800[20]). This is in contrast to the European standard in which the partial resistance of the steel deck is totally neglected. It should be mentioned that in the Brazilian standard, the contributions of the concrete and steel are determined according to different formulas. The effective area of the concrete rib is also specified differently. This especially holds for trapezoidal profiles as can be seen in Figure 2.27.

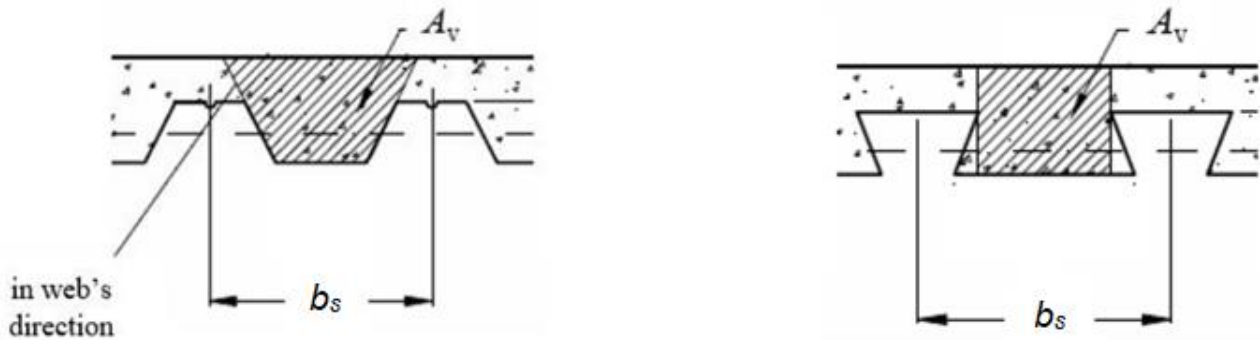


Figure 2.27 – Effective area of the concrete rib according to Brazilian standard: trapezoidal profile (left) and re-entrant profile (right)[20]

Abspoel, Stark & Prins[21] carried out a research program in close cooperation with Dutch Engineering[4] and Tuls[22] to gain more insight into the influence of the transverse shear force on the hogging moment capacity of composite slabs. This is of importance for continuously supported composite slabs and the current European standard lacks in information about this interaction. Therefore, they tested three ComFlor 210 slabs and two ComFlor 75 slabs (NL, refers to ComFlor 60 in the UK). Second point of interest was to validate the contribution of the steel deck to the transverse shear capacity of the composite slabs. The specimens were made of grade S350 for the steel deck, grade B500 for the reinforcement bars and mesh, and class C30/37 for the concrete section. The ComFlor 210 specimens contained one rebar $\text{Ø}12$ (rib reinforcement) and all specimens were provided with a reinforcement mesh and additional rebars on top. The ComFlor 210 and ComFlor 75 specimens had a nominal concrete topping of 70 mm and 90 mm respectively. No significant influence of the transverse shear force on the hogging moment capacity was found according to the experiments. None of the specimens failed in transverse shear, so quantitative determination of this resistance was not possible. Still, from the measured transverse shear forces it was concluded that the current European standard provides too conservative procedures for determination of the transverse shear capacity of composite slabs. This applied to both ComFlor 75 (NL) and ComFlor 210. A maximum cylinder load of 147.18 kN was measured for which the ComFlor 210 specimen (two ribs) still didn't fail in transverse shear (including hogging moment conditions). This load was directly equal to the transverse shear force acting on the specimen due to the used test setup (neglecting self-weight).

Pereira, Simões & Duarte[17] performed two tests on shallow composite slabs to evaluate the transverse shear resistance according to equation 2.13 (visualised in Figure 2.28). Comparison with equation 2.12 (Stark[18]) shows that $V_{Rd,p}$ is substituted by $V_{b,Rd}$, which makes that the contribution of the steel deck is now calculated according to the formula that is provided by the Eurocode 3. Consequently, the effect of shear buckling is taken into account for determination of the transverse shear capacity of the composite slab.

$$V_{t,Rd} = V_{Rd,c} + V_{b,Rd} = \max\left(C_{Rd,c}k(100\rho_l f_{ck})^{\frac{1}{3}}b_0d; 0.035k^{\frac{3}{2}}f_{ck}^{\frac{1}{2}}b_0d\right) + 2 \cdot \frac{h_w}{\sin(\varphi)} \frac{t f_{bv}}{\gamma_{M0}} \quad 2.13$$

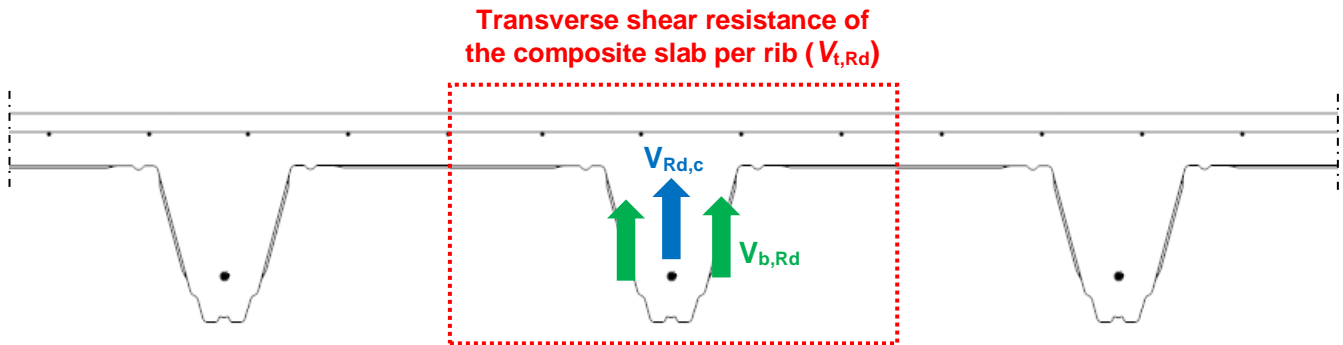


Figure 2.28 – Transverse shear resistance of composite slab per rib according to Pereira et al.[17]

The first tested slab collapsed due to the transverse shear force, since vertical cracks appeared near the loading zone and the values of measured slip were low. For this test, the transverse shear resistance according to the Eurocode 4 (section 2.5) was only 21.09% of the achieved capacity, while the resistance according to equation 2.12 was 98.61% of the achieved capacity. The proposed model therefore predicted the transverse shear resistance much closer to reality than the Eurocode 4 did. The second tested slab failed in longitudinal shear for the reason that ductile slip behaviour was observed with a maximum end-slip of approximately 13 mm. With this test it was therefore not possible to determine the transverse shear resistance quantitatively. However, it could again be concluded that Eurocode 4 is unnecessarily conservative: the calculated transverse shear resistance according to this standard corresponded to 38.74% of the achieved capacity. This means that according to procedures of Eurocode 4, the composite slab should already have failed in transverse shear instead of longitudinal shear. Statistically speaking, these two tests don't prove the rightness of equation 2.13, but they do support the supposition that the Eurocode 4 doesn't predict the transverse shear capacity accurately.

Hartmeyer & Kurz[27] also tried to come up with a new transverse shear model for composite slabs based on the observation that it is not accurately described by the Eurocode 4. Research has been carried out on composite slabs with shallow re-entrant profiled decks in combination with both normal and lightweight concrete. Only normal weight concrete is considered in this thesis. They have looked into more detail at the cracked state at failure and distinguished three different components that contribute to the transverse shear capacity in the ultimate limit state:

- The vertical force component of the uncracked compressive zone $V_{c,cz}$;
- The transverse shear capacity of the metal sheet $V_{p,R}$;
- The local aggregate interlock $V_{c,ct}$ (related to the tensile forces transmitted at the crack tip).

These components are shown in Figure 2.29. In experiments it was observed that across the major inclined 'bending shear crack'[27], transverse shear forces can be transferred to the metal deck up to its capacity. By reaching a critical load, local buckling of the metal deck was observed at the location of this critical crack. This is shown in Figure 2.30. The buckling allows a relative displacement of the crack's surfaces which activates aggregate interlock. The effectiveness of the interlock is mainly dependent on the concrete's properties, the bonding properties between the steel and concrete and the existing crack width at the moment of local buckling[27]. It was also observed that the inclined crack extended almost horizontally underneath the compression zone, until the section of maximum bending moment was reached. This led to reaching the ultimate capacity of the composite slab.

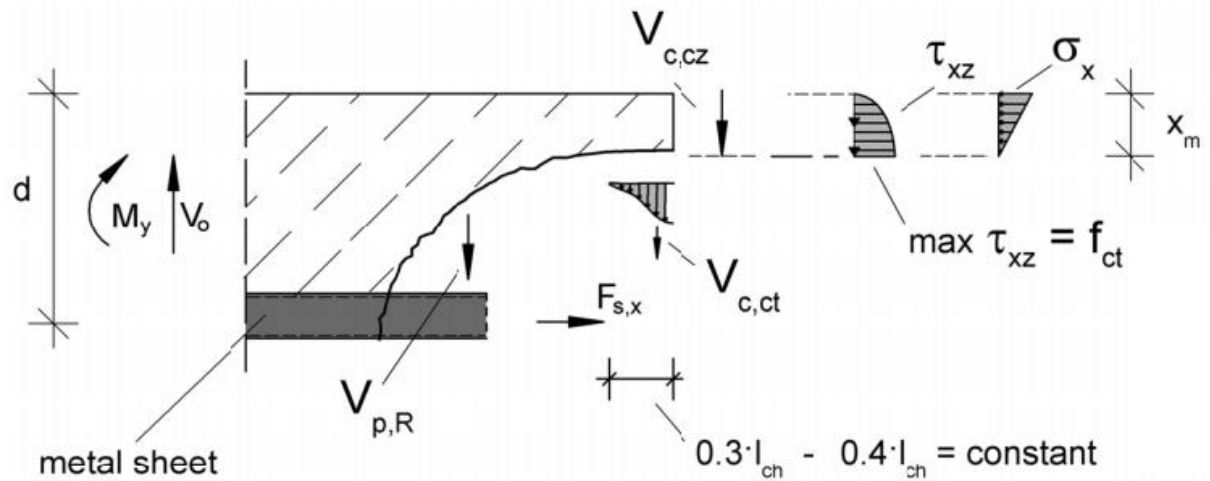


Figure 2.29 – Components that contribute to the transverse shear resistance of composite slabs according to Hartmeyer & Kurz[27]



Figure 2.30 – Buckling of the webs at the location of the inclined crack[27]

The height of the compression zone x_m depends on the composite action. The activated longitudinal shear stress at the interface determines the effective tensile force in the steel deck which is transferred into the concrete. Horizontal equilibrium of this tensile force ($\eta \cdot A_{pm} \cdot f_{ypm}$) and the compressive force in the concrete gives equation 2.14 to calculate x_m . The factor η has to be determined in accordance with Appendix B.3.6 of EN 1994-1-1[3] (see also the end of section 2.4). The height of the compressive zone x_m is calculated in the section of maximum moment (underneath the local line load) and can be used in equation 2.15 to calculate the contribution $V_{c,cz}$ to the total transverse shear resistance[27].

$$x_m = \frac{\eta \cdot A_{pm} \cdot f_{ypm}}{b_c \cdot f_{cm}} \quad 2.14$$

$$V_{c,cz} = \int_0^{x_m} \int_0^{b_c} \tau_{xz}(z) \cdot d_y \cdot d_z = \frac{2}{3} \cdot x_m \cdot b_c \cdot f_{ctm} \quad 2.15$$

With:

x_m	mean height of the compressive zone [mm];
$V_{c,cz}$	shear capacity of the uncracked compressive zone [N];
η	degree of shear connection according to partial shear method of EN 1994-1-1[3] [-];
f_{ypm}	yield strength steel deck [MPa]
A_{pm}	area of the steel deck [mm ²];
b_c	width of the concrete at the top [mm];
f_{cm}	mean cylindric compressive strength concrete [MPa];
f_{ctm}	mean tensile strength concrete [MPa].

For the effect of the aggregate interlock $V_{c,ct}$ an energetic approach was chosen by Hartmeyer & Kurz[27] based on investigations by Hillerborg, Mod er & Petersson (1976), and Walraven & Reinhart (1981) on the fracture process at the tip of the crack. Equation 2.16 can be used to calculate this contribution to the total transverse shear resistance of the composite slab. Since this part of the model is related to the tensile stresses at the crack tip, there is no need for description of the crack path[27].

$$V_{c,ct} = 0.12 \cdot l_{ch} \cdot b_c \cdot f_{ctm} = 0.12 \cdot \frac{G_f \cdot E_{cm}}{f_{ctm}^2} \cdot b_c \cdot f_{ctm} \quad 2.16$$

With:

$V_{c,ct}$	the local aggregate interlock [N];
l_{ch}	characteristic length of the crack [mm];
b_c	width of the concrete at the top [mm];
f_{ctm}	mean tensile strength of the concrete [MPa];
G_f	fracture energy: $G_f = 0.024 + 0.026 \cdot f_{ctm}$ (empirical relation as used in [27] for normal weight concrete) [N/mm];
E_{cm}	Young's modulus [MPa].

For the contribution of the steel deck $V_{p,R}$, Hartmeyer & Kurz[27] referred to information provided by the supplier of the steel decks. According to their model, the total mean transverse shear resistance $V_{t,Rm}$ of a composite slab is obtained by summing up the separate contributions as shown in equation 2.17. This method has been compared with experimental values and showed a good conformity[27]. To come to a design value, mean values have been converted to characteristic values and a safety factor has been added as shown in equation 2.18. The presented model is only valid for re-entrant composite slabs (with embossments) in combination with a safety factor of 1.35[27].

$$V_{t,Rm} = V_{p,Rm} + V_{c,cz} + V_{c,ct} = V_{p,Rm} + \left(\frac{2}{3} \cdot x_m + 0.12 \cdot \frac{G_f \cdot E_{cm}}{f_{ctm}^2} \right) \cdot b_c \cdot f_{ctm} \quad 2.17$$

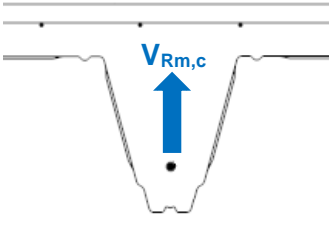
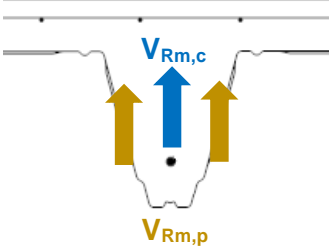
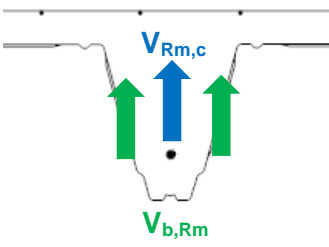
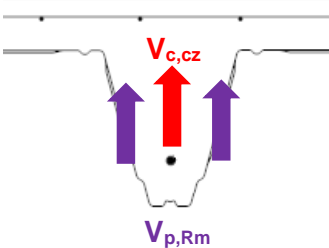
$$V_{t,Rd} = \frac{1}{\gamma_V} \cdot V_{t,Rk} = \frac{1}{1.35} \cdot \left(V_{p,Rk} + \left(\frac{2}{3} \cdot \frac{\eta \cdot A_p \cdot f_{ypk}}{b_c \cdot f_{ck}} + 0.12 \cdot \frac{G_f \cdot E_{cm}}{f_{ctk}^2} \right) \cdot b_c \cdot f_{ctk} \right) \quad 2.18$$

Trapezoidal profiles are generally manufactured with bigger heights of the webs, leading to larger transverse shear capacities[27]. Their bond capacities are usually worse than for re-entrant profiles, which makes that bigger crack widths may be expected at the time-moment of reaching the capacity of the steel deck[27]. It is therefore suggested by Hartmeyer & Kurz[27] that aggregate interlock shouldn't be considered for trapezoidal profiled composite slabs. They described a fundamental value for the transverse shear capacity $V_{t,0,Rm}$ in which the effect of the aggregate interlock is neglected (see equation 2.19). This value has been compared with tests on trapezoidal profiled composite slabs with lightweight concrete and showed a good correspondence[27]. For normal weight concrete, no comparison was made. In their paper it is proposed to put more effort in further investigation of the effect of additional rib reinforcement, as this should reduce the crack width and may activate the aggregate interlock for trapezoidal profiled composite slabs as well.

$$V_{t,0,Rm} = V_{p,Rm} + V_{c,cz} = V_{p,Rm} + \frac{2}{3} \cdot x_m \cdot b_c \cdot f_{ctm} \quad 2.19$$

As mentioned in the introductory part, this thesis focuses on the transverse shear capacity of deep composite slabs. Table 2.1 on the next page gives an overview of the different models that have been found in literature to calculate this capacity (mean values, $V_{t,Rm}$). A point of interest is how these models relate to the finite element results of this thesis, because the models aren't officially valid (Eurocode, $b_r/b_s > 0.6$) or derived (Stark[18]; Pereira et al.[17]; Hartmeyer & Kurz [27]) for deep composite slabs.

Table 2.1 – Overview of the different models to calculate the mean transverse shear capacity per rib

Eurocode 4 (refers to the procedure of Eurocode 2 as given below)		Parameters α = angle of web relative to the vertical axis b_0 = mean width concrete rib b_w = minimum width concrete rib in tensile area b_c = width of the composite slab at the top $C_{Rm,c}$ = empirical coefficient d = effective depth f_{bv} = shear strength steel considering buckling f_{cm} = mean compressive strength concrete f_{ctm} = mean tensile strength concrete f_y = yield strength steel h_l = height web, see Figure 2.24 h_w = height web, see Figure 2.24 k = size factor φ = angle of web relative to the horizontal axis ρ_l = reinforcement ratio t = thickness web x_m = height of compressive zone concrete
	<p><u>Transverse shear capacity composite slab:</u> $V_{t,Rm} = V_{Rm,c}$</p> <p><u>Partial resistance concrete section:</u> $V_{Rm,c} = \max \left(C_{Rm,c} k (100 \rho_l f_{cm})^{\frac{1}{3}} b_w d ; 0.035 k^{\frac{3}{2}} f_{cm}^{\frac{1}{2}} b_w d \right)$ $k \leq 2.0 ; \rho_l \leq 0.02$</p> <p><u>Partial resistance steel deck:</u> None</p>	
	<p><u>Transverse shear capacity composite slab:</u> $V_{t,Rm} = V_{Rm,c} + V_{Rm,p}$</p> <p><u>Partial resistance concrete section:</u> $V_{Rm,c} = \max \left(C_{Rm,c} k (100 \rho_l f_{cm})^{\frac{1}{3}} b_0 d ; 0.035 k^{\frac{3}{2}} f_{cm}^{\frac{1}{2}} b_0 d \right)$ $k \leq 2.0 ; \rho_l \leq 0.02$ Please notice the use of b_0 instead of b_w</p> <p><u>Partial resistance steel deck:</u> $V_{Rm,p} = 2 \cdot \cos(\alpha) \cdot h_l \cdot t \cdot \frac{f_y}{\sqrt{3}}$</p>	
	<p><u>Transverse shear capacity composite slab:</u> $V_{t,Rm} = V_{Rm,c} + V_{b,Rm}$</p> <p><u>Partial resistance concrete section:</u> $V_{Rm,c} = \max \left(C_{Rm,c} k (100 \rho_l f_{cm})^{\frac{1}{3}} b_0 d ; 0.035 k^{\frac{3}{2}} f_{cm}^{\frac{1}{2}} b_0 d \right)$ $k \leq 2.0 ; \rho_l \leq 0.02$ Please notice the use of b_0 instead of b_w</p> <p><u>Partial resistance steel deck:</u> $V_{b,Rm} = 2 \cdot \frac{h_w}{\sin(\varphi)} \cdot t \cdot f_{bv}$</p>	
	<p><u>Transverse shear capacity composite slab:</u> $V_{t,Rm} = V_{c,cz} + V_{p,Rm}$</p> <p><u>Partial resistance concrete section:</u> $V_{c,cz} = \frac{2}{3} \cdot x_m \cdot b_c \cdot f_{ctm}$</p> <p><u>Partial resistance steel deck:</u> $V_{p,Rm}$ is the transverse shear capacity of the steel deck as provided by the supplier</p>	

3. FINITE ELEMENT ANALYSIS

In this chapter the results of the Finite Element Analysis (FEA) of ComFlor 210 will be discussed. It has been chosen to analyse this type of composite slab, since most of the found research on deep composite slabs was also conducted to ComFlor 210 (Van Erp[16], Abspoel et al.[21]). It has been tried to quantitatively determine its transverse shear capacity with the finite element software Diana[14]. The FEA is started by merely modelling the concrete section of ComFlor 210 (neglecting the steel deck at the bottom), after which the total composite slab will be analysed to show the influence of the steel deck on the transverse shear capacity.

3.1. Geometry and loading conditions

To give the most accurate prediction of the transverse shear capacity, it is obvious that the FEA should be in 3D. In the Eurocode 4, no specific test method is given to determine the transverse shear capacity of a composite slab. Procedures for determination of the longitudinal shear capacity are well described though. As explained in section 2.4, with both the *m-k* method and partial shear method, four-point bending tests have to be carried out. It has been chosen to also simulate a four-point bending test for determination of the transverse shear capacity of ComFlor 210. This is shown in Figure 3.1. The corresponding distributions of transverse shear force and bending moment are also provided in this figure. The loading conditions make that the transverse shear force is constant over the shear span L_s and equal to the applied load V_t (i.e. line load integrated over its width). Therefore, when transverse shear failure occurs, it can be established that the transverse shear capacity of the slab is directly equal to the applied load V_t . Furthermore, the bending moment is constant between the loading points and its maximum value is only dependent on V_t and L_s (so not the span L). The part of the span between these loading points is called the region of constant bending moment.

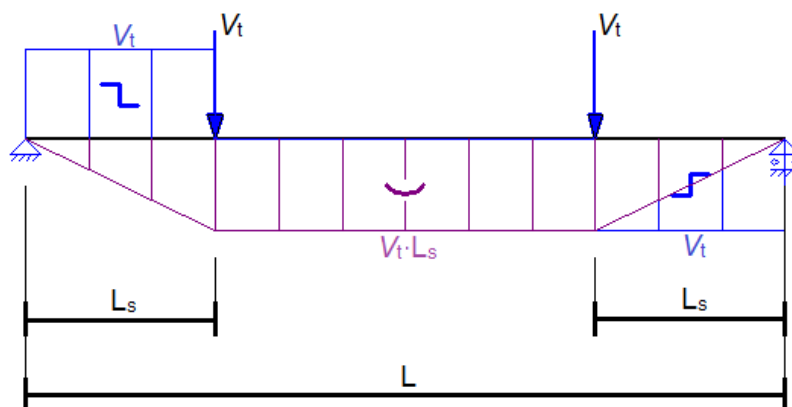


Figure 3.1 – Four-point bending test with corresponding bending moment and transverse shear force distribution

The setup for the finite element model is given in Figure 3.2 (side view). Due to symmetry around mid-span of the four-point bending test, only half of the span needs to be modelled. Proper boundary conditions are applied on the left side to account for this symmetry. As also shown in the figure, it has been chosen to model a steel support plate (80 mm x 56 mm x 20 mm) at the right lower side. With

this, it is tried to prevent compressive failure at the support due to the concentrated stresses in vertical direction, especially since the width of the support is relatively small (56 mm). Furthermore, the span L is chosen to be equal to 2000 mm with an overhang length L_o of 355 mm (see Appendix B for calculation). Both values are kept constant throughout the whole FEA. A span of 2000 mm is off course rarely applied in practice for deep composite slabs, but choosing a bigger span will unnecessarily increase the computation time of the FEA.

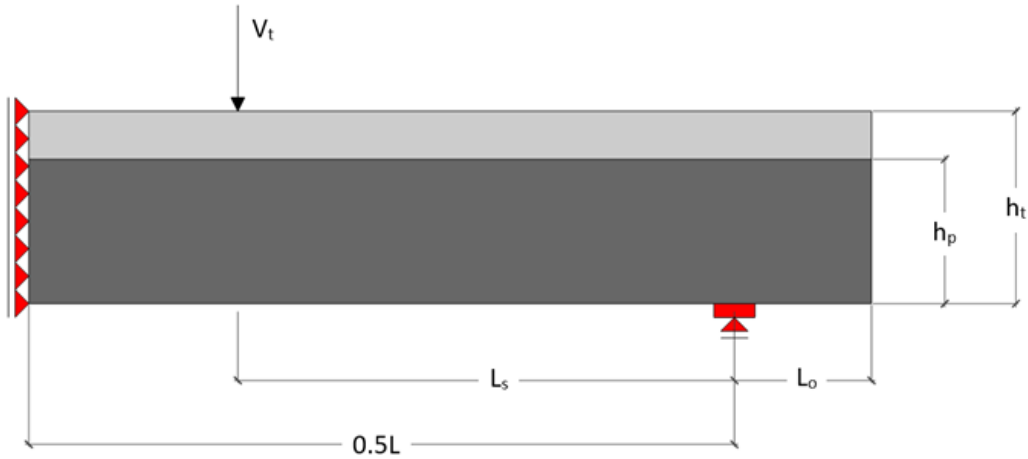


Figure 3.2 – Test setup of the FEA (side view)

FEA results are usually compared to real-life test results for sake of verification of the model. However, clear measurements of the transverse shear capacity of ComFlor 210 haven't been found. The research of Abspoel et al.[21] has been the only one in which some conclusions were made about the transverse shear capacity of ComFlor 210 based on real test values. In their research, a maximum transverse shear force of 147.18 kN was measured for which the ComFlor 210 still failed due to the hogging bending moment (concrete in tension, steel in compression). This indirectly implies that the transverse shear capacity of the specimen was even bigger than this measured 147.18 kN. Since this is the only test value of ComFlor 210 that could be found, it has been decided to start the FEA by analysing the same cross-section as in the research of Abspoel et al.[21].

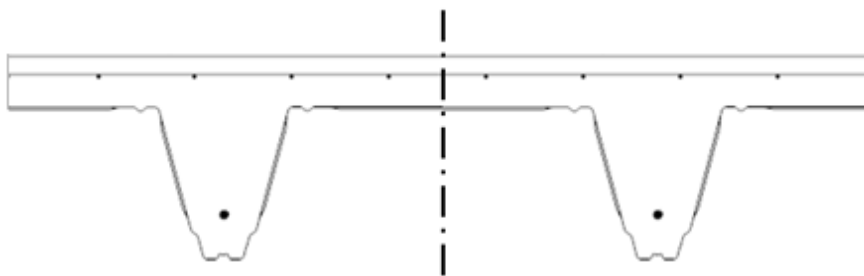
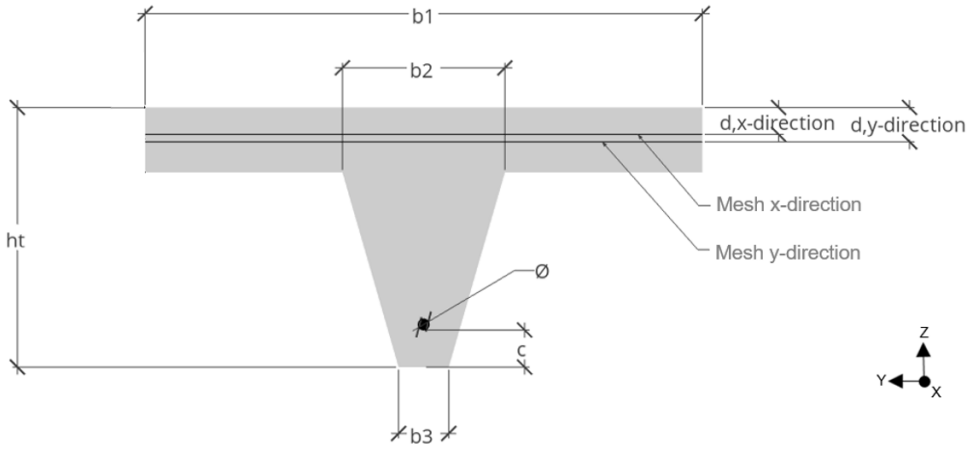
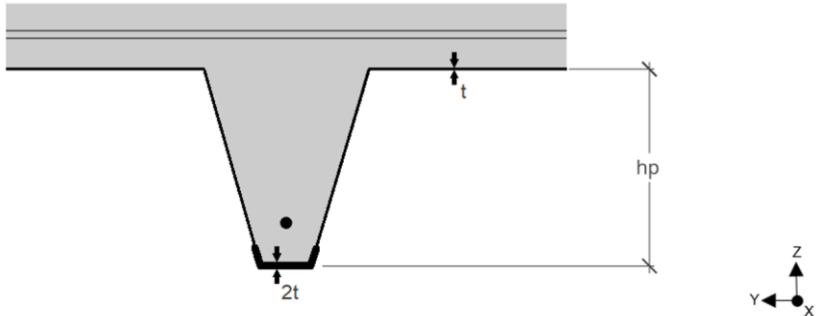


Figure 3.3 – Symmetry of cross-section with two ribs (ComFlor 210)[32]

In the research of Abspoel et al.[21], the tested ComFlor 210 contained two complete ribs. Due to the symmetry of two ribs around their middle (Figure 3.3), only one of them needs to be modelled. This makes that in total, due to double symmetry of the composite slab, only one quarter has been implemented in the FEA. Table 3.1 shows a very schematic representation of dimensions of ComFlor 210 (for one rib). The steel deck is drawn with straight parts for sake of simplicity. A distinction is made between the two types of analyses that will be executed in this thesis. First, only the concrete section of ComFlor 210 is analysed, so neglecting the steel deck at the bottom (but including all other reinforcement). This is shown in the upper image of Table 3.1. Then, the steel deck is added to the model, to investigate its influence on the transverse shear capacity of ComFlor 210. This is shown in

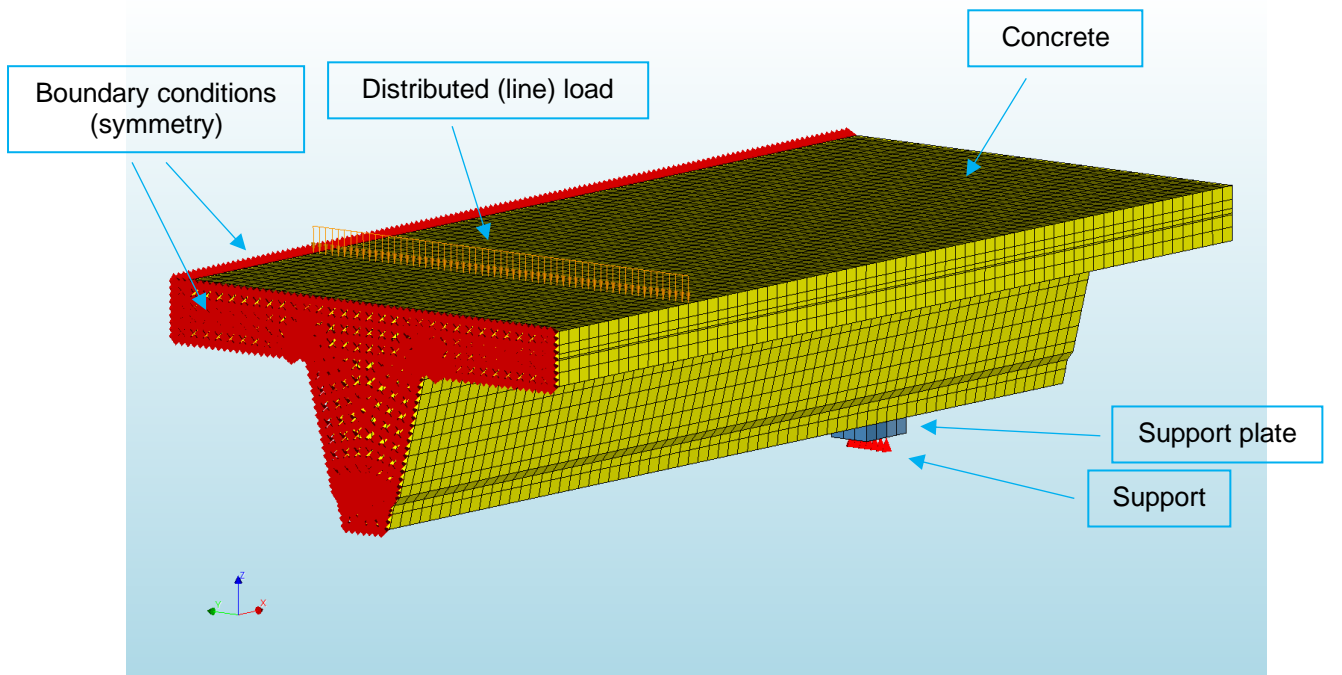
the lower image. As mentioned, all given dimensions are taken from the research of Abspoel et al.[21]. When any of these dimensions are changed in the FEA, it will be specifically mentioned. In the top layer of the slab, a reinforcement mesh and additional reinforcement are present. These additional rebars and the part of the mesh that reinforces in longitudinal direction, are simply assigned to the plane “mesh x-direction”. The part of the mesh that reinforces in the other direction is assigned to the plane “mesh y-direction”. The inclusion of these additional rebars in the top layer is the direct result of trying to analyse the same cross-section as in the research of Abspoel et al.[21].

Table 3.1 – Schematic representation of the dimensions for the two types of FEA’s (one rib)

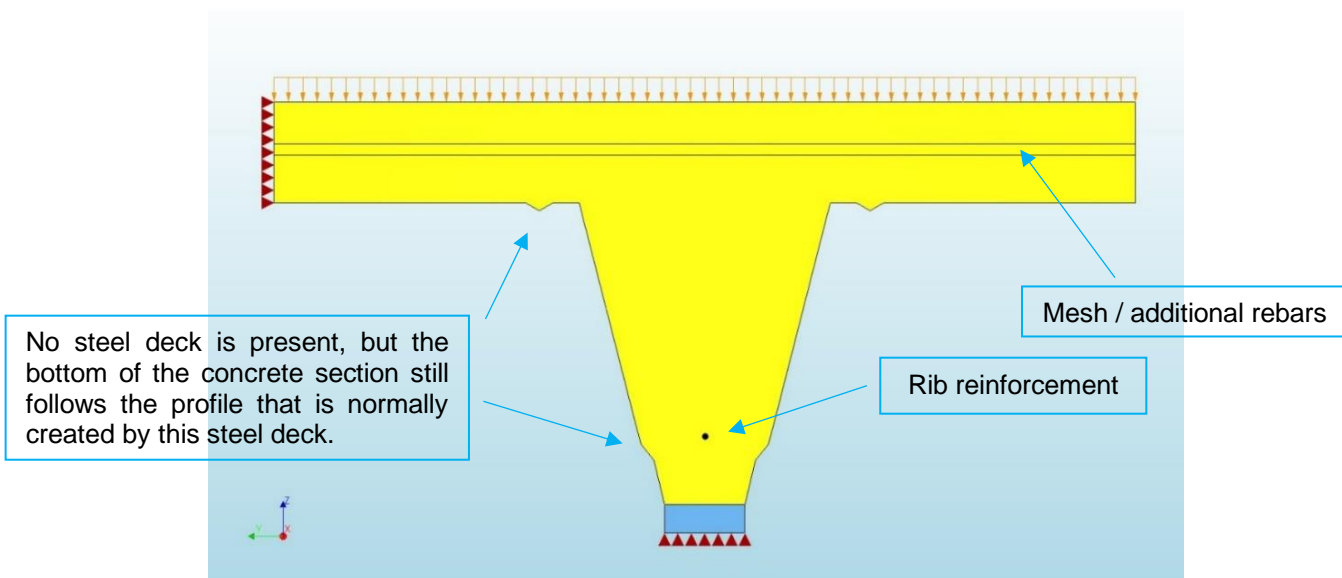
 <p style="text-align: center;"><u>FEA concrete section of ComFlor 210 (steel deck not included)</u></p>			
 <p style="text-align: center;"><u>FEA ComFlor 210</u> i.e. concrete section + steel deck</p>			
b1	600 mm	c	40 mm
b2	175 mm	t	0.96 mm (i.e. 1 mm excl. coatings)
b3	56 mm	Mesh x-direction	Ø8-150 + Ø12-150 (mm)
h_t	280 mm	Mesh y-direction	Ø8-150 (mm)
h_p	210 mm	d_{x-direction}	29 mm
Ø	12 mm	d_{y-direction}	37 mm

3.2. FEA concrete section of ComFlor 210

Although the main goal of the FEA is to determine the transverse shear capacity of ComFlor 210, the first point of interest is to validate this capacity for merely the concrete part of the composite slab. According to the Eurocode 4, the transverse shear capacity of a composite slab is only determined by its concrete part. The potential additional resistance provided by the steel deck is not considered. Therefore, determining the transverse shear capacity of the concrete section of ComFlor 210, actually equals the same procedure that is followed by the Eurocode 4 for calculation of the total transverse shear resistance of the composite slab. Figure 3.4 gives an overview of the finite element model for the analysis. Solid elements with quadratic interpolation have been used for the concrete and the support plate. All reinforcement has been modelled with embedded elements. The general dimensions of the cross-section are just as given in Table 3.1 (upper image).



a) 3D view



b) Front view (mesh not visible)

Figure 3.4 – Finite element model concrete section

3.2.1. Material properties

Table 3.2 gives an overview of the material properties for the FEA of the concrete section. The strength values are taken from the research of Abspoel et al.[21]. Figure 3.5, Figure 3.6 and Figure 3.7 are provided in addition to clarify some of the mentioned terms in Table 3.2. For the tensile diagram of Hordijk, the area underneath this graph is equal to G_f/h i.e. the fracture energy divided by the crack bandwidth. The crack bandwidth h is used to calculate the crack width from the crack strain ($w = \epsilon * h$). It defines over what length the crack width w is smeared out. As also mentioned in Table 3.2, it has been chosen to use a rotating crack model. This means that the orientation of a crack within an element is always perpendicular to the tensile principal direction, so that no shear stress is present along this crack. Any change in principal direction, due to redistribution of stresses for instance, leads to rotation of the crack. This is shown in Figure 3.6. It may be clear that rotation of an existing crack sounds somewhat unphysical. However, the big advantage of this rotating crack model is that there is no need for specifying relationships for shearing along the crack.

Table 3.2 – Material properties FEA concrete section (as specified in DIANA[14])

Concrete	
Mean compressive strength (f_c)	41.8 MPa
Compressive curve	Thorenfeldt (Figure 3.5)
Mean tensile strength (f_t)	3.1 MPa
Tensile curve	Hordijk (Figure 3.5)
Mode-I tensile fracture energy (G_f)	0.1046 N/mm
Young's modulus (E_c)	33789 MPa
Poisson's ratio (ν)	0.2
Crack model	Rotating (Figure 3.6)
Rib reinforcement and mesh	
Shape of diagram	Bilinear (Figure 3.7)
Yield strength (f_y)	536 MPa ($\epsilon_y = 2.68 \cdot 10^{-3}$)
Ultimate strength (f_u)	574 MPa ($\epsilon_u = 5 \cdot 10^{-2}$)
Young's modulus (E_s)	200000 MPa
Support plate	
Young's modulus (E_s)	210000 MPa
Poisson's ratio (ν)	0.3

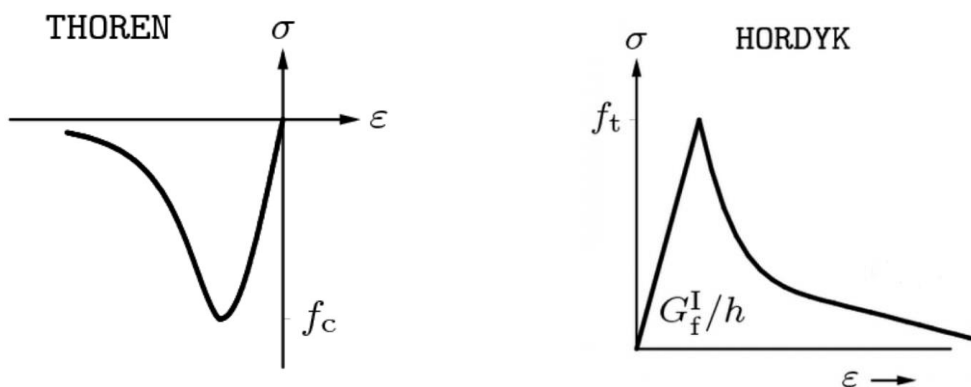
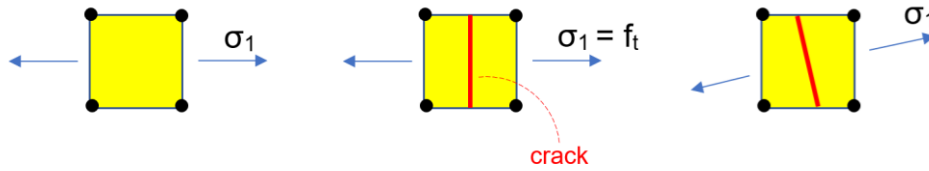


Figure 3.5 – Compressive (left) and tensile (right) behaviour of concrete in the FEA[14]



A crack develops in an element by exceeding the tensile strength of the material in the principal direction;
 When this principal direction rotates, the crack rotates too;
 No shearing occurs along the crack.

Figure 3.6 – Rotating crack model

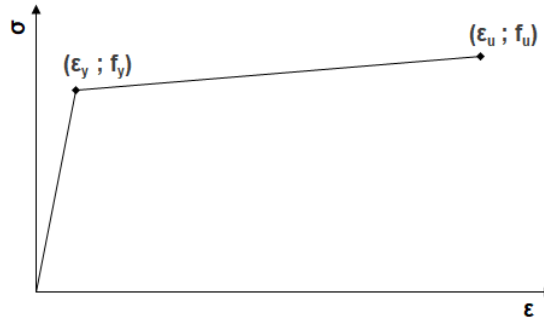


Figure 3.7 – Bilinear stress-strain diagram for steel

3.2.2. Analysis procedure

As discussed in section 2.3, transverse shear failure may become the governing failure mode for short shear spans. It has been explained that, when assuming an equal transverse shear capacity over the full span of the slab, reduction of the shear span will lead to transverse shear failure. However, as also described by the Eurocode 2, more of the applied load is directly transferred to the support when the shear span becomes smaller. To reduce this effect of direct load transfer and accurately measure the transverse shear capacity, the shear span L_s should be bigger than a certain limit value. In the Eurocode 2, the effect of direct load transfer is considered as follows: when the shear slenderness ratio (a_v/d) is smaller than 2.0, the measured shear force V_t should be multiplied with $\beta = a_v/(2d)$. This reduction takes into account the effect of direct load transfer. The distance a_v is taken as the horizontal distance between the applied load and the edge of the support plate, in accordance with clause 6.2.2 of EN 1992-1-1 [24] (see Figure 3.8). In this thesis, a_v is related to the shear span L_s in the following way: $L_s = a_v + 40 \text{ mm}$.

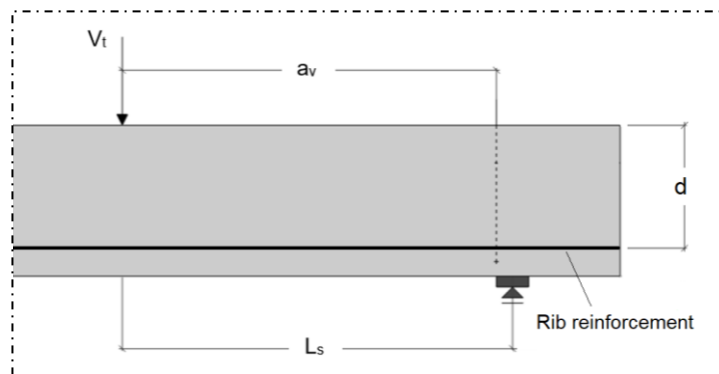


Figure 3.8 – Definition of different parameters

However, Rombach & Henz [29] concluded in their research that direct load transfer is still possible up to shear slenderness ratios of 3.0. This is based on test results of concrete slabs without shear

reinforcement (stirrups). For that reason, it has been chosen to start the FEA with a shear slenderness ratio of 3.0. When transverse shear failure doesn't occur, the shear span L_s (and so the shear slenderness ratio a_v/d) is further reduced. With this, it is expected that either transverse shear failure occurs, or that the effect of direct load transfer becomes decisive and makes that bending failure is the governing mode for every shear slenderness ratio.

Because of the non-linear material properties that have been assigned to the concrete, a non-linear analysis is required as well to solve the problem. The load is applied in a force-controlled incremental way, in combination with the so-called arc-length method to overcome convergence problems due to softening behaviour of the concrete (cracking). This is illustrated in Figure 3.9. To overcome a limit point in a regular force-controlled process, negative load steps should be specified after this limit point to find convergence. This means that the location of the limit point should be known a priori, which is generally not the case. By using the arc-length method, this problem is solved because the method doesn't have difficulties with finding convergence after limit points (during softening, see Figure 3.9). Regarding the iteration process within every load step, regular Newton-Raphson method has been used. This method is shown in Figure 3.10. With this method, the stiffness is adapted every iteration to find convergence of a certain load step. Convergence is found when both energy and displacement norms are satisfied with a tolerance of 0.005 and 0.05 respectively. When convergence isn't found after 30 iterations, the analysis moves on with the next load step instead of stopping the analysis. This is because quite often, when the cracking process in the concrete is somewhat unstable, the analysis can't find convergence for these specific load steps. This can lead to a consecutive series of non-converging load steps as also shown in Figure 3.11 (red bars). Off course, the range of this series shouldn't be too big (like a maximum of 3 load steps as shown in the figure) and it should also not happen over the whole analysis. When this occurs, the size of the load step should be reduced. Post-processing of the results regarding this non-convergence is very important to check whether the FEA results are still reliable. In the FEA, only physical non-linearity has been considered.

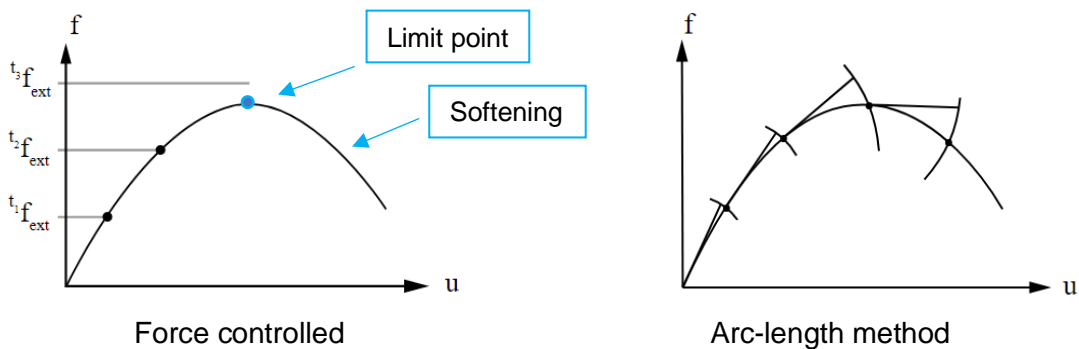


Figure 3.9 – Incremental loading[14]

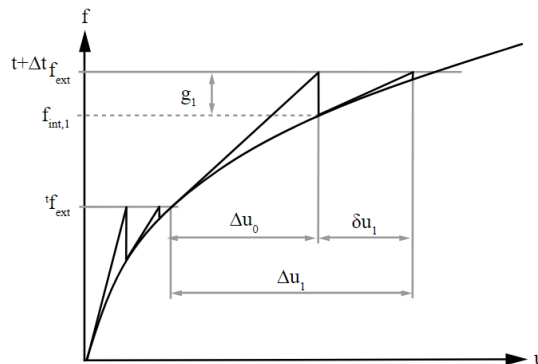


Figure 3.10 – Iterative process: Regular Newton-Raphson method[14]

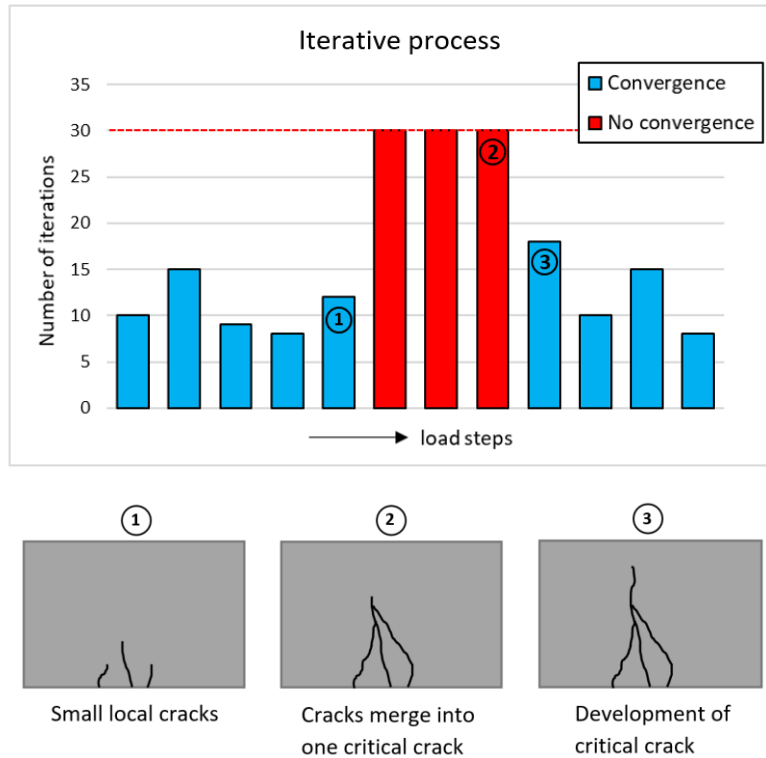


Figure 3.11 – Convergence of the FEA with respect to crack development in concrete

3.2.3. Results and discussion

Figure 3.12 shows the load-displacement curves of the FEA for 4 different shear slenderness ratios a_v/d . The shear slenderness ratio defines at which distance the force V_t is located from the support. For instance, a shear slenderness ratio of 2 means that the distance between the load and the edge of the support plate (a_v) is 2 times the effective depth of the slab (d). For the ratios 2.50 and 1.54, the ultimate load-carrying capacity wasn't reached, because too few load steps had been specified in the FEA (values written in red in Figure 3.12). Still, it can be concluded that bending failure was the governing mode for every analysis. Quite ductile behaviour has been observed, which occurred due to yielding of the rib reinforcement at the locations of these vertically oriented bending cracks. This is shown in Figure 3.13. Inclined cracking is also clearly visible, but opening of the vertically oriented cracks at the left from the applied load (region of constant bending moment) caused failure in every simulation. In Table 3.3, the bending moment capacity of the concrete section has been derived from two different analyses. Both values show good conformity when being compared. It can be seen in Figure 3.12 that the failure load increases when the shear slenderness ratio is reduced: when the load is close to the support, more load is needed to reach the bending moment capacity.

Table 3.3 – Derivation of bending moment capacity from FEA results

Shear slenderness ratio a_v/d	2.99	2.05
Ultimate load V_t	23.65 kN	33.28 kN
Effective depth d	$280 - 40 - 6 = 234$ mm	$280 - 40 - 6 = 234$ mm
a_v (see Figure 3.8)	$2.99 \cdot 234 = 700$ mm	$2.05 \cdot 234 = 480$ mm
Shear span $L_s (= a_v + 40$ mm)	$700 + 40 = 740$ mm	$480 + 40 = 520$ mm
Bending moment capacity M_R	$23.65 \cdot 0.740 = 17.50$ kNm	$33.28 \cdot 0.520 = 17.30$ kNm

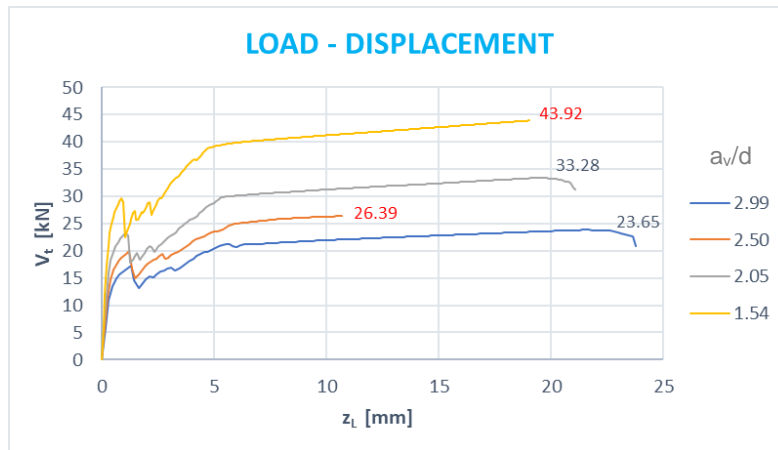


Figure 3.12 – Load-displacement curves FEA concrete section for different shear slenderness ratios

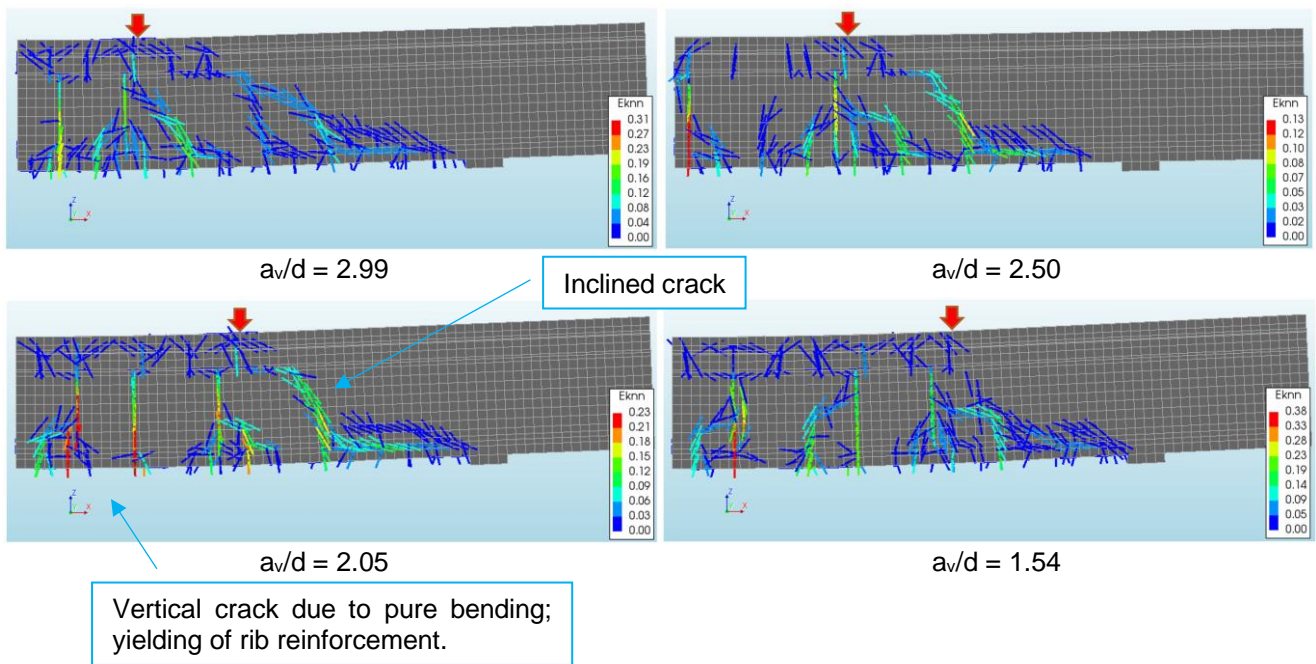


Figure 3.13 – Crack strain plots at failure for FEA concrete section

Since bending failure occurred in all previous analyses, it has been chosen to adjust the cross-section by doubling the diameter of the rib reinforcement. The rib reinforcement now has a diameter of 24 mm instead of 12 mm. It is expected that this will mainly increase the bending moment capacity of the concrete section, so that transverse shear failure may become governing. Keep in mind that a rib reinforcement diameter of 24 mm may be rarely seen in practice, but it is not too unrealistic for experimental purposes. The increased rib reinforcement diameter leads to a reduced concrete cover c at the bottom (34 mm instead of 40). All other dimensions and parameters are kept the same as described before in Table 3.1.

Failure of the finite element model has been simulated for shear slenderness ratios 3.50, 2.99, 2.50 and 2.05. Figure 3.14 shows the load-displacement curves of the analyses. Figure 3.15 shows the corresponding cracking patterns at failure. It is clearly visible that the concrete section failed in transverse shear for every shear slenderness ratio. The cracking patterns match with what is known as “flexural shear failure” [28]. In short, this failure mode is characterized by the formation of bending cracks within the shear span, which start to curve towards the loading point under influence of the transverse shear force. Opening of these inclined cracks within the shear span led to total failure of the concrete element.

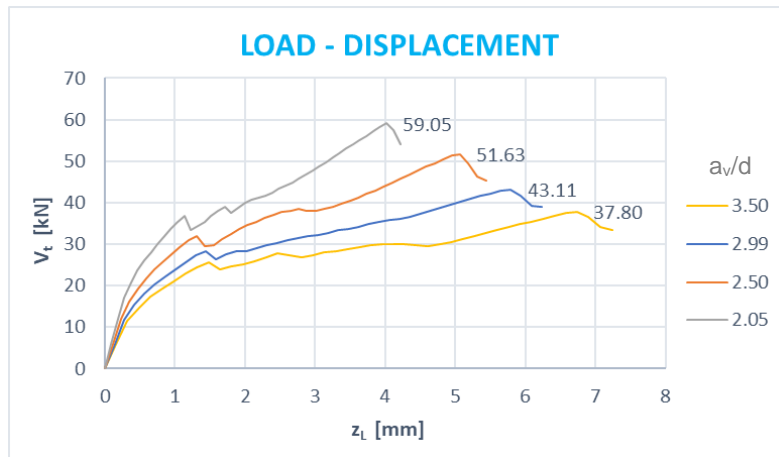


Figure 3.14 – Load-displacement curves FEA concrete section for different shear slenderness ratios (rib reinforcement: Ø24 mm instead of Ø12 mm)

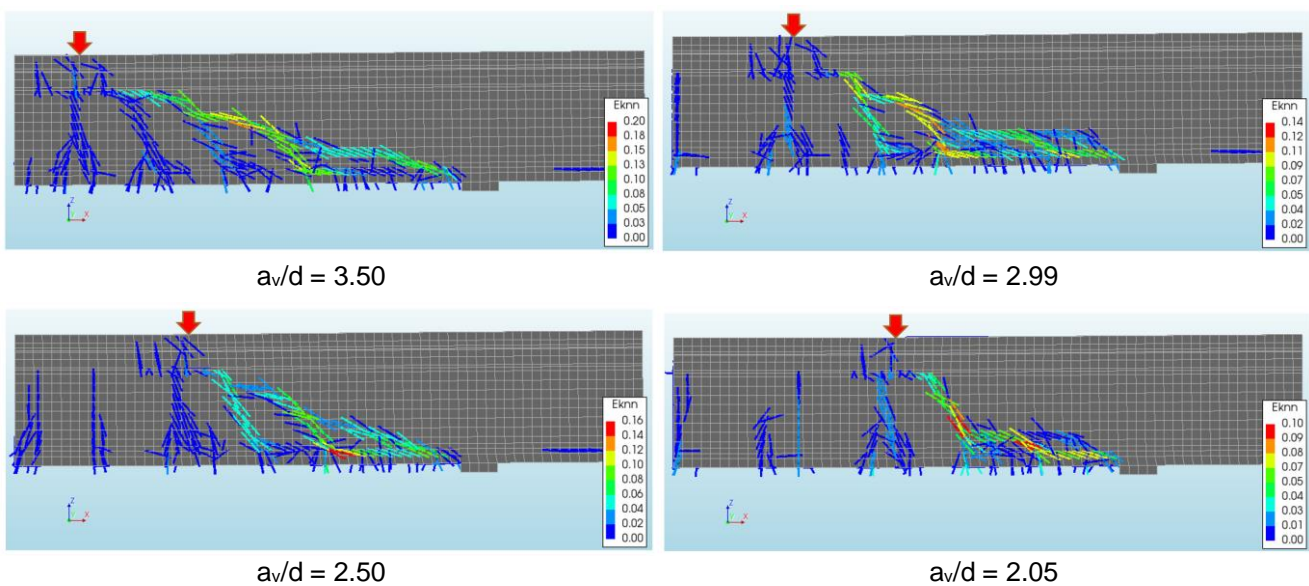


Figure 3.15 – Crack strain plots at failure for FEA concrete section (rib reinforcement: Ø24 mm instead of Ø12 mm)

From the load-displacement curves in Figure 3.14 it may be established that the failure load increases when the shear slenderness ratio is reduced. This is the result of direct load transfer to the support and can be explained on basis of the following. Figure 3.16 shows the crack formation in the concrete element for the FEA analysis with shear slenderness ratio $a_v/d = 2.50$. Different snapshots are given, marked with corresponding dots in the load-displacement curve. Starting from the beginning of the analysis, it may be established that the load keeps increasing until the first major crack arises in the concrete. This occasion is marked with a green dot (1) and leads to a setback in the load-displacement graph. The crack is located in the section underneath the loading point. What follows next is a clear reduction in overall stiffness as a result of the proceeding crack formation. At the occasion corresponding to the yellow dot (2), the most right inclined crack start to arise. This crack has been fully developed at the moment of the orange dot (3), after which horizontal cracking starts to occur along the rib reinforcement (dowel cracking[28]). Although it may be expected that this horizontal cracking initiates total failure of the concrete section, still significant more load is needed to cause this. The difference between the starting of this dowel cracking and reaching the failure load is more than 10 kN. This additional load-carrying capacity is provided by the sort of arch-like structure[28] that arises in the concrete section after crack formation.

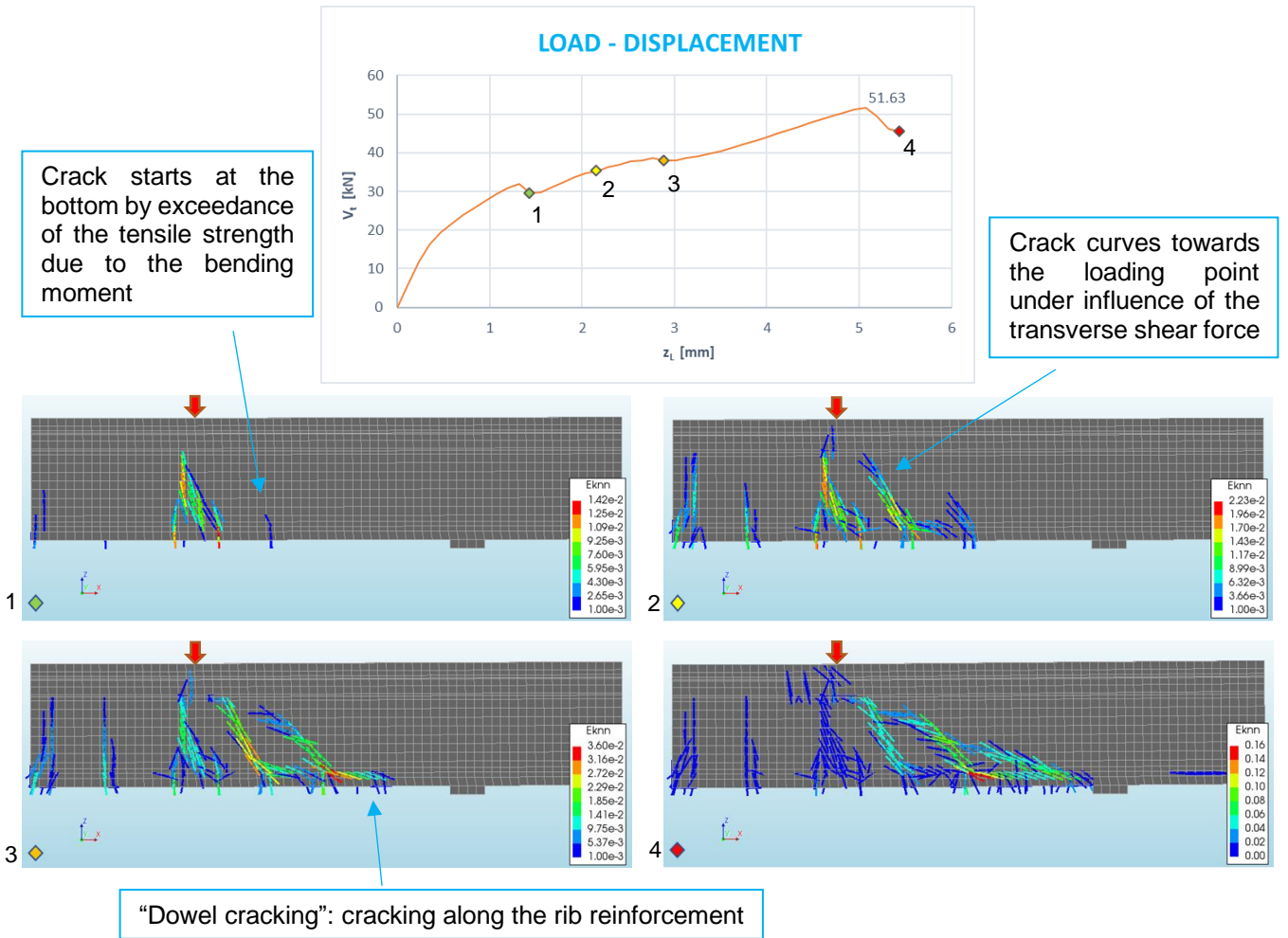


Figure 3.16 – Flexural shear failure of the concrete section (FEA $a_v/d = 2.50$; $\varnothing 24$ mm)

The functioning of this arch structure is illustrated in Figure 3.17. It shows that even after full crack formation, the load P can still be carried by the diagonally oriented compressive struts, for which the reinforcement acts as a tensile chord [28]. For high shear slenderness ratios, formation of the critical inclined crack often leads to total failure of the reinforced concrete member, because the arch structure isn't able to carry the load [28]. When the shear slenderness ratio is reduced, it generally holds that the capacity of the arch structure is improved due to the bigger inclination of the compressive strut with respect to the longitudinal axis (because the load is closer to the support). Due to the bigger inclination of the strut, more compressive load is taken by this strut for the same load P . This can even give a different kind of transverse shear failure mode, namely “shear compression failure” [28]. This failure mode is characterized by compressive failure of the diagonal strut (i.e. splitting cracks). This haven't been observed in any analysis of this thesis.

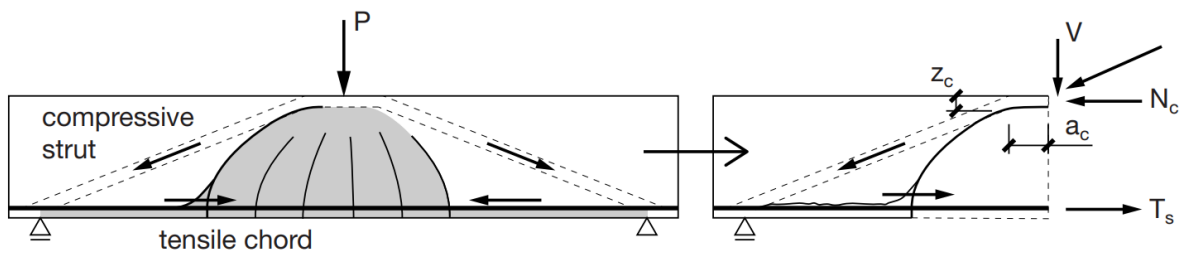


Figure 3.17 – Arch-like structure in reinforced concrete members [28]

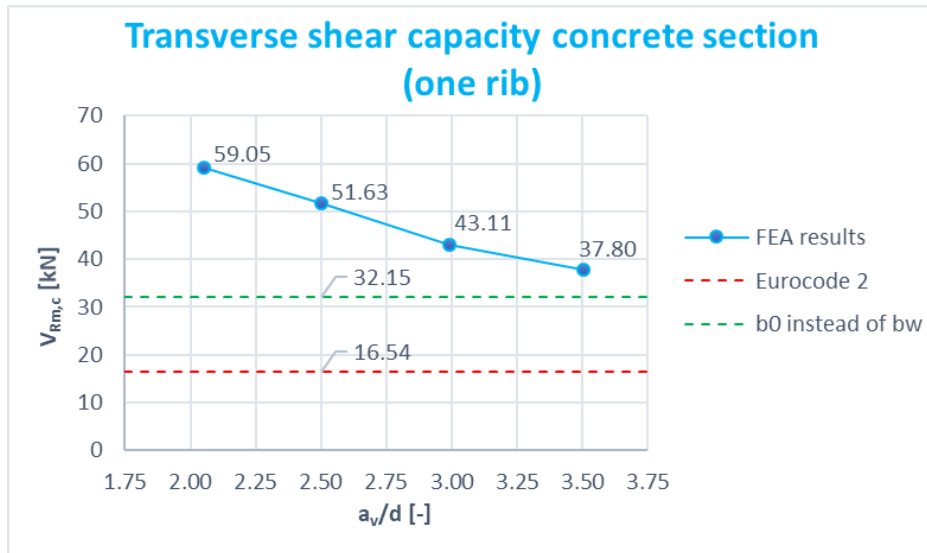


Figure 3.18 – Comparison of FEA results with calculated resistances (rib reinforcement: Ø24 mm instead of Ø12 mm)

Figure 3.18 shows the transverse shear capacity $V_{Rm,c}$ of the concrete section for every shear slenderness ratio that has been analysed. This picture clearly shows the dependency of $V_{Rm,c}$ on the shear slenderness ratio a_v/d . A difference of 21.25 kN in capacity can be found between the two ultimate shear slenderness ratios (3.50 and 2.05). The FEA shows that even for shear slenderness ratios bigger than 3.0, direct transfer of the load to the support is still possible. For shear slenderness ratio 3.50, a 12.3% lower capacity has been found compared to that of 2.99. Looking at Figure 3.18, it seems that an exponential curve could be drawn through the results of the FEA. Assuming that this is true, it can be established that for big shear slenderness ratios, the transverse shear capacity approaches a constant value (asymptote) that excludes any effect of direct load transfer.

The transverse shear capacity according to the Eurocode 2 is also given in Figure 3.18. The calculation procedure according to this standard is provided in the first row of Table 2.1 at the end of chapter 3. A factor $C_{Rm,c}$ of 0.15[28] has been used to calculate the mean transverse shear capacity $V_{Rm,c}$ of the concrete section. The calculation is shown below.

$$k = \min\left(1 + \sqrt{\frac{200}{d}}; 2.0\right) = \min\left(1 + \sqrt{\frac{200}{234}}; 2.0\right) = \min(1.925; 2.0) = 1.925$$

$$\rho_l = \min\left(\frac{A_{sl}}{b_w \cdot d}; 0.02\right) = \min\left(\frac{0.25 \cdot \pi \cdot (24)^2}{56 \cdot 234}; 0.02\right) = \min(0.0345; 0.02) = 0.02$$

$$V_{Rm,c} = \max\left(C_{Rm,c} k (100 \rho_l f_{cm})^{\frac{1}{3}} b_w d; 0.035 k^{\frac{3}{2}} f_{cm}^{\frac{1}{2}} b_w d\right)$$

$$= \max\left(0.15 \cdot 1.925 \cdot (100 \cdot 0.02 \cdot 41.8)^{\frac{1}{3}} \cdot 56 \cdot 234; 0.035 \cdot 1.925^{\frac{3}{2}} \cdot 41.8^{\frac{1}{2}} \cdot 56 \cdot 234\right)$$

$$= \max(16540; 7917)$$

$$= 16540 \text{ N} = 16.54 \text{ kN}$$

The calculated capacity according to the Eurocode 2 is quite conservative. The lowest transverse shear capacity that has been found in the FEA is equal to 37.80 kN and this is still 2 times bigger than the calculated resistance of 16.54 kN. According to the Eurocode 2, it is only allowed to use the smallest width in the tensile area b_w (56 mm) for calculation of $V_{Rm,c}$. However, the concrete cross-section has a great varying width over its height as also illustrated in Table 3.1: starting at 56 mm at the bottom (b3),

175 mm at top of the tapered rib (b_2) and finally a width of 600 mm at the top (b_1). It is suggested to replace this parameter b_w in calculation by the mean width of the concrete rib b_0 , as also proposed by Stark[18] and Pereira et al.[17]. For calculation of this parameter b_0 , it is assumed that the concrete rib smoothly transits from 56 mm at the bottom to 175 mm at the top. With this, the mean width of the rib is simply calculated as $(175+56)/2 = 115.5$ mm. This b_0 is located at mid-height of the steel deck (i.e. $0.5 \cdot h_p = 0.5 \cdot 210 = 105$ mm). This is illustrated in Figure 3.19.

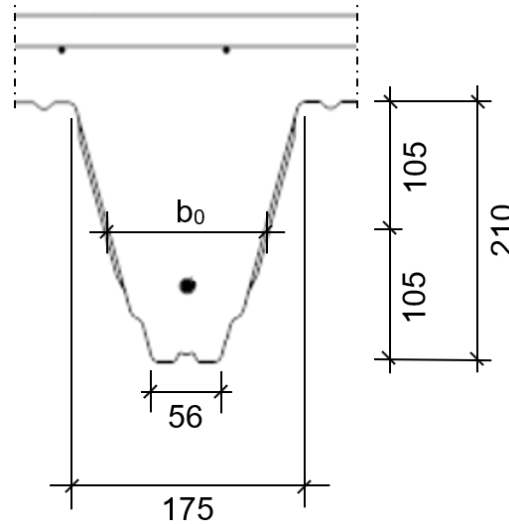


Figure 3.19 – Mean width of the concrete rib b_0 (ComFlor 210)

Replacing b_w by b_0 makes that the transverse capacity $V_{Rm,c}$ is calculated as follows:

$$k = 1.925 \text{ (not affected)}$$

$$\rho_l = \min\left(\frac{A_{sl}}{b_0 \cdot d}; 0.02\right) = \min\left(\frac{0.25 \cdot \pi \cdot (24)^2}{115.5 \cdot 234}; 0.02\right) = \min(0.0167; 0.02) = 0.0167$$

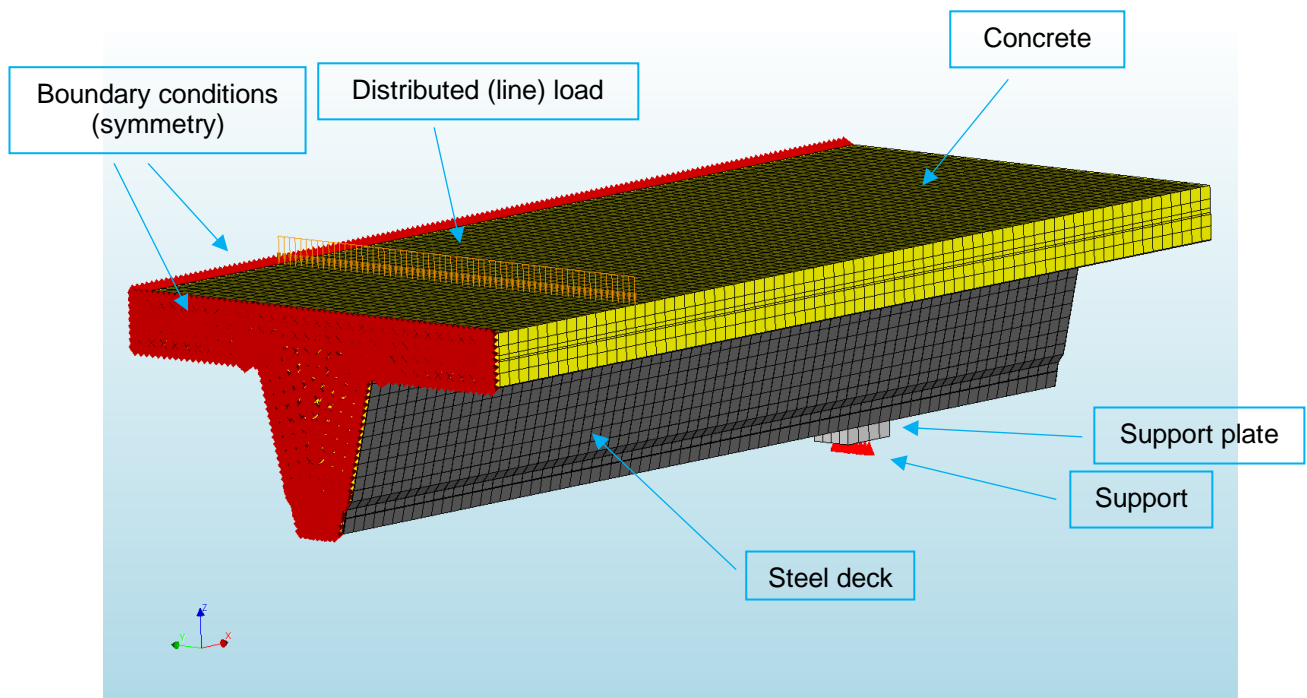
$$\begin{aligned} V_{Rm,c} &= \max\left(C_{Rm,c} k (100 \rho_l f_{cm})^{\frac{1}{3}} b_0 d; 0.035 k^{\frac{3}{2}} f_{cm}^{\frac{1}{2}} b_0 d\right) \\ &= \max\left(0.15 \cdot 1.925 \cdot (100 \cdot 0.0167 \cdot 41.8)^{\frac{1}{3}} \cdot 115.5 \cdot 234; 0.035 \cdot 1.925^{\frac{3}{2}} \cdot 41.8^{\frac{1}{2}} \cdot 115.5 \cdot 234\right) \\ &= \max(32149; 16328) \\ &= 32149 \text{ N} = 32.15 \text{ kN} \end{aligned}$$

This value approaches the lowest found resistance of 37.80 kN much more closely, and therefore supports the proposal to use b_0 instead of b_w in the Eurocode's formula (as shown above). The improvement of this adjusted calculation is also clearly visible in Figure 3.18. The calculated transverse shear capacity of 32.15 kN seems to provide a reasonable asymptote to the FEA results of this thesis.

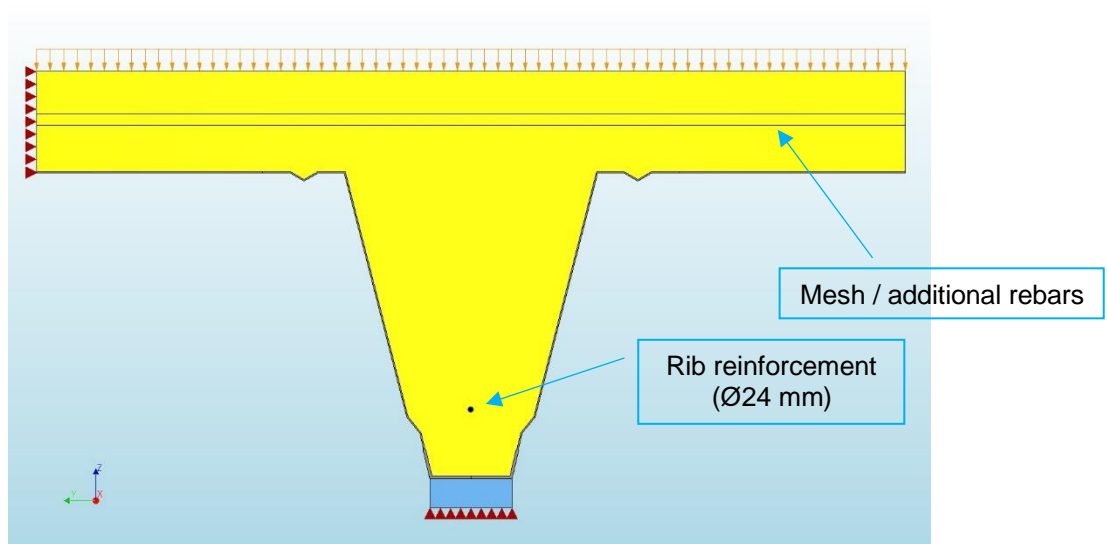
3.3. FEA ComFlor 210

After verification of the transverse shear capacity of the concrete section, this thesis will now focus on the influence of the steel deck on this capacity. On basis of the literature review it may be expected that the steel deck will give a significant improvement of the transverse shear capacity. A FEA of ComFlor 210 has been executed to investigate this expectation. Figure 3.20 gives an overview of the finite element model. Information about the geometry and loading conditions has already been provided in section 3.1. With respect to the dimensions given in Table 3.1, please be aware that the rib reinforcement in the finite element model contains a diameter \varnothing of 24 mm instead of 12 mm (all other

dimensions are still the same). This has been applied to be consistent with the last FEA of the concrete section, so that comparison of the results is possible. A consequence of this decision is that the analysed cross-section of ComFlor 210 isn't completely in accordance with the research of Abspoel et al.[21], which was initially suggested. Solid elements with quadratic interpolation have been used for the concrete, steel deck and support plate. For the steel deck, at least 2 elements over its thickness have been implemented to account for local bending of the plate. Furthermore, a small transition zone has been included between the different thicknesses at the bottom of the steel deck, to reduce the stress concentration at this location (Figure 3.21). Interface elements have been used for implementation of the slip behaviour between the steel deck and concrete.



a) 3D view



b) Front view (mesh not visible)

Figure 3.20 – Finite element model ComFlor 210

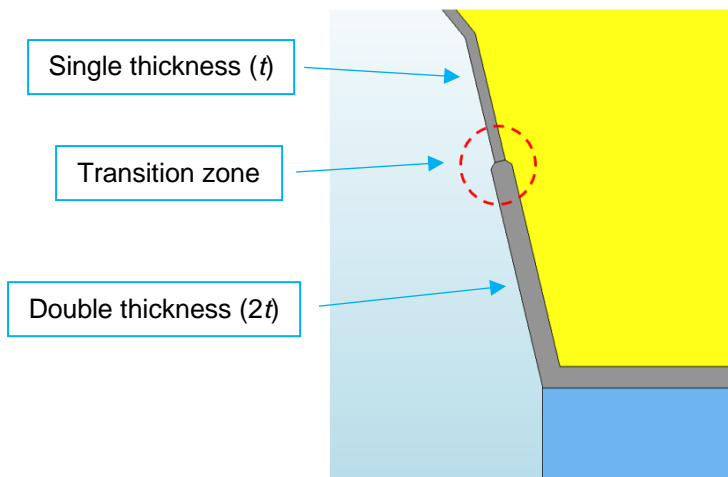


Figure 3.21 – Small transition zone between the different thicknesses at the bottom of the steel deck

3.3.1. Material properties

The material properties of the concrete part and reinforcement have already been provided in section 3.2.1. These parameters are kept the same for the FEA of ComFlor 210. As known from the literature review, the profile of the steel deck contains embossments which are of importance for the longitudinal shear capacity due to the mechanical interlock between the concrete and steel. These embossments also influence the cross-sectional area of the steel deck that is effective in transmission of stresses. Because of the wrinkling of the steel sheet due to the embossments, it flattens out when it is loaded in tension. This initial reduced stiffness makes that the embossments in the steel deck are less effective in the transmission of stresses than the adjacent parts. Therefore, in EN 1994-1-1[3] it is prescribed that the parts with embossments should be neglected when determining the effective area of the steel deck. This is of course very conservative since some tensile stresses will be transmitted through these parts. Especially since the concrete partly prevents the embossments from flattening out (illustrated in Figure 3.22). As mentioned in section 2.4, Van Erp[16] therefore assumed an effectiveness of 12.5% for the parts of the steel deck with embossments, based on his findings. A 1 mm thickness will then be reduced to 0.125 mm in design. A visual representation of the effective cross-section for ComFlor 210 is given in Figure 3.23.

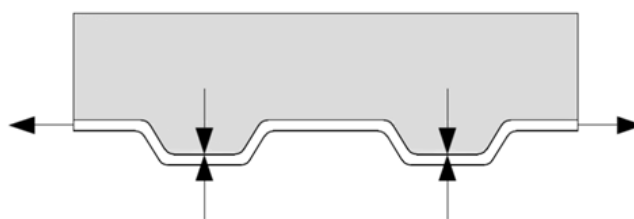


Figure 3.22 – Concrete preventing the embossments from flattening out[16]

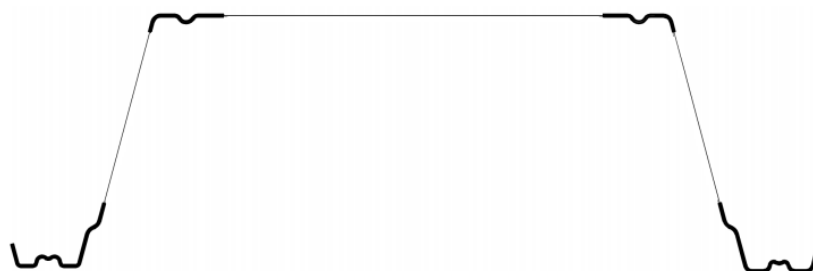


Figure 3.23 – Effective cross-section ComFlor 210: bold parts are fully effective; other parts have a reduced effectiveness due to the embossments.[16]

The use of an effective cross-section with thickness reduction (as shown in Figure 3.23) is commonly used in the design of composite slabs or other thin-walled cold-formed steel sections. This reduction in thickness is of course not representative for the real-life behaviour of the embossments, which makes it also not very suitable for application in the FEA. To account for the reduced effectiveness of the embossments, it is therefore chosen to change the material properties of these parts as also proposed by Veljković[34]. Figure 3.24 shows the stress-strain relations for different parts of a steel deck based on tensile tests[34]. Comparing the dimpled sheeting (spec. 3) with the flat sheeting (spec. 6), shows that the initial Young's modulus is reduced as well as the yield strength. Veljković[34] assumed a reduction of 53% for both material parameters. The dimpled sheeting also has a steeper hardening plateau. For FEA purposes, Veljković[34] used the approximated stress-strain relationships as shown in Figure 3.25. From these relationships it can be established that the ultimate strength is reduced as well (approx. 27%).

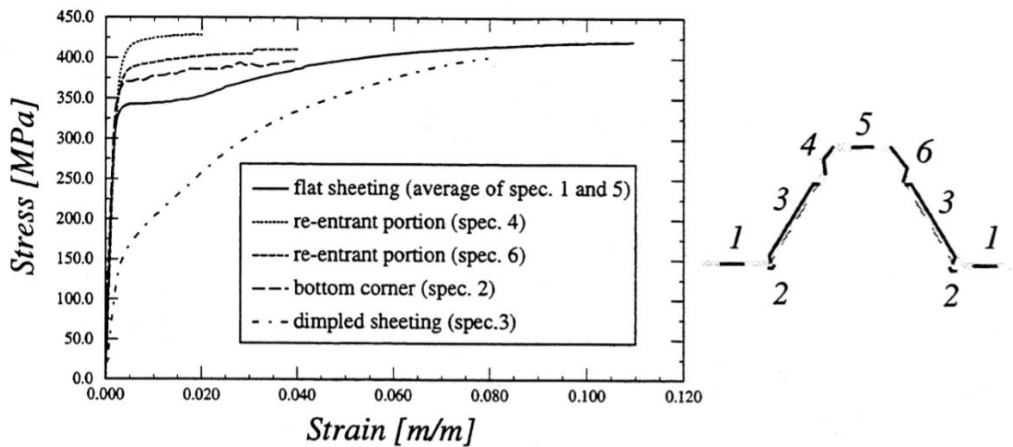


Figure 3.24 – Stress-strain diagrams for different parts of a steel deck based on tensile tests[34]

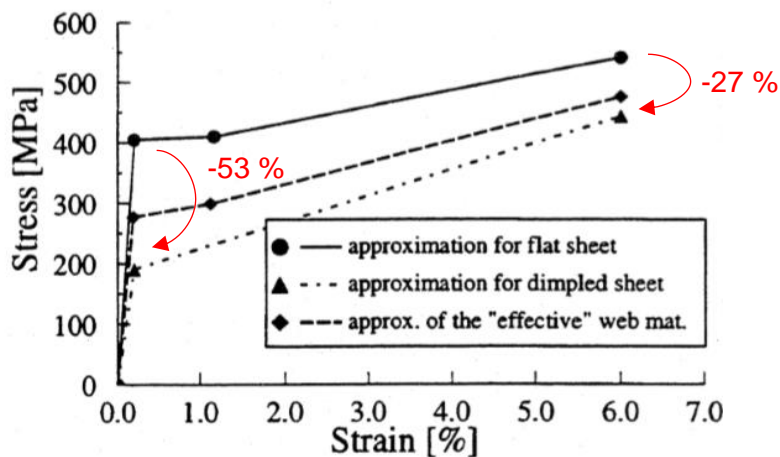


Figure 3.25 – Approximated stress-strain relationships for the steel deck in the FEA of Veljković[34]

Figure 3.26 shows the cross-section of the steel deck as how it has been implemented in the FEA. The longitudinal stiffeners in the webs and upper flanges are included in the model, but they are approached by straight parts. Furthermore, all rounded corners are modelled as straight corners. The geometry of the lower flange is also approached by straight parts, with a double thickness to account for the overlap. As can be seen in the figure, large parts of the upper flange and webs are less effective due to the embossments. Reduced material properties have been assigned to these parts of the cross-section. All material parameters for the steel deck in the FEA are shown in Table 3.4, of which the non-reduced parameters again are in accordance with the research of Abspoel et al.[21].

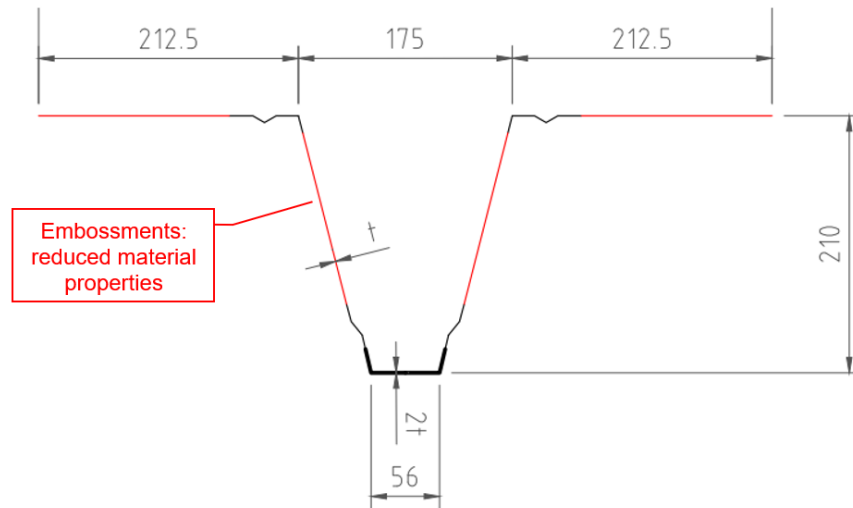


Figure 3.26 – Cross-section steel deck as used in the FEA (unit: mm)

Table 3.4 – Material properties FEA ComFlor 210 (as specified in DIANA[14])

Concrete; reinforcement; support plate.	
See Table 3.2	
Steel deck	
Shape of diagram	Bilinear (Figure 3.7)
Yield strength (f_y)	409 MPa ($\epsilon_y = 1.95 \cdot 10^{-3}$)
Ultimate strength (f_u)	490.8 MPa ($\epsilon_u = 16 \cdot 10^{-2}$)
Young's modulus (E_s)	210000 MPa
Reduced yield strength ($f_{y,red}$)	192.15 MPa ($\epsilon_y = 1.83 \cdot 10^{-3}$)
Reduced ultimate strength ($f_{u,red}$)	306.75 MPa ($\epsilon_u = 16 \cdot 10^{-2}$)
Reduced Young's modulus ($E_{s,red}$)	105000 MPa
Poisson's ratio ν	0.3

Regarding the provided material properties in Table 3.4, please notice the following:

- The applied reduction in yield strength is equal to 53% in accordance with Veljković[34];
- The Young's modulus has been reduced with 50% and the ultimate strength has been reduced with 37%. As mentioned earlier, these values should have been 53% and 27% (derived from the paper of Veljković[34]). Some small calculation errors were made by the author in determining the reduced material properties which led to this deviation in percentages. However, since these reduced properties are already quite an assumption, the effect of these calculation errors is neglected.
- An ultimate strain value ϵ_u of 16% has been assumed (for reduced and non-reduced properties) in accordance with NEN 10346[38].

The reduced material properties for the embossments are mainly based on the reduced effectiveness of these parts in the longitudinal direction (local x-direction). This is illustrated in Figure 3.27a. However, whether these reduced material properties correctly describe the behaviour of the embossments in any direction may be doubted. It is illustrated in Figure 3.27b and -c that for these other loading conditions, the material seems to be less affected by the wrinkling of the plate. Therefore, it may be expected that the steel deck behaves more or less orthotropic at the locations of the embossments. With respect to this orthotropy, detailed information is missing. For that reason, it has been chosen to apply an isotropic material model for the embossments with reduced properties, to be on the conservative side.

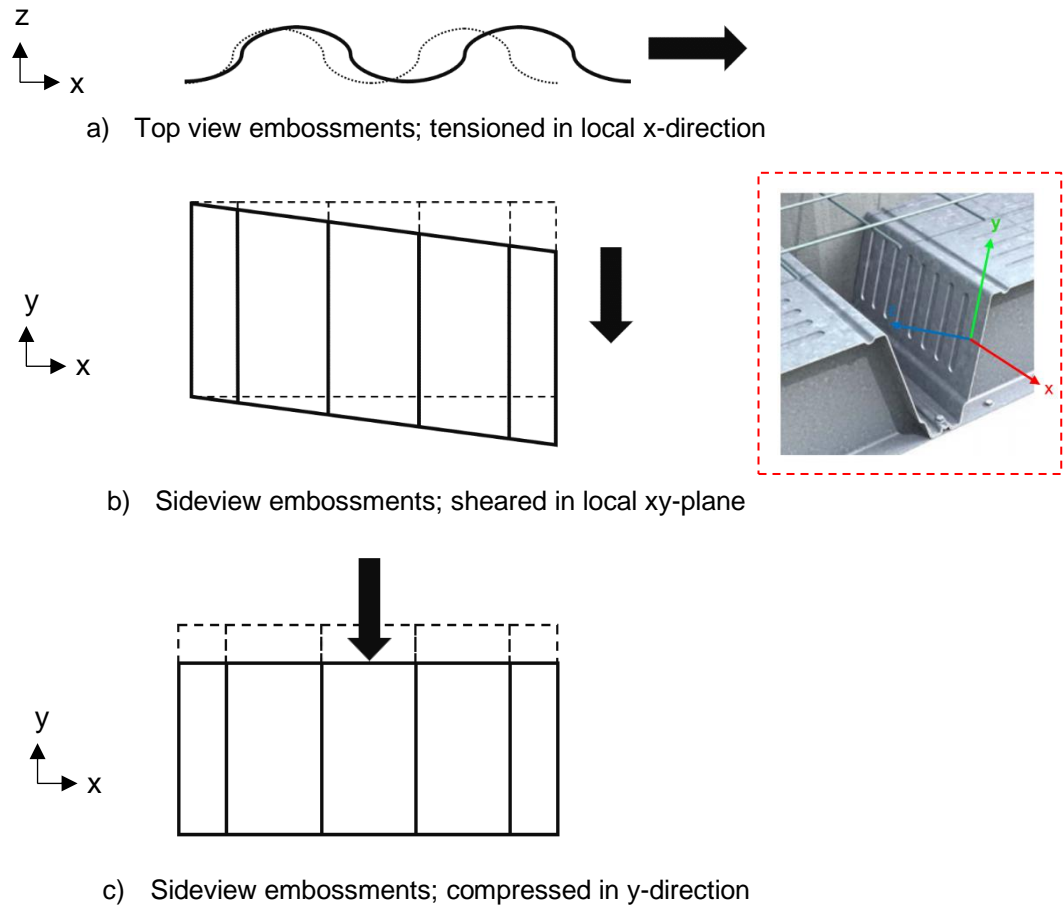


Figure 3.27 – Behaviour embossments for different loading conditions

Figure 3.28 shows the type of interface element that has been applied in the finite element model to simulate the interaction between the steel deck and concrete. This element can describe the behaviour in normal direction (local z-axis) and shear directions (local x- and y-axis). The local x-axes of all interface elements are aligned with the global x-axis of the finite element model. The bonding in this direction is the strongest due to the orientation of the embossments (shown in Figure 3.29). The bond-slip diagram for this x-direction is shown in Figure 3.30. The shape of the diagram is based on research by Ríos, Cifuentes, Martínez-De La Concha & Medina-Reguera[35] on numerical modelling of shear-bond behaviour in composite slabs. As can be seen, the diagram exists out of 3 different linear segments: starting with (almost) full interaction, then a branch of partial interaction and finally a descending part[35]. This shape of the diagram can generally be observed in the load-displacement curves of composite slabs for longitudinal shear failure[16][35]. The provided values that characterise this bond-slip relation are based on the experiments by Van Erp[16]. Calculation of these values is given in Appendix C. In contrast to the slip behaviour in x-direction, simple linear material properties have been assigned to the local y- and z-direction of the interface elements. To this y-direction, a 1000 times smaller stiffness (0.000154 N/mm^3) has been implemented compared to that of the x-direction (0.154 N/mm^3), since it is assumed that the embossments don't effectively restrain the slip in this y-direction (Figure 3.29). To the z-direction, which represents the contact between the steel and concrete, a very high linear stiffness has been applied (154000 N/mm^3). Separation between the concrete and steel will therefore not occur.

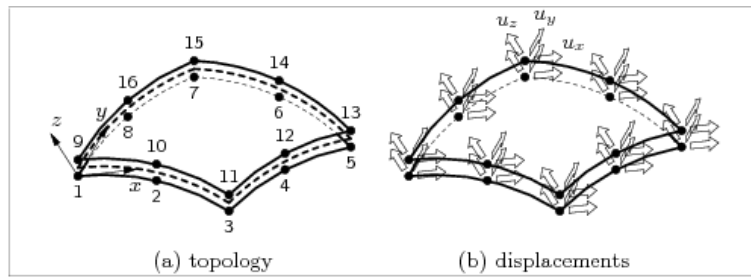


Figure 3.28 – 3D surface interface element in Diana[14]

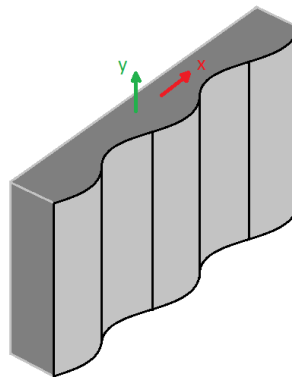


Figure 3.29 – Orientation of the local directions with respect to the embossments

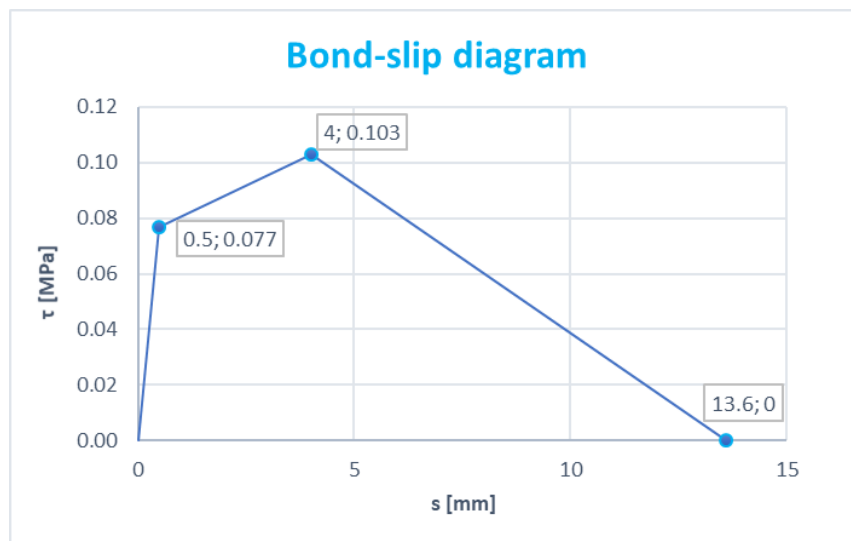


Figure 3.30 – Bond-slip behaviour for local x-direction of interface elements[16][35]

3.3.2. Analysis procedure

It has been chosen to use a shear slenderness ratio a_v/d of 2.99 (shear span $L_s = 740$ mm). From the former analysis of the concrete section, it was concluded that direct transfer of the load to the support is still possible for bigger shear slenderness ratios. However, this will also increase the chance on longitudinal shear failure or bending failure as known from section 2.3. Both physical and geometrical non-linearity have been considered in the FEA. The presence of this slipping interface has been the main reason to also include geometrical non-linear behaviour in the analysis. For further information about the solution procedure, please see section 3.2.2. Convergence is found when both energy and force norms are satisfied with a tolerance of 0.005 and 0.05 respectively.

3.3.3. Results and discussion

Figure 3.31 shows the load-displacement curve of ComFlor 210 (blue), together with the load-displacement curve of the former analysis of the concrete section (orange). The rib reinforcement diameter and shear slenderness ratio were the same in both analyses.

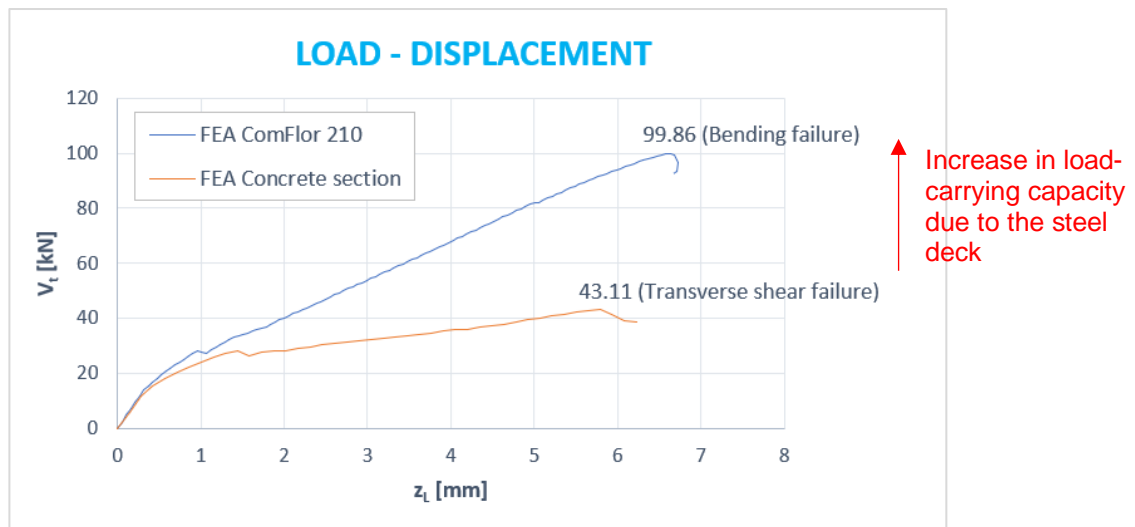


Figure 3.31 – Results FEA ComFlor 210 and FEA concrete section (rib reinforcement $\text{Ø}24$ mm; $a_v/d = 2.99$)

The composite slab (ComFlor 210) failed at a load of 99.86 kN. Unfortunately, bending failure was the governing mode. The composite slab failed by crushing of the concrete top layer (compressive zone), just underneath the application of the line load. This is shown in Figure 3.32 at the locations of the red dashed circles, where the compressive stresses in longitudinal direction start to drop to zero. Figure 3.33 shows the Von Mises stresses in the steel deck at maximum load. Yielding at the bottom of the steel deck did occur within the region of constant bending moment. The effect of this yielding isn't directly visible in the load-displacement diagram of Figure 3.31. This is caused by the fact that the stress in the rib reinforcement (455.86 MPa) stayed below its yield strength (536 MPa), before failure of the composite slab occurred. Figure 3.34 shows the cracks in the composite slab at maximum load. It may be established that opening of the cracks has been very limited. From Figure 3.32 it may also be observed that a rather big longitudinal crack was present in the top part of the composite slab (location where the principal stresses are almost zero). This crack resulted from the secondary bending in y-direction, for which the mesh in the top layer acted as reinforcement. The maximum value of slip in longitudinal direction was equal to 1.02 mm, so longitudinal shear failure didn't occur.

The FEA of the concrete section reached a maximum load of 43.11 kN as a consequence of transverse shear failure. When both analyses are being compared, it may be concluded that the steel deck does significantly improve the transverse shear resistance of the composite slab. Adding the steel deck to the finite element model led to an increase in the load-carrying capacity from 43.11 kN to 99.86 kN. Although this later failure load characterizes the bending moment capacity of the composite slab ($= 99.86 \cdot 0.74 = 73.90$ kNm), it also provides a minimum value for its transverse shear resistance (>99.86 kN). So, according to the FEA of ComFlor 210, the composite slab has a minimal transverse shear capacity of 99.86 kN. For barely the concrete part of this composite slab, the transverse shear capacity is equal to 43.11 kN. So, according to the analyses, the additional transverse shear resistance provided by the steel deck is minimally equal to $99.86 - 43.11 = 56.75$ kN.

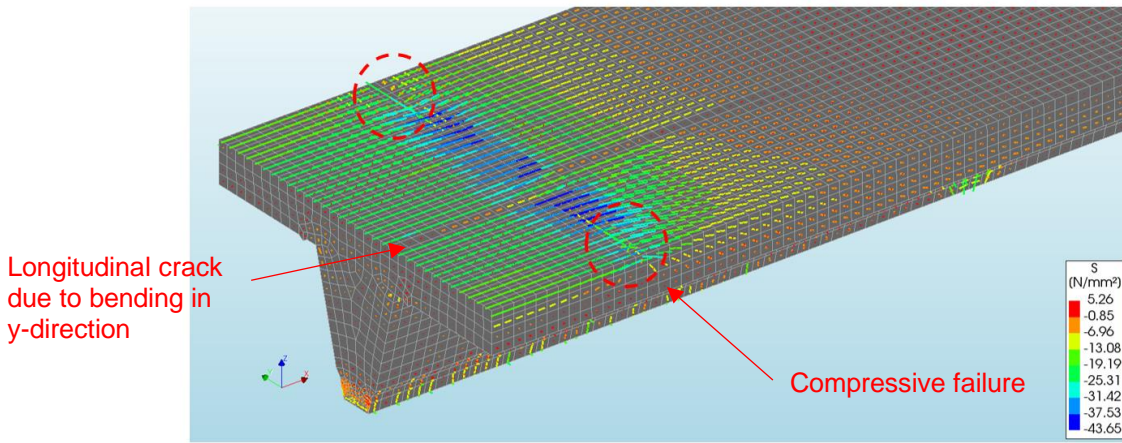


Figure 3.32 – Principal stresses in concrete at maximum load (FEA ComFlor 210)

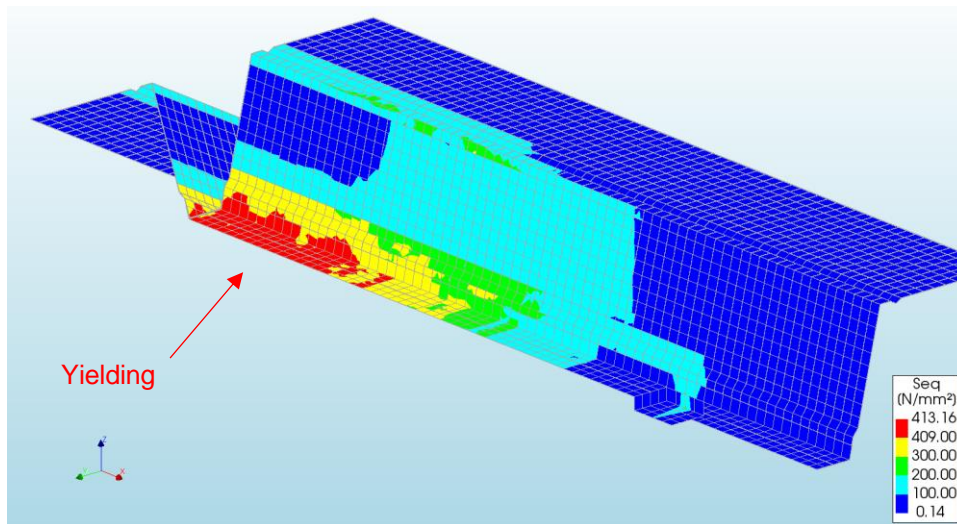


Figure 3.33 – Von Mises stresses in steel deck at maximum load (FEA ComFlor 210, plotted in integration points)

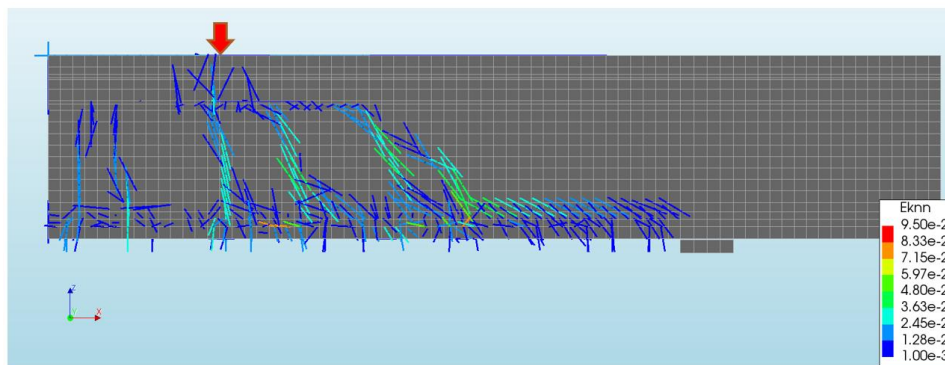


Figure 3.34 – Crack strain plot at maximum load (FEA ComFlor 210)

Figure 3.35 shows the principal stresses in the steel deck at maximum load (FEA ComFlor 210). Only one side of the steel deck is shown in this figure, but it can be assumed that the stress distribution in the steel deck is the same for the other side (i.e. the other web). It can be seen that, within the shear span, the webs of the steel deck are mainly subjected to tensile stresses in the principal directions. Most of these principal stresses even show sort of uniaxial state: tensile stress in one direction, (almost) no stress in the other direction. This stress state is quite unexpected when we consider the steel deck to be barely responsible for carrying a part of the transverse shear force. This difference in expectation

versus observation is also shown in Figure 3.36. The most obvious explanation for this, is that the stresses in the steel deck's webs are significantly influenced by the cracking in the concrete, making that the webs are subjected to tensile stresses in both longitudinal direction (σ_x) and transverse direction (σ_y) within the shear span L_s . Off course, the steel deck's webs are subjected to shear stresses as well (τ_{xy}). With the tensile stresses bridging the cracks, the steel deck acts as reinforcement to the concrete. As shown in Figure 3.35, the tensile (principal) stresses in the webs are mostly below their yield strength (i.e. 192.15 MPa for embossments; 409 MPa for normal parts). A small part of the embossments in the webs is above its yield strength (green tensors), but since the embossments do have a quite steep hardening plateau, opening of the cracks is still prevented. From the FEA of the concrete section, it is known that transverse shear failure would have been observed in case of absence of the steel deck. It has been shown that opening of the inclined cracks within the shear span caused transverse shear failure of the concrete element. By including the steel deck to the finite element model, opening of these inclined cracks is restrained. The steel deck acts as transverse shear reinforcement to the concrete, which makes that the transverse shear capacity is increased.

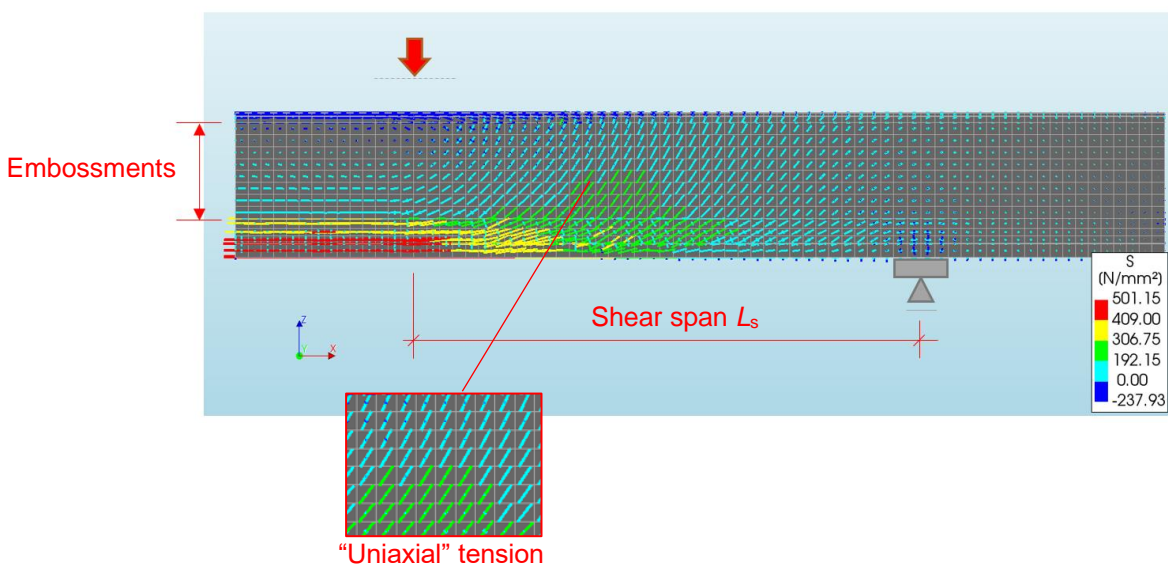


Figure 3.35 – Principal stresses in steel deck at maximum load (FEA ComFlor 210)

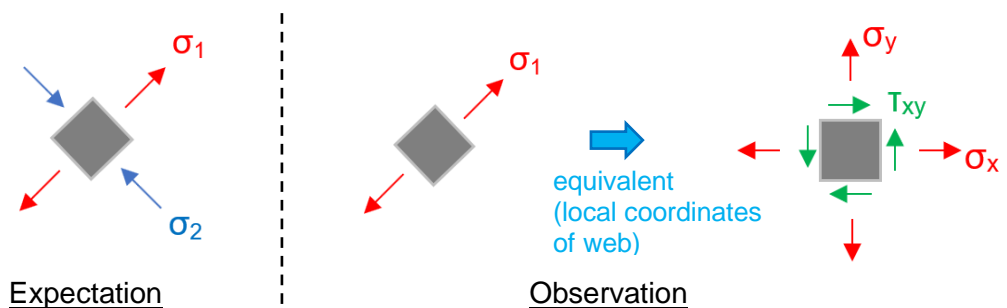


Figure 3.36 – Principal stresses around mid-height of steel deck's webs (FEA ComFlor 210)

From this FEA of ComFlor 210, it may also be questioned whether shear buckling is expected to occur when considering transverse shear failure of a deep composite slab. The dark blue tensors in Figure 3.35 represent the compressive stresses in the steel deck. It can be seen that the upper flanges of the steel deck are mostly in compression, and so are the webs closely above the support. However, within the shear span, no significant dark blue tensors can be observed in the webs. The webs are mainly subjected to tensile stresses in one diagonal direction; the compressive stresses in the other diagonal direction are very low or absent (Figure 3.36). Since these compressive stresses are the reason for shear buckling of the webs (see Appendix A), it is doubted whether this kind of buckling may be observed in case of transverse shear failure of a deep composite slab.

In Figure 3.37 it is shown that opening of an inclined crack generally leads to a horizontal displacement in global x-direction and a vertical displacement in global z-direction. This horizontal opening of the crack is definitely restrained by the steel deck's webs, since the transfer of stresses between the concrete and steel is assured by the embossments in this direction. However, for vertical opening of the crack, the local transfer of stresses between the steel deck's webs and concrete is assumed to be nihil. It has been explained in section 3.3.1 that, due to the orientation of the embossments, low linear stiffness properties have been assigned to the interface elements in local y-direction. Slip between the concrete and the steel deck's webs is therefore free to occur in this direction, making that the steel deck's webs aren't locally reinforcing the cracks for this vertical opening. This seems a bit contradictory with the observation in the FEA that the steel deck's webs are subjected to tensile stresses in both longitudinal direction (σ_x) and transverse direction (σ_y) within the shear span. However, this can be explained on basis of the following. In the FEA, detachment between the steel deck and concrete couldn't occur. With the ends of the webs being fully attached to the concrete, vertical opening of the cracks (global z-direction) makes that the webs can still be stressed in the local y-direction. So, due to the chosen interface properties, the steel deck's webs are able to reinforce the concrete by resisting the tensile stresses from the inclined cracks in both longitudinal direction and vertical direction.

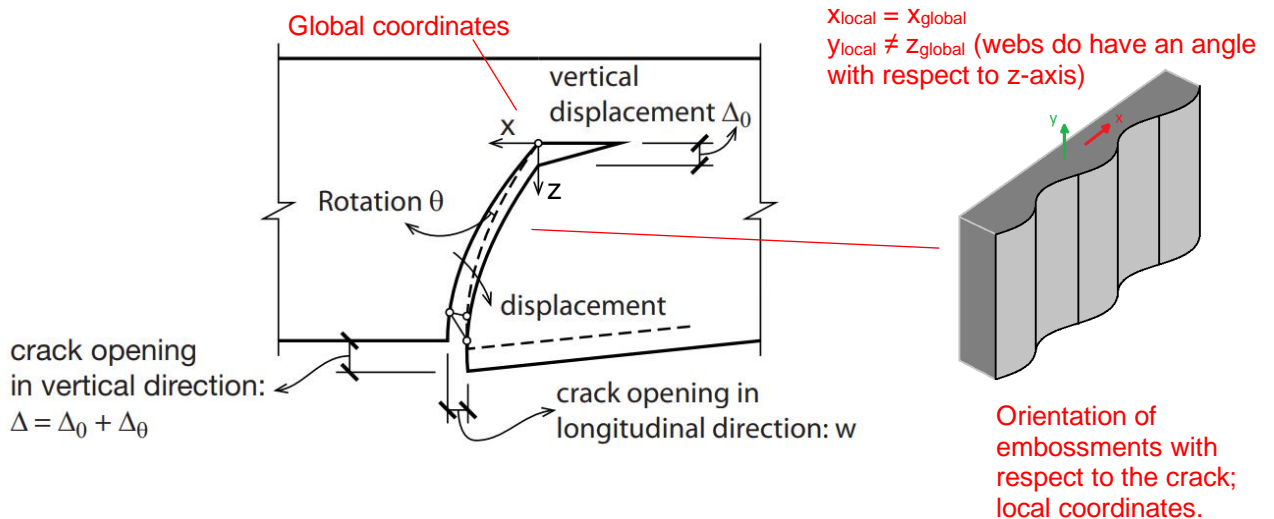


Figure 3.37 – Opening of an inclined crack[28]

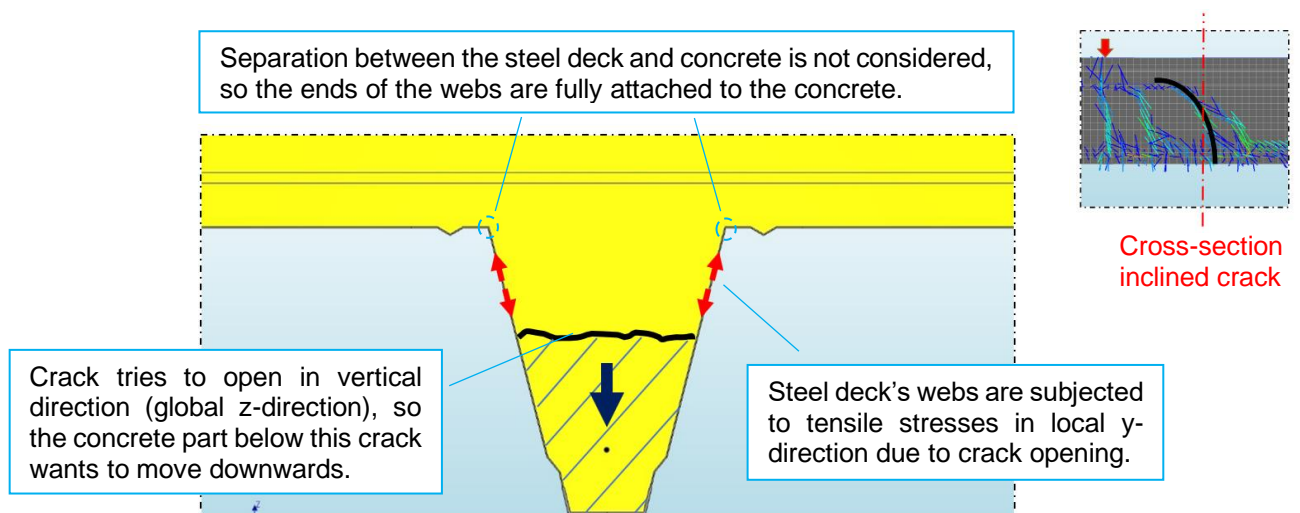


Figure 3.38 – How vertical opening of the inclined cracks is restrained by the webs in the finite element model

With the statement that the steel deck's webs are able to reinforce the inclined cracks in a vertical sense, it may be established that the functioning of this is comparable to stirrups in ordinary reinforced concrete beams. These stirrups are positioned at a certain mutual distance in the concrete beam, whereby they bridge the existing transverse shear cracks (Figure 3.39a). The stirrups take over the tensile stresses that can't be resisted by the cracks, whereby they prevent these cracks from opening. For the transverse shear resistance of such reinforced concrete members, it is assumed by the Eurocode 2 that the internal distribution of stresses can be described with a strut-and-tie model as shown in Figure 3.39b and -c. The upper chord of this model represents the concrete compressive zone, as the lower chord represents the tensile rebars. The vertical and diagonal members of the model represent the stirrups and concrete compressive struts respectively. The process for transfer of the transverse shear force F from loading point to support can be explained as follows. First, the external force F flows from the top of the beam through the concrete to the bottom of the adjacent stirrup. A diagonally oriented compressive strut arises in the concrete. This strut is loaded by a force $F\sqrt{2}$. At the bottom of the stirrup, this force is guided to the top of the beam due to the tensile forces that arise in the stirrup. The total tensile force that is taken by the stirrup is equal to F . Once arrived at the top, again the force flows diagonally from the top of the beam to the bottom of the next stirrup. The process is repeated until the support is reached. It may be established that the total transverse shear resistance of the concrete beam is determined by the partial resistances of the struts (compressive failure) and stirrups (yielding). In clause 6.2.3 of EN 1992-1-1[24], formulas are provided to calculate these partial resistances.

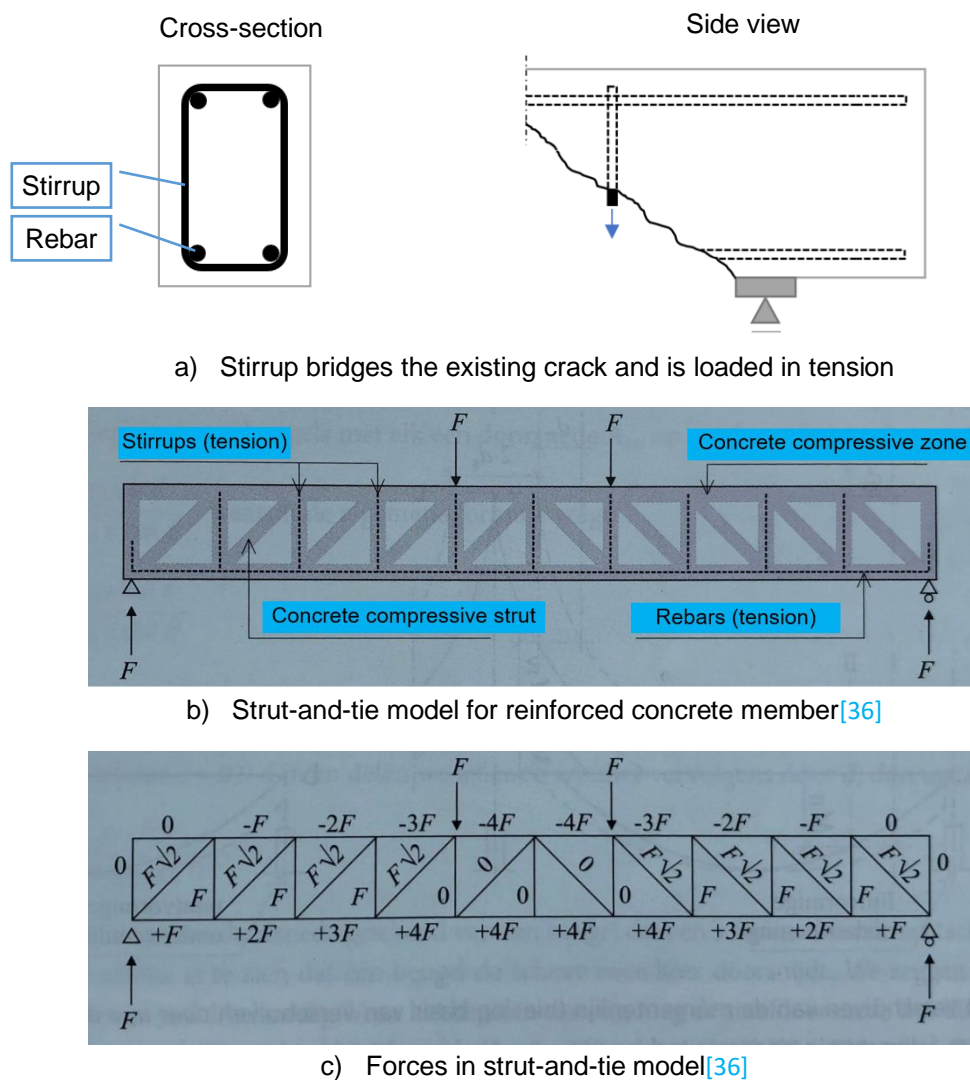


Figure 3.39 – Strut-and-tie model for reinforced concrete beams with stirrups

With respect to the transverse shear capacity of deep composite slabs, it is wondered whether the same kind of strut-and-tie model can be applied. The proposal for such a strut-and-tie model is shown in Figure 3.40 (for one rib). The diagonal members represent the compressive struts in the concrete rib and the vertical members represent the tensile stresses in the steel deck's webs. It is assumed that these tensile stresses in the steel deck can be represented by one vertical member, in the middle of the shear span L_s . This assumption is based on the stress distribution of Figure 3.41, which shows the normal stresses in global z-direction in the steel deck for one web (FEA of ComFlor 210). It clearly shows a peak in the middle of the shear span. The choice for one vertical member within the shear span restricts the model to two concrete compressive struts (see Figure 3.40). When the strut-and-tie model is applied to the finite element model of this thesis, it gives that the compressive struts have an angle θ of 34.3° with respect to the longitudinal axis. The Eurocode 2 gives restrictions for this angle, namely $21.8^\circ \leq \theta \leq 45^\circ$, which is satisfied. The compressive principal stresses in the concrete are shown in Figure 3.42. The orientation of these compressive stresses corresponds well with the compressive struts in the model of Figure 3.40.

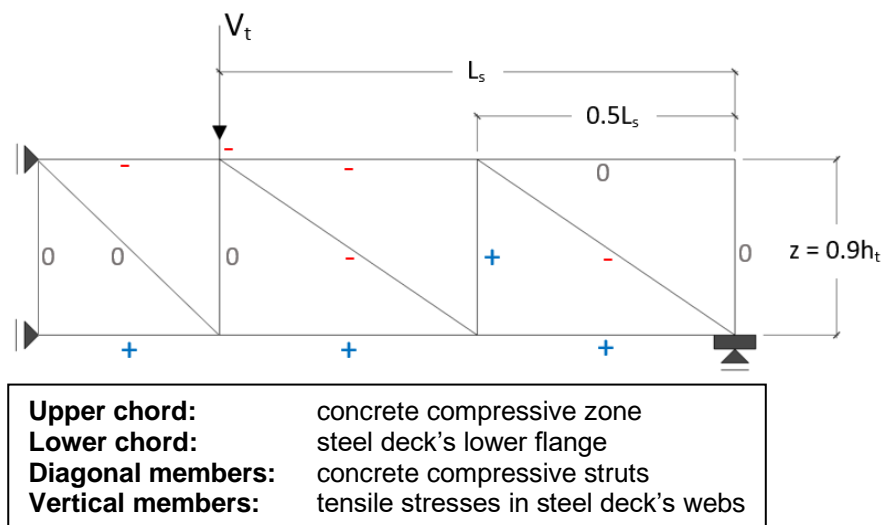


Figure 3.40 – Strut-and-tie model for load transfer in deep composite slabs

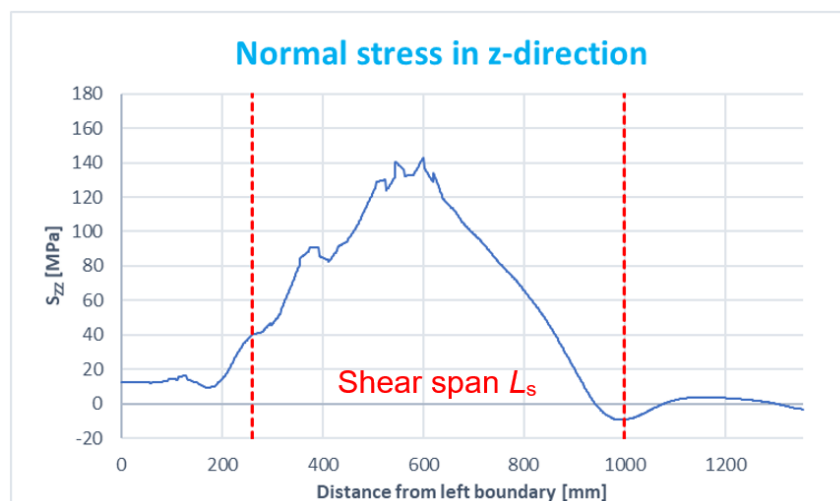


Figure 3.41 – Normal stress in global z-direction in steel deck at mid-height (for one web; maximum load (failure); FEA ComFlor 210)

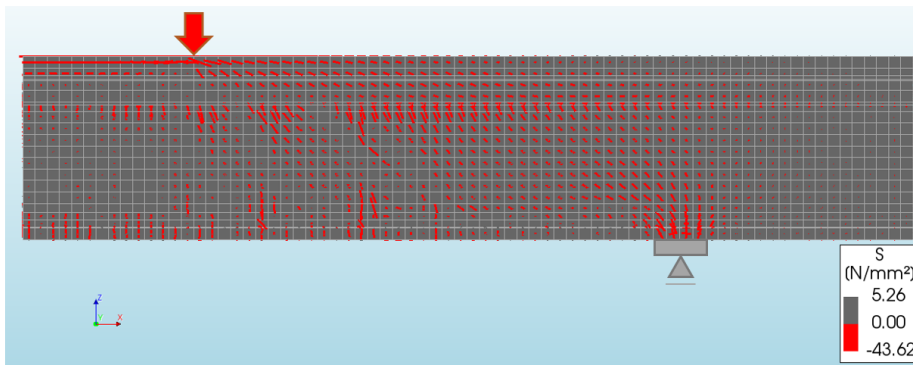


Figure 3.42 – Principal compressive stresses in concrete at maximum load (FEA ComFlor 210)

The validity of the proposed strut-and-tie model (Figure 3.40) as calculation method for the transverse shear capacity of deep composite slabs, haven't been confirmed by the analysis. The description of the load transfer in the composite element by this 2D model can be assessed as a big simplification. This especially holds for the stress state in the steel deck's webs: the strut-and-tie model assumes that the steel deck's webs can only be stressed in vertical direction (i.e. global z-direction = vertical component of local y-direction of the webs), but this is off course never the case. Furthermore, it is also not clear how to convert the steel deck's webs into such linear members for the strut-and-tie model. Using an effective length (in x-direction) may be the most obvious solution to this.

However, when considering that the steel deck's webs act as transverse shear reinforcement in a similar way as stirrups, does provide a valid argument for the significant increase in transverse shear capacity like observed in the FEA. The efficiency of the load-transferring mechanism (strut-and-tie model) seems to be the main reason for the increase. However, the model relies on a good collaboration between the concrete and steel deck. Using a strut-and-tie model as proposed, with different materials for the various members, is only valid when transfer of load between the different materials is assured. For that reason, accurate description of the interface behaviour between the concrete and steel deck plays an important role as well.

With respect to this interface behaviour, it is being questioned whether the adhesive capacity between the steel deck and concrete is big enough, so that the assumption of no separation makes a good approach. Suppose both materials to be completely free to separate from each other, then the steel deck loses its function as stirrup. With the embossments only restraining the slip in longitudinal direction and the ends of the webs not being attached to the concrete, opening-up of the cracks can no longer result in tensile stresses in the steel deck's webs in local y-direction (σ_y). On the other hand, due to the possible mechanical interlock of the embossments in this y-direction (Figure 3.43), the steel deck's webs may still be stressed in this direction when restraining the inclined cracks from opening.

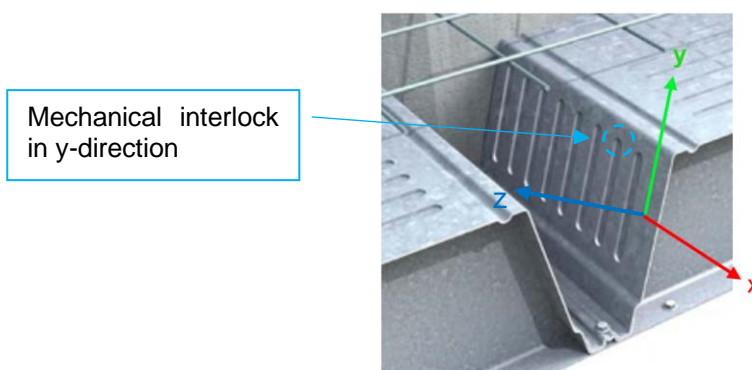


Figure 3.43 – Local directions of both the interface and the steel deck's web

So, when considering the transverse shear capacity of deep composite slabs, the following may be established. The steel deck's webs have the potential to act as transverse shear reinforcement in the same way as stirrups in reinforced concrete. The load is assumed to be mainly transferred by compressive struts in the concrete ribs and vertical tensile stresses in the steel deck's webs. These tensile stresses in the webs restrain the cracks in the concrete from opening, so good collaboration between the separate materials is necessary. In the finite element model, this collaboration has been assured by assuming that the steel deck and concrete couldn't separate from each other. In reality, for the steel deck's webs to effectively restrain the crack opening in a vertical sense, most probably relies on the mechanical interlock of the embossments in the local y-direction. Therefore, accurate description of the total interface behaviour between the steel deck and concrete is a critical aspect to determine whether this stirrup-functioning of the webs really occurs. With respect to this interface behaviour, detailed information is missing as listed below:

- How does the embossments restrain the slip in local y-direction?
- How big is the adhesive strength between the steel deck and concrete in local z-direction?
- What is the influence of separation between the steel deck and concrete (in local z-direction) on the slip behaviour (in local x- and y-directions)?

So, the assumption that the steel deck and the concrete can't separate from each other, is considered to be the biggest simplification of the finite element model. However, due to the above-mentioned missing links, accurate implementation of the interface properties is not possible. Still, in the next section it is tried to find a lower bound value for the transverse shear capacity of ComFlor 210, by using other interface properties.

3.4. FEA ComFlor 210: a lower bound value for the transverse shear capacity

From the FEA results in former section 3.3, it could be concluded that the steel deck does give a significant improvement of the transverse shear capacity. Due to the chosen properties of the interface, the steel deck's webs were able to reinforce the concrete in a similar way as stirrups in regular reinforced concrete beams. However, it is doubted whether these interface properties are correct and if this stirrup-functioning of the steel deck's webs is representative for the actual transverse shear behaviour of deep composite slabs.

So, it is wondered what will happen to the transverse shear resistance when the steel deck and concrete are free to separate from each other. This behaviour is quite easy to implement in the finite element model by specifying a no-tension relationship for the interface elements in local z-direction. In reality, it could be that some adhesive strength is present between the steel deck and concrete. But since this is not known, assuming that the interface contains no tensile strength in local z-direction may be considered as a conservative approach. Implementation of this no-tension behaviour for the interface in local z-direction, also affects the slip behaviour in longitudinal direction (local x-direction of the interface elements). It isn't hard to imagine that the effect of mechanical interlock from the embossments becomes less when the steel deck separates from the concrete. However, the crosslink between this behaviour in local z-direction and local x-direction isn't known. In the finite element model of section 3.3, it has been assumed that the embossments mainly restrain the slip in local x-direction, so that slipping in local y-direction is (nearly) free to occur. Opening of the interface therefore doesn't affect the behaviour in local y-direction. However, when it is assumed that the embossments also restrain the slip in local y-direction, and a more accurate behaviour is implemented in the finite element model (like for the local x-direction), then opening of the interface affects the behaviour in both x- and y-directions.

To overcome this ignorance about an appropriate longitudinal shear relationship (local x-direction) when considering separation between the steel deck and concrete (in local z-direction), it is suggested to assume that slipping in this longitudinal direction is almost free to occur (like for the local y-direction). A full sliding connection for the interface in longitudinal direction is likely to give numerical problems, so some slip restraining properties should be implemented. However, by setting a low linear stiffness for the interface in local x-direction (so the slip is not effectively restrained) and including separation between the steel deck and concrete (for tensile conditions in local z-direction), it is tried to investigate if the steel deck is still possible to provide additional transverse shear resistance.

3.4.1. Material properties & analysis procedure

The no-tension behaviour for the local z-direction of the interface elements can be specified in Diana[14] with a predefined function. It is needed to specify a stiffness, a critical interface opening and a stiffness reduction factor. For this stiffness, a value of 1540 N/mm³ has been applied. This stiffness mainly defines the compressive behaviour of the interface. Compressive failure of the concrete occurs at a stress value of 41.8 MPa, which means that the interface has the potential to show a negative relative displacement of 41.8/1540 = 0.027 mm before failure of the concrete occurs. In real life, this isn't possible since the steel deck and concrete can't move through each other. However, this inaccuracy is neglected because the relative displacement is very small. Increasing the stiffness may improve this inaccuracy, but it tried to prevent large stiffness differences between the different directions of the interface elements to overcome convergence problems. The critical interface opening is set to 1e-6 mm and the stiffness reduction factor is set to 1e-6. This means that when the critical interface opening is reached (for tensile conditions), the stiffness is reduced to 1e-6·1540 = 0.00154 N/mm³.

For the longitudinal shear behaviour (local x-direction of the interface elements), a linear stress-slip relationship has been applied with a stiffness that is 100 times smaller than the initial stiffness in the finite element model of section 3.3. The longitudinal shear behaviour for the current analysis and the former analysis are shown in Figure 3.44 with the orange and blue lines respectively. The reduction in stiffness has been chosen carefully: when the stiffness becomes very low, it is likely to give convergence problems.

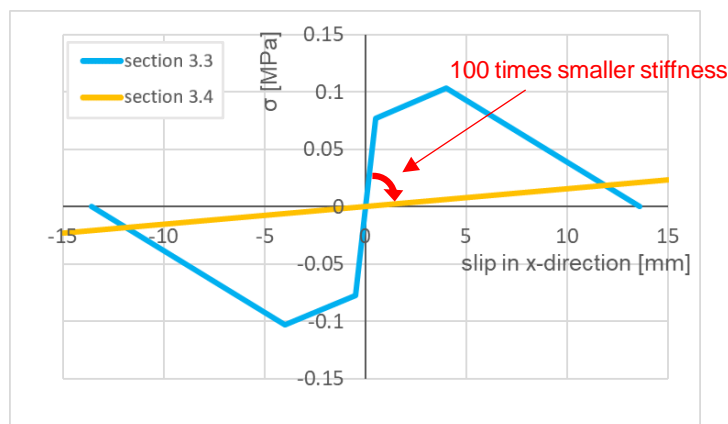


Figure 3.44 – Differences in longitudinal shear behaviour for FEA in section 3.3 and 3.4

So, regarding the interface properties, the following can be summed up:

- For the behaviour in local z-direction, the stress-displacement graph follows a linear diagram with a stiffness of 1540 N/mm³ for compressive conditions. As soon as the relative displacement reaches a positive value of 1e-6 mm (opening), this stiffness is reduced to 0.00154 N/mm³ for tensile loading conditions. With this low tensile stiffness and high compressive stiffness, it is tried to simulate that the steel deck and concrete can separate from each other, but can't move through each other at the

interface. However, with this compressive stiffness being non-infinite, some small negative relative displacement is allowed for the interface elements. Also, with the tensile stiffness being larger than zero, some tensile stresses will always be transmitted between the steel deck and concrete when the interface opens. It is assumed that both inaccuracies can be neglected.

- The longitudinal slip behaviour in x-direction follows a linear diagram with a stiffness of 0.00154 N/mm³. Longitudinal slip is not effectively restrained due to this small stiffness, but some composite behaviour is still guaranteed to prevent convergence problems.
- The slip behaviour in local y-direction of the interface elements is left unchanged with respect to the former FEA in section 3.3 (linear diagram with stiffness of 0.000154 N/mm³).

Please be aware that the assumed interface properties are totally non-realistic parameters and can't be used for accurate simulation of composite behaviour of ComFlor 210. However, it is tried to simulate an imaginary experiment in which the interface is barely capable in preventing the concrete and steel deck to move through each other. So, when an external load is applied on top of the composite slab, it gives that the steel deck deflects together with the concrete section. Due to this combined deflection, both elements are stressed as shown in Figure 3.45. Equilibrium at the considered cross-section makes that $V_t = V_c + V_{webs}$. So, a part of the load is carried by the concrete section (V_c) and a part of the load is carried by the transverse shear force in the webs of the steel deck (V_{webs}). The described calculation methods in section 2.7 all rely on the same kind of superposition. It is expected that including the steel deck to the finite element model still gives an increase in transverse shear capacity, even when the composite behaviour is limited.

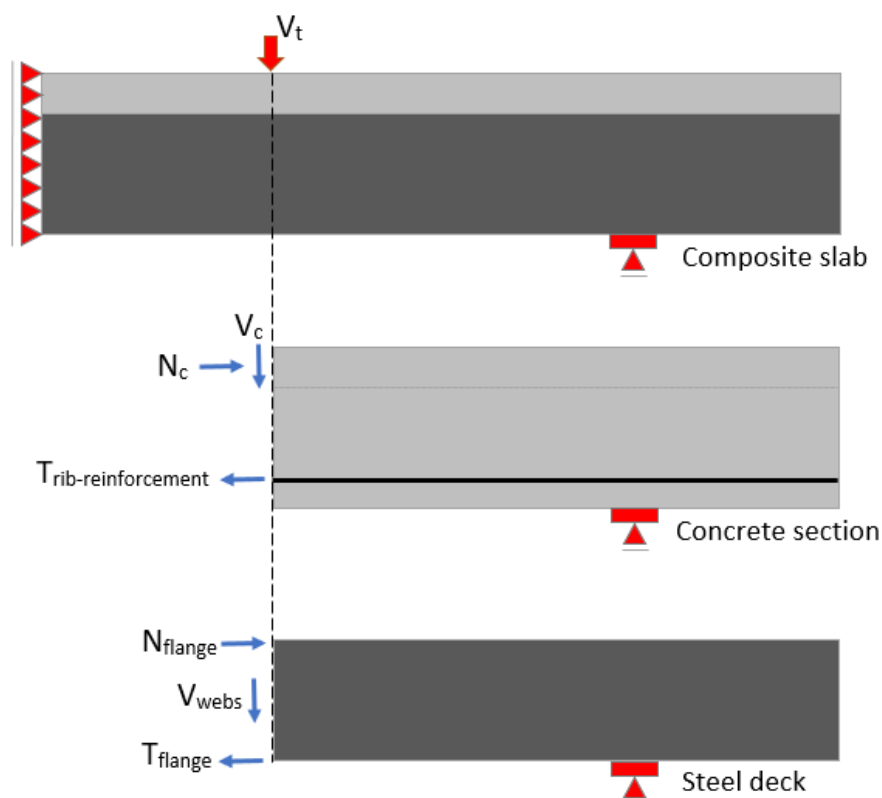


Figure 3.45 – General forces in composite slab due to external loading

For more information about the material properties of the concrete and steel deck, see section 3.2.1 & 3.3.1. Again, in this FEA of ComFlor 210, the rib reinforcement diameter is equal to 24 mm and a shear slenderness ratio of 2.99 (shear span $L_s = 740$ mm) is used. For more information about the analysis procedure, see section 3.3.2.

3.4.2. Results and discussion

The load-displacement graph of the executed FEA of ComFlor 210 is plotted in Figure 3.46 with a green line. The results of the other two FEA's (section 3.2 and 3.3) are also shown in this figure (orange and blue lines). The rib reinforcement diameter and shear slenderness ratio were the same in all analyses.

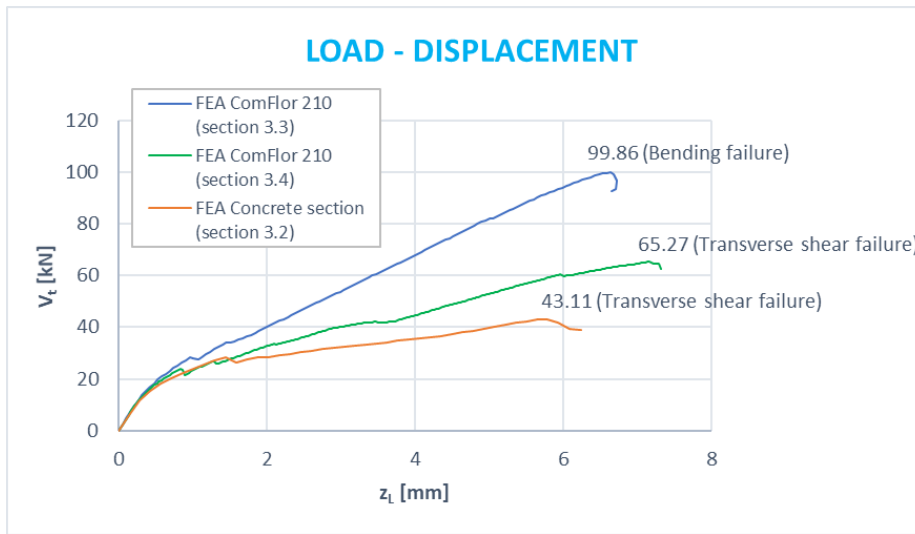


Figure 3.46 – Load-displacement graphs FEA's ComFlor 210 and FEA concrete section (rib reinforcement $\varnothing 24$ mm; $a_v/d = 2.99$)

In section 3.3, the composite slab failed in bending at a load of 99.86 kN (blue graph in Figure 3.46). By changing the interface properties of the composite slab (see section 3.4.1) and redoing the FEA, this failure load is reduced to 65.27 kN (green graph in Figure 3.46). The composite slab now failed in transverse shear instead of bending. Figure 3.47 shows the formation of this clear inclined crack within the shear span. Compressive failure of the concrete's compressive zone underneath the location of the external load became decisive in the same way as in the former analysis of ComFlor 210 (section 3.3, Figure 3.32). However, yielding of the bottom flange of the steel deck haven't been observed this time. The same holds for yielding of the rib reinforcement. The combination of this and the cracking pattern in the concrete, makes that the failure mode is assessed as transverse shear failure.

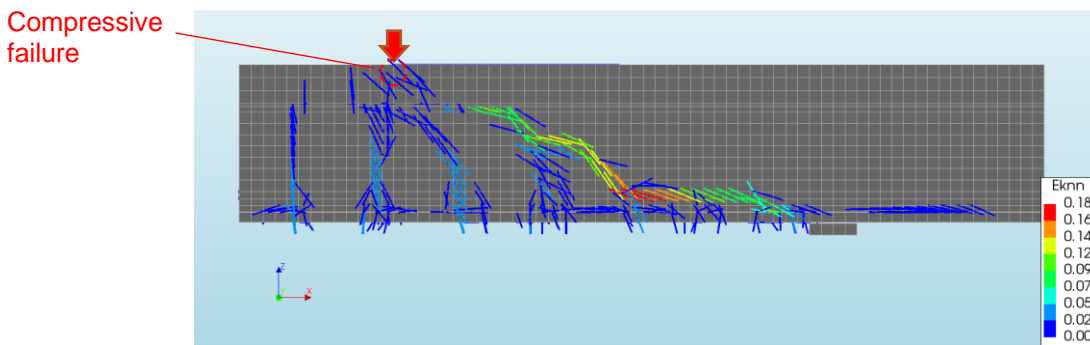


Figure 3.47 - Crack strain plot at maximum load

So, allowing the steel deck and concrete to separate from each other and reducing the composite behaviour between the two elements, led to a reduction in load-carrying capacity of ComFlor 210. Still, by making the comparison with the FEA of the concrete section (orange graph in Figure 3.46), it can be concluded that the steel deck does give a significant increase in transverse shear capacity. According to both analyses, the additional resistance provided by the steel deck is equal to $65.27 - 43.11 = 22.16$ kN. This confirms the expectation that, even when the steel deck and concrete are not effectively acting together due to these bad interface properties, the steel deck is still able to

provide additional transverse shear resistance. The steel deck deflects together with the concrete due to the external load, making that it is stressed and takes part in resisting this external load.

Figure 3.48 shows the compressive (blue) and tensile (red) principal stresses in the steel deck just after the first load step of the FEA. The analysis is clearly in the linear-elastic stage and the stress distribution in the steel deck is as expected. The upper flange of the steel deck is in compression as the lower flange is in tension. Within the shear span, the principal stresses around mid-height of the webs are rotated at an angle of approx. 45° due to the shear stresses. By considering the structural behaviour of the steel deck in the ULS as an extension of this initial stress state, it is easy to explain the observed buckling behaviour of the steel deck as shown in Figure 3.49. This figure actually shows the opening of the interface in local z-direction, but this representative for the buckling behaviour of the steel deck. By allowing the steel deck and concrete to separate from each other, the steel deck becomes susceptible to local flange buckling, shear buckling and buckling of the webs above the support due to the introduced compressive stresses. Comparing Figure 3.49 with Figure 3.48 shows that the observed buckling pattern in the steel deck corresponds well with these initial compressive stress trajectories. However, the local buckling of the steel deck makes that the stress distribution in the ULS is very irregular and difficult to assess. This is shown in Figure 3.50. From this figure, it may also be seen that the maximum principal stress values (649.23 MPa and -575.47 MPa) are beyond the specified material strengths, which shouldn't be possible. However, this is due to the extrapolation of the stresses from the integration points to the outer surfaces of the elements. The combination of local buckling and the limited number of elements over the plate thickness of the steel deck is likely to cause this inaccuracy. Figure 3.50 shows the Von Mises stresses in the steel deck at maximum load, plotted in the integration points of the elements. From this it may be concluded that the steel deck is hardly at yielding, except for this location above the support at the inside of the webs. This yielding occurred due to the very local bending at this kink in the steel deck's webs.

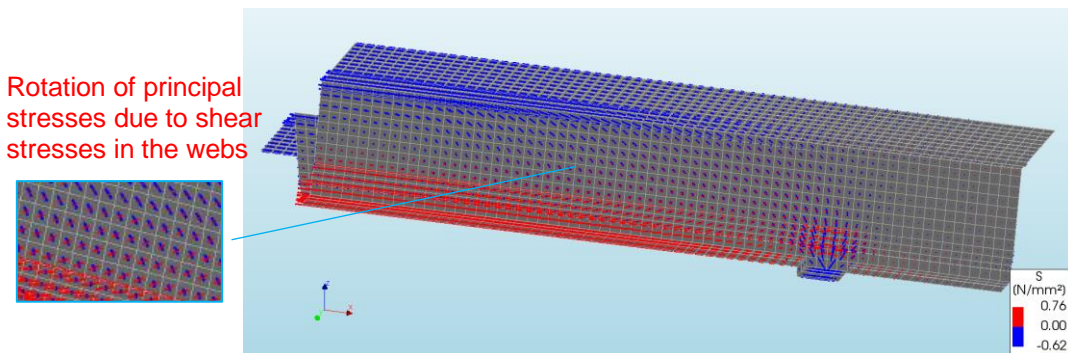


Figure 3.48 – Principal stresses in steel deck just after the first load step: blue is compression, red is tension.

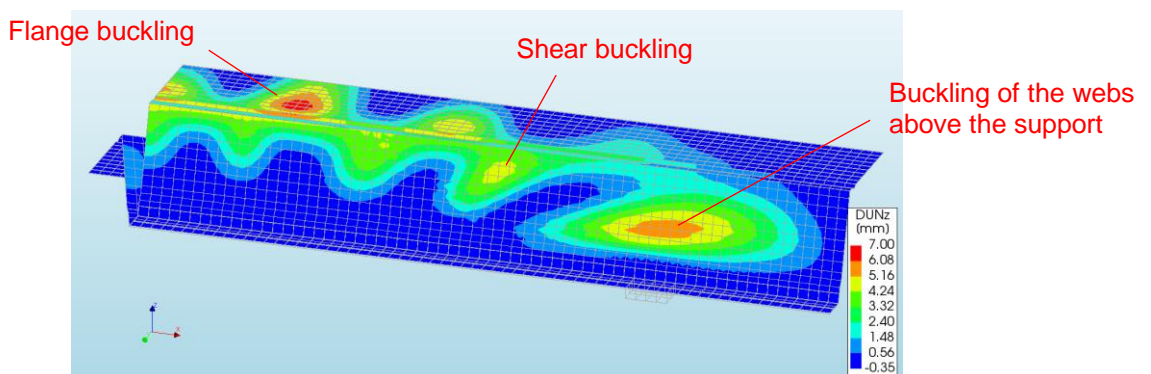
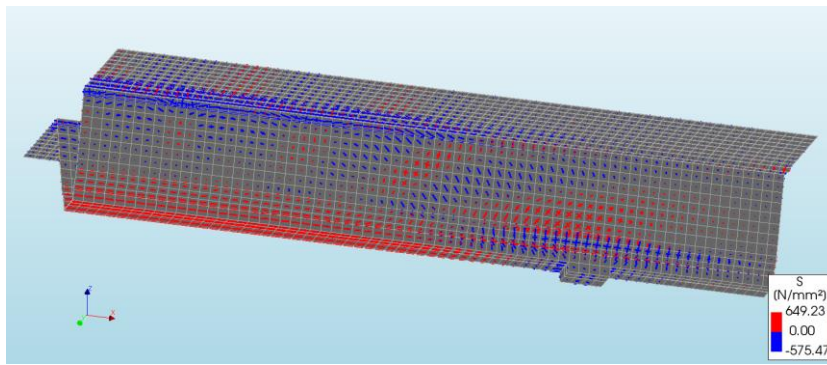
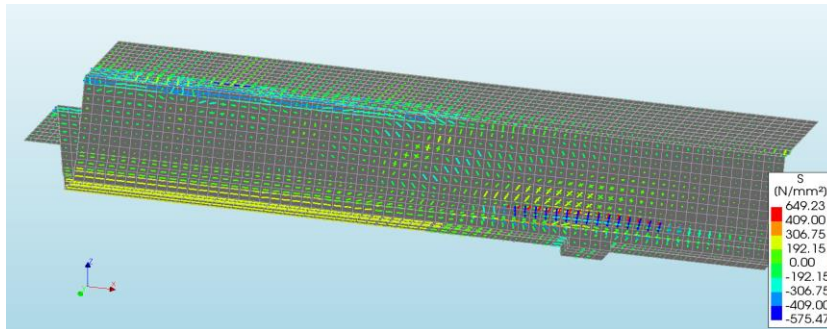


Figure 3.49 – Relative displacement of interface elements in local z-direction at maximum load

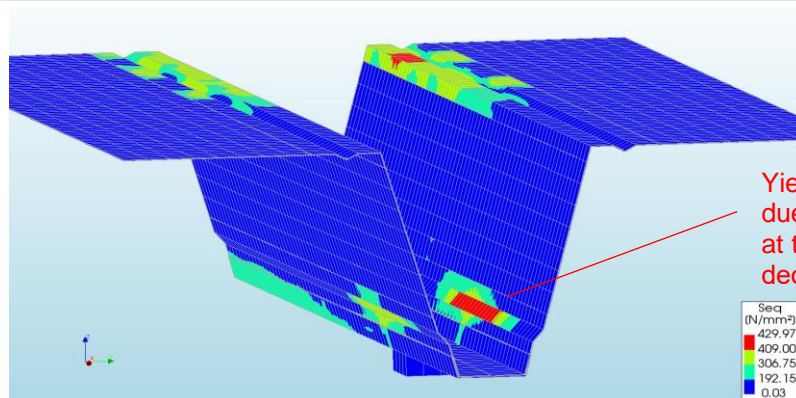
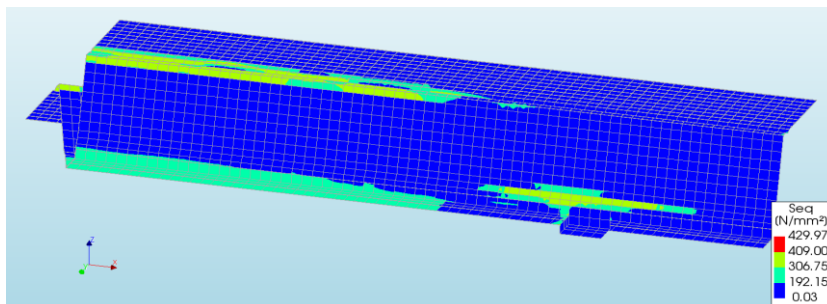


a) Blue is compression, red is tension



b) Discrete colour scale

Figure 3.50 – Principal stresses in steel deck at maximum load (stresses at the outer surfaces of the elements)



Yielding above support due to very local bending at this kink in the steel deck's webs

Figure 3.51 – Von Mises stresses in steel deck at maximum load (values in integration points of elements)

In former section 3.3, it is mentioned that shear buckling isn't expected to occur when considering the transverse shear capacity of ComFlor 210. This statement is based on the stress distribution in the steel deck's webs during failure of the composite slab in the FEA (Figure 3.35). However, by changing the interface properties of the finite element model, it is shown that the steel deck becomes more

susceptible to local buckling, including shear buckling of the webs. So, the interface behaviour plays an important role for this local buckling of the steel deck. Of course, when the steel deck can't separate from the concrete at the interface, like in the FEA of section 3.3, local buckling of the steel deck becomes nearly impossible: the steel deck first has to detach from the concrete by reaching the concrete's tensile strength in the elements close to the interface. Therefore, the inclusion of this no-tension relationship for the interface elements in local z-direction makes it easier for the steel deck's webs to buckle. In addition, due to the chosen interface properties, it can be assumed that only function of the steel deck's webs is to resist a part of the transverse shear force. When there are no other factors that influence the stress distribution in the steel deck's webs (like cracking in the concrete for instance), it may give that the steel deck becomes more susceptible to shear buckling as well. However, regarding the observed buckling behaviour of the steel deck, it may be question whether the finite element model accurately covers this. It has been explained in section 3.3.1 that reduced material properties have been applied to the parts of the steel deck with embossments. But, when considering local buckling of these parts, it is expected that the embossments give an increased resistance due to the actual geometry: the moment of inertia for out-of-plane bending is increased by the embossments.

4. DISCUSSION

- How big is the transverse shear capacity of the concrete section and how does this relate to the current Eurocode 2: Concrete structures (EN 1992)?

As explained, the transverse shear capacity of a composite slab according to the Eurocode 4 is only determined by its concrete part. The Eurocode 4 (composite structures) prescribes that the calculation procedures of Eurocode 2 (concrete structures) should be used when it comes to the transverse shear resistance of the total composite slab. Nothing is mentioned about the potential influence of the steel deck. So, for calculation of the transverse shear capacity of the composite slab, only the resistance provided by the concrete section is being considered. For that reason, the first point of interest is to validate the calculation procedures of Eurocode 2 for the transverse shear resistance of this concrete section. The formulas that are provided by the Eurocode 2 are empirically derived for reinforced concrete members, which generally have a different lay-out compared to the concrete ribs in deep composite slabs.

In section 3.2, the results of the FEA of the concrete section have been discussed. Applying a $\varnothing 24$ mm bar as rib reinforcement resulted in transverse shear failure of the finite element model for every analysed shear slenderness ratio a_v/d . This rebar diameter may be rarely applied in practice (for deep composite slabs), but it has been used in the FEA to make sure that bending failure didn't become decisive, as this was the case with a $\varnothing 12$ mm rebar. The reinforcement ratio ρ_l of the finite element model can be calculated at $0.0345 (= 0.25\pi \cdot \varnothing^2 / (b_w \cdot d))$ when using a $\varnothing 24$ mm rebar. According to the Eurocode 2, only a maximum reinforcement ratio ρ_l of 0.02 is allowed to use in calculation of the transverse shear capacity. Therefore, instead of doubling the rebar diameter like done in the FEA, it may had been better to double the reinforcement ratio ρ_l in order to control this parameter a bit more.

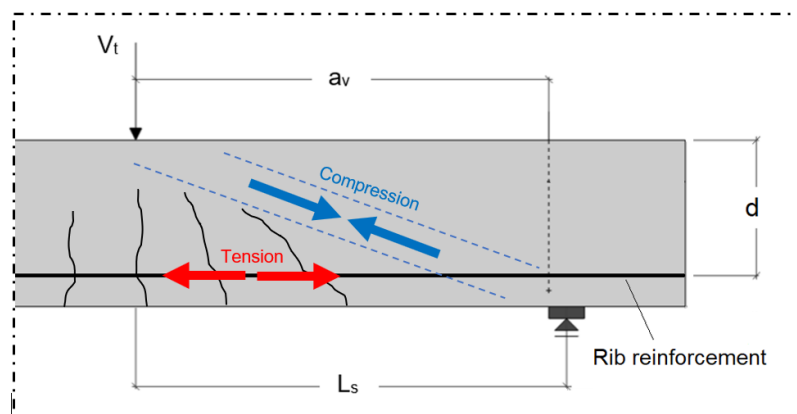
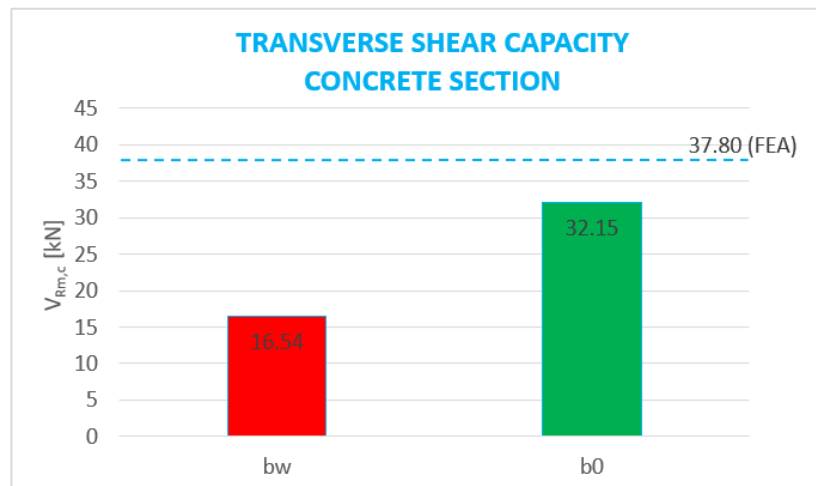


Figure 4.1 – Direct transfer of the load to the support by this compressive strut in the concrete rib

The results of the FEA clearly showed that the effect of direct load transfer must be excluded for accurate determination of the transverse shear capacity of the concrete element. The load shouldn't be too close to the support, so that the beneficial effect of this arising arch-like structure (concrete compressive strut and tensile rib reinforcement) in the concrete element is eliminated. This is shown in Figure 4.1. For that reason, the shear slenderness ratio a_v/d (or shear span L_s) should be bigger than a certain limit value. Using a shear slenderness ratio of 3.0 resulted in a transverse shear capacity of 43.11 kN. The analysis with a shear slenderness ratio of 3.5 gave a lower capacity of 37.80 kN. So, it

may be established that there is still some dependency of the transverse shear capacity on the shear slenderness ratio a_v/d for values bigger than 3.0.

When following the procedures of Eurocode 2, the transverse shear capacity can be calculated at 16.54 kN for the analysed cross-section (one concrete rib of ComFlor 210). This is not even half of the lowest found value in the FEA (37.80 kN). As mentioned before, the reinforcement ratio ρ_l of the analysed cross-section is equal to 0.0345, but only a maximum value of 0.02 may be used in the calculation according to the Eurocode 2. However, when this limitation is neglected and the actual reinforcement ratio (0.0345) is used to calculate the transverse shear capacity, a resistance of 19.84 kN is obtained (instead of 16.54 kN). This is still far below the found capacity in the FEA. Therefore, it is proposed to change the Eurocode’s calculation method by adjusting the effective width that is used in calculation of the transverse shear capacity of the concrete rib. According to the Eurocode 2, only the smallest width in the tensile area b_w can be used. In analogy to Stark[18] and Pereira et al.[17], it is proposed to use the mean width of the concrete rib b_0 . This gives a calculated resistance of 32.15 kN, which makes a much better prediction when being compared to the FEA results of this thesis. This is illustrated in Figure 4.2. Furthermore, using the mean width b_0 of the concrete rib also gives that the reinforcement ratio ρ_l now can be calculated at $0.0167 (= 0.25\pi \cdot \varnothing^2 / (b_0 \cdot d))$, which is below 0.02.



$$V_{Rm,c} = C_{Rm,c} k (100 \rho_l f_{cm})^{\frac{1}{3}} (b_w \text{ or } b_0) d \geq 0.035 k^{\frac{3}{2}} f_{cm}^{\frac{1}{2}} (b_w \text{ or } b_0) d$$

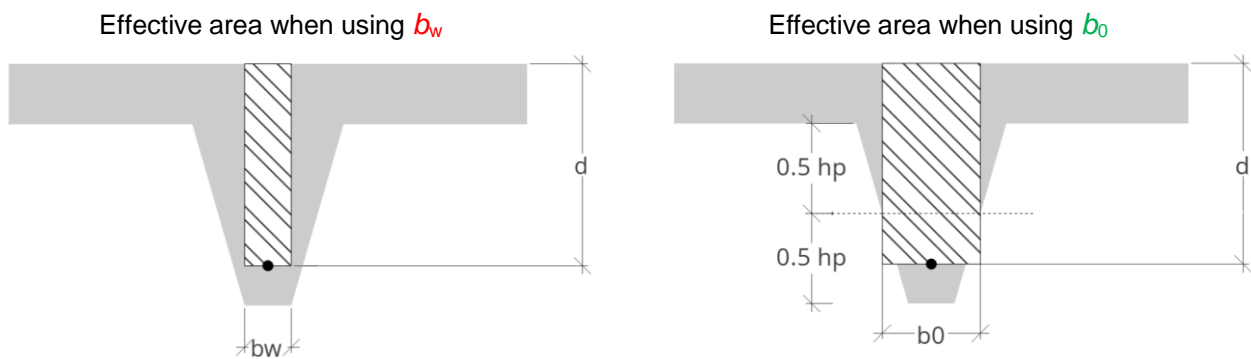


Figure 4.2 – Calculated transverse shear capacity of the concrete rib vs. FEA result

- What is the influence of the steel deck on the transverse shear capacity and how does this relate to the current Eurocode 4: Composite structures (EN 1994)?

After verification of the transverse shear capacity of the concrete section, the steel deck has been added to the finite element model to determine its influence on this capacity. Two different FEA’s of

ComFlor 210 have been executed, of which the results are described in section 3.3 and 3.4. From both analyses it can be concluded that the steel deck does give a significant improvement of the transverse shear capacity. However, due to the complexity of the problem and the strong non-linear behaviour of the composite slab, it is difficult to give an exact explanation for the improvement. Still, 3 main factors can be distinguished which give reasons for the increase in transverse shear capacity:

- Steel deck acting as reinforcement to the concrete like stirrups;
- Steel deck acting as reinforcement to the concrete like longitudinal rebars;
- Steel deck being able to resist a part of the transverse shear force in its webs.

The above-mentioned factors will be discussed separately.

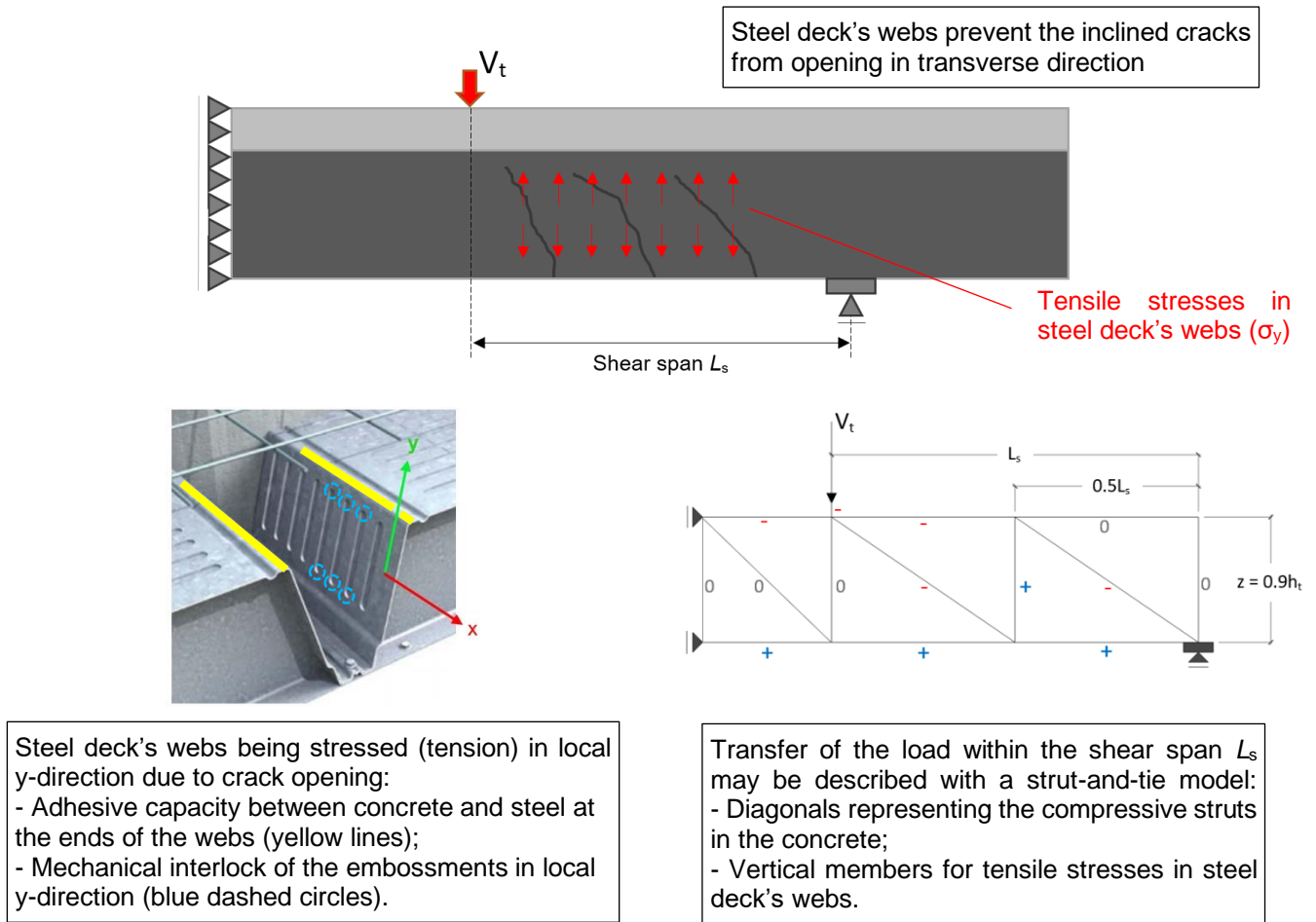


Figure 4.3 – Stirrup-functioning of steel deck's webs in deep composite slabs

It has been explained in section 3.3.3 that the steel deck's webs have the potential to reinforce the concrete in a similar way as stirrups. This means that vertical opening of the inclined cracks (in global z-direction) is restrained by tensile stresses σ_y in the steel deck's webs in local y-direction. This is shown in Figure 4.3. However, for the steel deck's webs to effectively restrain the crack opening this way, the interface behaviour becomes very important. Either the ends of the webs should be connected to the concrete (as has been the case in the FEA of 3.3: no separation at the interface), or the embossments in the webs should restrain the slip in this local y-direction due to the local mechanical interlock. Assuming that these conditions are satisfied, then the load-transferring mechanism in the deep composite slab may be approached with a strut-and-tie model like proposed in Figure 4.3. The validity of this strut-and-tie model for the transverse shear resistance of the deep composite slab haven't been confirmed in this thesis. Before further elaboration of the model, it should mainly become clear whether

this stirrup-functioning of the steel deck's webs is representative for the actual transverse shear behaviour of deep composite slabs. More knowledge should be gained on how to accurately describe the interface behaviour in the multiple directions (local x-, y- and z-direction).

As explained in section 3.3.1, due to the orientation of the embossments in the steel deck, it is assumed that the slip at the interface is mainly restrained in the longitudinal direction. So, due to the composite behaviour, opening of the cracks in the concrete is restrained by the steel deck in this direction (shown in Figure 4.4). The tensile stresses that are released from the cracks are transferred to the steel deck. The steel deck may be considered to reinforce the concrete in a similar way as the rib reinforcement. Evaluating the Eurocode's formula for calculation of the transverse shear resistance of the bare concrete section (rib), it can be established that the resistance is increased for bigger reinforcement ratios ρ_l . So, assuming that the reinforcement ratio ρ_l is increased by the steel deck, leads to an increase in transverse shear resistance according to this formula. Therefore, the steel deck is likely to provide additional transverse shear resistance this way.

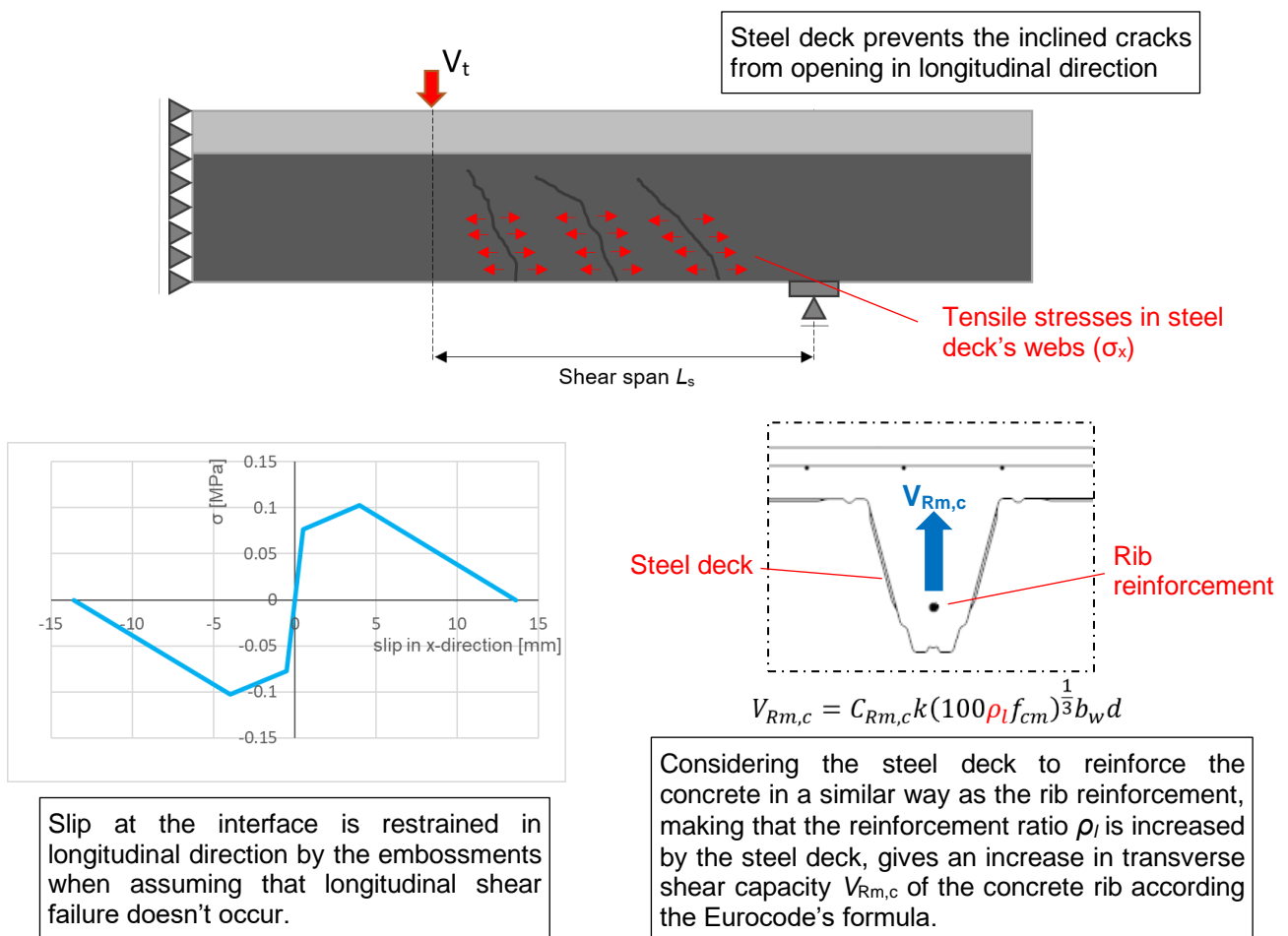


Figure 4.4 – Steel deck acting as reinforcement in longitudinal direction

In the foregoing, the steel deck is considered to act as reinforcement to the concrete, which causes the transverse shear capacity to increase. In addition, the steel deck can be assessed as separate structural element as well, being able to carry a part of the load. Due to shape of the profile, the steel deck can resist a part of the transverse shear force in its webs as shown in Figure 4.5. Since the concrete section can't move through the steel deck at the interface, both elements are being stressed by the external load due to the combined deflection of the concrete and the steel deck. With a part of the load being carried by the steel deck's webs, it makes that the transverse shear resistance is increased by the steel deck.

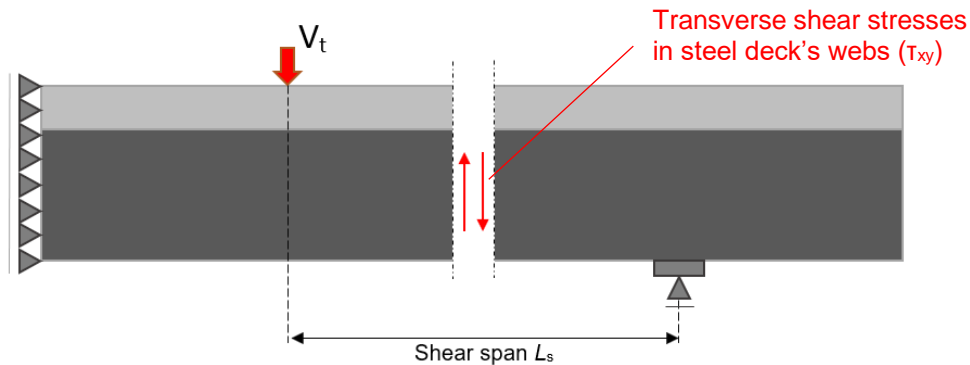


Figure 4.5 – Transverse shear stresses in steel deck’s webs

According to the FEA of ComFlor 210 in section 3.3, the steel deck provides a minimal increase in transverse shear capacity of 56.75 kN per rib (can even be higher). In the FEA, the steel deck and concrete couldn’t separate from each other and a more or less realistic longitudinal shear behaviour had been implemented. Therefore, it can be assumed that all of the mentioned factors (Figure 4.3 - Figure 4.5) have played a role in this big increase in transverse shear capacity of 131.6% with respect to the resistance of the concrete section. However, especially because of the doubt whether this stirrup-functioning of the webs (Figure 4.3) is valid for the transverse shear behaviour of deep composite slabs, a second FEA has been executed as described in section 3.4. Due to the bad interface properties in this later FEA of ComFlor 210, the first two factors (Figure 4.3 and Figure 4.4) are no longer valid. Still, an increase in transverse shear capacity of 22.16 kN has been found. So, even when the composite behaviour between the steel deck and concrete is bad, meaning that the steel deck isn’t effectively reinforcing the cracks, the steel deck provides an increase in transverse shear capacity of 51.4%. Therefore, the presence of these big webs in deep composite slabs is considered to be an important factor for the transverse shear capacity, as the webs resist a part of the transverse shear force.

So, for the transverse shear capacity of deep composite slabs, the following may be established:

- When the composite behaviour between the concrete and the steel deck is neglected, then the additional transverse shear resistance provided by the steel deck solely depends on the webs being able to resist a part of the transverse shear force (Figure 4.5). According to the FEA of ComFlor 210, the steel deck provides an additional 22.16 kN per rib in this case, which is equivalent to an increase of 51.4% in transverse shear capacity with respect to the resistance of the bare concrete section.
- When considering that the composite behaviour in longitudinal direction is guaranteed by the embossments, it may be expected that the transverse shear capacity of the composite slab is increased because of the beneficial effect of the steel deck reinforcing the cracks in longitudinal direction (Figure 4.4).
- When the interface behaviour between the concrete and steel deck is such, that the steel deck’s webs are not only restraining the crack opening in longitudinal direction, but also in transverse direction, then the transverse shear capacity becomes significantly bigger. The effectiveness of the load being transferred by compressive struts in the concrete and tensile stresses in the steel deck’s webs seems to be the main reason for this (Figure 4.3).
- How to calculate the transverse shear capacity of deep composite slabs?

With the Eurocode 4 failing in providing an adequate calculation method for the transverse shear capacity of deep composite slabs, it is tried to come up with an appropriate replacement. The FEA of

this thesis will therefore be compared to three other models as described in the literature review: Stark[18], Pereira et al.[17] and Hartmeyer & Kurz[27]. All these models are based on the same assumption that, for engineering’s purposes, the total transverse shear capacity of the composite slab should be calculated by adding the partial transverse shear resistances of the concrete section and the steel deck. Comparison of the models with the FEA result of section 3.4 is given in Figure 4.6 (for calculations, see Appendix D).

It has been chosen to compare the calculation models with the FEA result of section 3.4, because this is the most conservative one. Due to the bad composite behaviour in this analysis, the steel deck could only provide additional transverse shear resistance to the concrete by resisting a part of the transverse shear force in its webs. Because of the non-realistic interface properties, it can be doubted whether the executed FEA is representative for the actual transverse shear behaviour of the composite slab. However, for accurate assessment of the transverse shear capacity of ComFlor 210 by means of FEA, more detailed information about the interface behaviour is needed. The FEA of ComFlor 210 in section 3.3 contained a more realistic longitudinal slip behaviour, but due to the assumption that the steel deck and concrete couldn’t detach from each other, it may have given an overestimation of the transverse shear capacity.

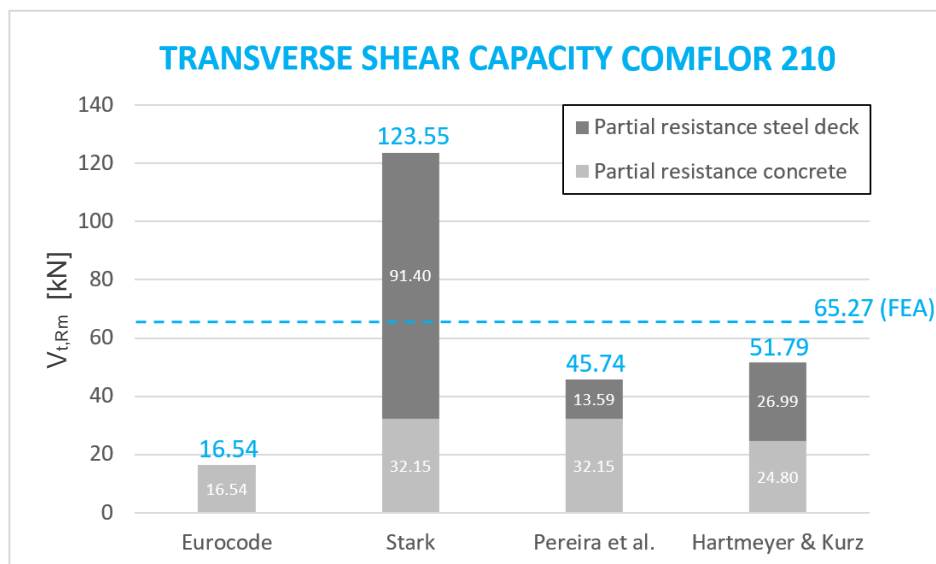


Figure 4.6 – Comparison of different calculation models with the FEA result of section 3.4 (capacity in kN for one rib of ComFlor 210)

The transverse shear capacity according to the Eurocode 4 is also given in Figure 4.6, from which it is easy to see that the standard is unnecessarily conservative. Considering the other models, it can be established that the model of Stark[18] overestimates the transverse shear capacity of the composite slab when being compared to FEA. The model gives a capacity of 123.55 kN, of which 91.40 kN is based on the partial resistance of the steel deck. This seems to be the main reason for overestimation of the capacity. The model supposes that the webs of the steel deck reach their full shear yield capacity before total failure of the composite slab, but this haven’t been observed in any of the analyses. In contrast to the model of Stark[18], the other two models do give a safe calculation procedure as shown in Figure 4.6. With the model of Pereira et al.[17], the partial resistance of the steel deck is significantly reduced (13.59 kN) when being compared to the model of Stark[18]. This is because the model of Pereira et al.[17] takes into account the effect of shear buckling of the steel deck’s webs, leading to a reduction in resistance. Although the model of Hartmeyer & Kurz[27] gives a slightly better prediction, it is considered to be less suitable as calculation method, because it requires test values for the partial

resistance of the steel deck. A value of 44.98 N/mm (resistance per width of the steel deck) has been used as mentioned in the report of Tuls[22]. So, it is recommended to use the model of Pereira et al.[17] as replacement for the procedures of the Eurocode 4, for the following reasons:

- With the Eurocode 4 (composite structures) lacking in detailed information about the transverse shear capacity of composite slabs, it may be established that it is simply not known how to correctly calculate it and to take into account the additional resistance that is provided by the steel deck. However, by combining the procedures of Eurocode 2 (concrete structures) and Eurocode 3 (steel structures) as proposed by Pereira et al.[17], a more accurate transverse shear capacity of ComFlor 210 can be calculated, while still being safe.
- For calculation of the partial transverse shear resistance of the concrete section ($V_{Rm,c}$), the model of Pereira et al.[17] uses the mean width of the concrete rib (b_0) instead of the smallest width (b_w). This has been confirmed by the FEA to give a better prediction.
- It is not perfectly clear whether shear buckling is an effect that needs to be accounted for. In section 3.4, it has been shown that the steel deck's webs may be susceptible to this kind of local buckling. But, due to the complex interface behaviour in real-life and/or the increased resistance against local buckling of the embossments, it may be that shear buckling will never be observed in experiments for deep composite slabs. However, since the model of Pereira et al.[17] does consider as reduced shear strength (f_{bv}) for the steel deck's webs to take into account the effect of shear buckling, it may be assessed as a safe method to use until there is more known about this aspect.

At last, it can be established that for both hogging and sagging bending moment conditions, the transverse shear capacity of ComFlor 210 is underestimated. Based on real experiments, Abspoel et al.[21] found a minimal value of 73.59 kN (one rib) for hogging bending moment conditions. In this thesis, a value of 65.27 kN is found for sagging bending moment conditions. The FEA that resulted in this capacity included very bad interface properties (section 3.4), from which it can be expected that in real life the transverse shear capacity of ComFlor 210 is even bigger. The dependency of the transverse shear capacity on this interface behaviour is clearly shown when comparing both FEA's of ComFlor 210 in section 3.3 and 3.4. As explained in the beginning of section 3.1, it was intended to analyse the exact same cross-section as in the research of Abspoel et al.[21]. However, in the FEA of the concrete section (section 3.2), the rib reinforcement diameter had to be increased to make sure that bending failure didn't become decisive. This adjustment has been continued in the rest of the thesis, making that considered cross-section in FEA of ComFlor 210 isn't completely in accordance with the research of Abspoel et al.[21]. However, due to this initial assumption, additional rebars were included in the top layer of the finite element model (in accordance with Abspoel et al.[21]). It may be established that this is quite unnecessary to do for sagging bending moment conditions and it is assumed that it hardly affects the transverse shear capacity in this case.

5. CONCLUSION

The current Eurocode 4 (composite structures) suggests that the transverse shear capacity of a composite slab solely depends on the resistance of its concrete section (i.e. concrete ribs). The standard simply refers to the calculation procedures of the Eurocode 2 (concrete structures), so that the transverse shear capacity of a composite slab is calculated according to this empirical formula which was originally derived for regular reinforced concrete members. No information is provided about the contribution of the steel deck to the transverse shear capacity of the composite slab, while the Eurocode 3 (steel structures) implies that this steel deck can resist a certain transverse shear force in its webs. Therefore, it is expected that the Eurocode 4 provides an unnecessarily conservative design principle for the transverse shear capacity of composite slabs. This expectation has been investigated for deep composite slabs in this thesis by means of non-linear finite element modelling. The finite element study was started with merely analysing the concrete section of ComFlor 210, after which the steel deck had been added to the finite element model to investigate its influence on the transverse shear capacity. When evaluating the FEA results, the following can be concluded:

- The empirical formula provided by the Eurocode 2 gives an inaccurate prediction of the transverse shear capacity of the concrete section (i.e. concrete ribs). Using the mean width of the concrete rib (b_0), instead of the minimum width in the tensile area (b_w), has proved to give a better prediction of the transverse shear capacity of this concrete section.
- The steel deck provides a minimum increase of 51.4% in transverse shear capacity for ComFlor 210, with respect to the resistance of its concrete section, because of the steel deck's webs being able to resist a part of the transverse shear force. When considering that the bonding at the interface will activate the reinforcing properties of the steel deck as well, this increase in transverse shear capacity is expected to become even bigger. This expectation is based on the observation in the FEA that when the steel deck acts as reinforcement to the concrete in both longitudinal direction (like rebars) and transverse direction (like stirrups), an increase of 131.6% in transverse shear capacity is obtained.
- The Eurocode 4 provides a too conservative calculation method for transverse shear capacity of ComFlor 210: a capacity of 16.54 kN can be calculated for the considered cross-section (one rib), while a capacity of 65.27 kN is found in the FEA as a lower bound value.
- The model of Pereira et al.[17], which simply combines the procedures of the Eurocode 2 and 3, gives a better prediction of the transverse shear capacity of ComFlor 210 (45.74 kN per rib), while still being safe compared to the FEA results of this thesis. Please notice that with respect to the Eurocode 2, the model does use the mean width of the concrete rib (b_0) instead of the minimum width (b_w), as mentioned in the first concluding remark.

Recommendations

From the FEA results, it is concluded that the Eurocode 2 gives inaccurate predictions for the transverse shear capacity of the concrete ribs. In trying to find a good calculation method for the total transverse shear capacity of the composite slab, this inaccuracy of the Eurocode 2 already seems a critical aspect. Therefore, it is recommended to start a second FEA program, as an extension to this thesis, which solely focusses on the transverse shear capacity of the concrete ribs. Varying the model parameters (like: compressive strength, rib reinforcement diameter, effective depth, etc.) should verify whether the

Eurocode 2 is inaccurate for every case and if the calculation procedure can be improved with the proposal of using b_0 instead of b_w (see chapter 4). The FEA program may be supported by real experiments.

Furthermore, more detailed information about the interface behaviour is necessary for the verification of the transverse shear capacity of deep composite slabs by means of FEA. The new constitutive relationships for the interface should include the following:

- The total slip restraining properties of the embossments: not only for the longitudinal direction (local x-direction), but also for the transverse direction (local y-direction);
- The effect of opening of the interface (in local z-direction) on the slip restraining properties of embossments (in local x- and y-directions).

At last, it may be established that the execution of real experiments is a must for verification of the transverse shear capacity of ComFlor 210. In the FEA, a lot of assumptions have been made to come to a finite element model, like the specification of the interface properties; the application of reduced material properties for the embossments and neglecting their actual geometry; not considering the local effects of cold forming, etc. These assumptions can only be validated with experiments.

Bibliography

- [1] Şamhâl, E. (2005). *Lecture 1.1: Composite Construction*. Retrieved from <https://web.itu.edu.tr/~haluk/COMPOSITE%201.pdf>
- [2] BCSA, Steel for Life, & SCI. (n.d.). *Composite construction*. Retrieved from https://www.steelconstruction.info/Composite_construction
- [3] CEN. (2004). *EN 1994-1-1, Eurocode 4: Design of composite steel and concrete structures - Part 1-1: General rules and rules for buildings*.
- [4] Dutch Engineering Raadgevend Ingenieurs Bureau B.V. (2013). *Staal-beton Vloersystemen*. Retrieved from https://www.dutchengineering.nl/media/vk_1198/files/67579_DutchEngineering_Brochure_Online.pdf
- [5] Toniolo, G. (2009). *Composite Slabs with Lightweight Concrete*. Retrieved from https://www.politesi.polimi.it/bitstream/10589/2347/1/2010_07_Penza.pdf
- [6] Hedao, N. A. and Gupta, L. M. (2008). State of the Art Report on Thin-walled Cold-formed Profiled Steel Decking. In ORG. Missouri University of Science and Technology (Ed.), *Nineteenth International Specialty Conference on Cold-Formed Steel Structures* (pp. 307–323).
- [7] SFIA. (n.d.). *How Cold-Formed Steel is Made*. Retrieved from <https://sfia.memberclicks.net/how-cold-formed-steel-is-made>
- [8] Stark, J. W. B., & Abspoel, R. (2010). *STEEL STRUCTURES 3, CT4121, Part: Cold Formed Sections*. Delft University of Technology.
- [9] Rackham, J. W., Couchman, G. H., & Hicks, S. J. (2009). *Composite Slabs and Beams using Steel Decking: Best Practice for Design and Construction (Revised Edition)*. The Metal Cladding & Roofing Manufacturers Association.
- [10] Simms, W. I., & Hughes, A. F. (2011). *Composite design of steel framed buildings, in accordance with Eurocodes and the UK National Annexes*. SCI.
- [11] Leskelä, M. V. (2017). *BEHAVIOUR AND DESIGN OF STEEL-CONCRETE COMPOSITE STRUCTURES*. Lahti: Peikko Group Corporation.
- [12] Schuurman, R. (2001). *Physical Behaviour of Shear Connections in Composite Slabs* (doctoral thesis, Delft University of Technology, The Netherlands). Retrieved from <http://resolver.tudelft.nl/uuid:75b035c6-bc9a-4d61-bbd4-8c82c8543572>
- [13] Abbas, H. S., Bakar, S. A., Ahmadi, M., & Haron, Z. (2015). Experimental studies on corrugated steel-concrete composite slab. *GRADEVINAR*, 67(3), 225-233. <https://doi.org/10.14256/JCE.1112.2014>
- [14] Diana FEA BV. (2019). DIANA Finite Element Analysis (10.3) [Software]. Retrieved from <https://dianafea.com/diana-downloads>
- [15] Johnson, R. P. (2004). *Composite Structures of Steel and Concrete: Beams, Slabs, Columns, and Frames for Buildings* (4e ed.). Oxford, United Kingdom: Wiley.
- [16] Van Erp, P. (2017). *Horizontal Shear Resistance of ComFlor 210* (Master's thesis, Delft University of Technology, The Netherlands). Retrieved from <http://resolver.tudelft.nl/uuid:613a4ebf-7d48-48f6-9c07-4a84fca028bc>
- [17] Pereira, M., Simões, R., & Duarte, J. (2017). ANALYSIS OF THE VERTICAL SHEAR DESIGN MODEL FOR STEEL-CONCRETE COMPOSITE SLABS. *ce/papers*, 1(4), 405-414. <https://doi.org/10.1002/cepa.540>
- [18] Stark Partners. (2012). *VERTICAL SHEAR RESISTANCE OF COMPOSITE FLOORS WITH ComFlor 60 (EVALUATION OF TESTS REPORTED IN SPO/ICON-RT-11-10-VO1 (IMPERIAL COLLEGE))*.
- [19] Popo-Ola, S. O. (2012). *Test Report on Shear Line Load Tests on Composite Slabs with CF60 Decking* (Report nr. SPO/ICON-RT-11-10-V01). London, United Kingdom: Imperial College.

- [20] ABNT. (2008). *ABNT NBR 8800, Projeto de estruturas de aço e de estruturas mistas de aço e concreto de edifícios*. Rio de Janeiro: Associação Brasileira de Normas Técnicas.
- [21] Abspoel, R., Stark, J., & Prins, H-J. (2018). The influence of vertical shear on the hogging bending moment resistance of ComFlor composite slabs. In V. Albero, A. Espinos, C. Ibabez, A. Lapuebla, & M. L. Romero (Eds.), *Proceedings 12th international conference on Advances in Steel-Concrete Composite Structures - ASCCS 2018* (pp. 183-190). Valencia, Spain: Universitat Politecnica de Valencia. <https://doi.org/10.4995/ASCCS2018.2018.7056>
- [22] Tuls, J. J. (2017). *Influence of a Vertical shear Force on the Hogging Bending Moment Resistance in Composite Slabs* (Master's thesis, Delft University of Technology, The Netherlands). Retrieved from <http://resolver.tudelft.nl/uuid:21663b9c-2840-485a-bc36-b039ad71ef5a>
- [23] Tata Steel. (2017). *ComFlor® manual: composite floor decking design and technical information*. Retrieved from https://www.tatasteelconstruction.com/static_files/Tata%20Steel/content/products/Building%20Systems/Comflor/ComFlor%20manual.pdf
- [24] CEN. (2004). *EN 1992-1-1, Eurocode 2: Design of concrete structures - Part 1-1: General rules and rules for buildings*.
- [25] CEN. (2006). *EN 1993-1-3, Eurocode 3 - Design of steel structures - Part 1-3: General rules - Supplementary rules for cold-formed members and sheeting*
- [26] CEN. (1992). *ENV 1994-1-1, Eurocode 4: Ontwerp en berekening van staal-betonconstructies - Deel 1-1: Algemene regels en regels voor gebouwen*
- [27] Hartmeyer, S., & Kurz, W. (2013). Evaluation of the Shear Force Behaviour of Composite Slabs. In Bradford, M. & Uy, B. (Eds.), *Composite Construction in Steel and Concrete VII - Proceedings of the 2013 International Conference on Composite Construction in Steel and Concrete* (pp. 731-742). Reston, Virginia: American Society of Civil Engineers. Retrieved from <https://app.knovel.com/hotlink/pdf/id:kt010XWGGC/composite-construction/evaluation-shear-force>
- [28] Yang, Y. (2014). *Shear behaviour of reinforced concrete members without shear reinforcement: A new look at an old problem* (doctoral thesis, Delft University of Technology, The Netherlands). <https://doi.org/10.4233/uuid:ac776cf0-4412-4079-968f-9each67e8846>
- [29] Rombach, G., & Henze, L. (2017). Shear Capacity of Concrete Slabs Without Shear Reinforcement Under Concentrated Loads Close to Support. In D. A. Hordijk, & M. Luković (Eds.), *High Tech Concrete: Where Technology and Engineering Meet* (pp. 676–683). https://doi.org/10.1007/978-3-319-59471-2_80
- [30] CEN. (2005). *EN 1993-1-1, Eurocode 3: Design of steel structures - Part 1-1: General rules and rules for buildings*.
- [31] Stark, J. & Stark, R. (2009). *Staal-Beton: toepassing en berekening van staal-beton constructies voor gebouwen volgens Eurocode 4 bij normale temperatuur en brand*. Delft: Bouwen Met Staal.
- [32] Tata Steel. (n.d.). ComFlor Steel Composite Metal Deck Design Software (v9.0.34) [Software]. Retrieved from https://www.tatasteelconstruction.com/en_GB/Products/structural-buildings-and-bridges/Composite-floor-deck/Comflor%C2%AE-Active
- [33] Tuladhar, R. (2014). Shear failure of RC beam [photo]. Retrieved from <https://i.ytimg.com/vi/zn3-VM9Eurw/maxresdefault.jpg>
- [34] Veljković, M. (1996). *BEHAVIOUR AND RESISTANCE OF COMPOSITE SLABS: Experiments and Finite Element Analysis* (doctoral thesis, Luleå University of Technology, Sweden).
- [35] Ríos, J. D., Cifuentes, H., Martínez-De La Concha, A., & Medina-Reguera, F. (2017). Numerical modelling of the shear-bond behaviour of composite slabs in four and six-point bending tests. *Engineering Structures*, 133, 91–104. <https://doi.org/10.1016/j.engstruct.2016.12.025>
- [36] Braam, C. R., Lagendijk, P., & Dees, W. C. (2011). *Constructie leer Gewapend Beton*. Boxtel, the Netherlands: Aeneas.
- [37] Composite Profiles UK. (2018). comflor-decking [photo]. Retrieved from <https://www.compositeuk.com/services-solutions/comflor-metal-decking/>
- [38] CEN. (2015). *EN 10346, Continuously hot-dip coated steel flat products for cold forming - Technical delivery conditions*.

Appendix A

Shear buckling strength of steel decks used in composite slabs

Due to shearing of a steel deck's web, compressive and tensile stresses arise in the diagonal directions (principal directions). This is illustrated in Figure A.1. These compressive stresses can lead to local buckling, because of the thinness of the web. This phenomenon is known as shear buckling.

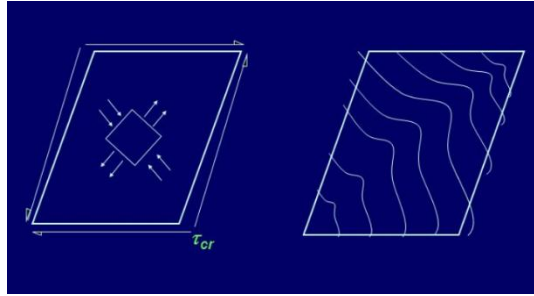


Figure A.1 – Shear buckling of a plate

For considering the effect of shear buckling on the transverse shear resistance of a steel deck, the Eurocode 3 introduces a shear buckling strength f_{bv} . The determination of this strength parameter is prescribed in clause 6.1.5 of EN 1993-1-3[25]. All the following information is directly copied from the mentioned standard.

Table 6.1: Shear buckling strength f_{bv}

Relative web slenderness	Web without stiffening at the support	Web with stiffening at the support ¹⁾
$\bar{\lambda}_w \leq 0,83$	$0,58 f_{yb}$	$0,58 f_{yb}$
$0,83 < \bar{\lambda}_w < 1,40$	$0,48 f_{yb} / \bar{\lambda}_w$	$0,48 f_{yb} / \bar{\lambda}_w$
$\bar{\lambda}_w \geq 1,40$	$0,67 f_{yb} / \bar{\lambda}_w^2$	$0,48 f_{yb} / \bar{\lambda}_w$

¹⁾ Stiffening at the support, such as cleats, arranged to prevent distortion of the web and designed to resist the support reaction.

(2) The relative web slenderness λ_w should be obtained from the following:

- for webs without longitudinal stiffeners:

$$\bar{\lambda}_w = 0,346 \frac{s_w}{t} \sqrt{\frac{f_{yb}}{E}} \quad \dots (6.10a)$$

- for webs with longitudinal stiffeners, see figure 6.5:

$$\bar{\lambda}_w = 0,346 \frac{s_d}{t} \sqrt{\frac{5,34 f_{yb}}{k_\tau E}} \quad \text{but} \quad \bar{\lambda}_w \geq 0,346 \frac{s_p}{t} \sqrt{\frac{f_{yb}}{E}} \quad \dots (6.10b)$$

with:

$$k_\tau = 5,34 + \frac{2,10}{t} \left(\frac{\Sigma I_s}{s_d} \right)^{1/3}$$

where:

I_s is the second moment of area of the individual longitudinal stiffener as defined in 5.5.3.4.3(7), about the axis a – a as indicated in figure 6.5;

s_d is the total developed slant height of the web, as indicated in figure 6.5;

s_p is the slant height of the largest plane element in the web, see figure 6.5;

s_w is the slant height of the web, as shown in figure 6.5, between the midpoints of the corners, these points are the median points of the corners, see figure 5.1(c).

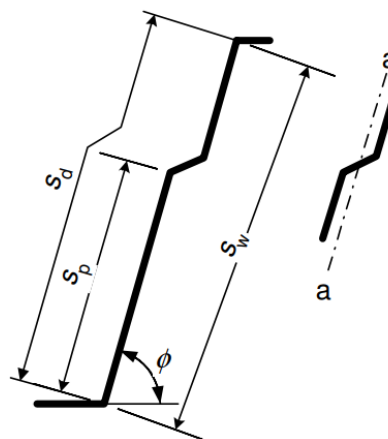
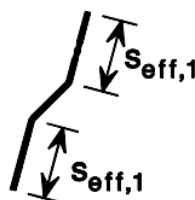


Figure 6.5: Longitudinally stiffened web

Definition of I_s in clause 5.5.3.4.3(7):

I_s is the second moment of area of a stiffener cross-section comprising the fold width s_{sa} and two adjacent strips, each of width $s_{eff,1}$, about its own centroidal axis parallel to the plane web elements, see figure 5.13. In calculating I_s the possible difference in slope between the plane web elements on either side of the stiffener may be neglected;



Cross-section for determining I_s

More information on how to determine $s_{eff,1}$ can be found in EN 1993-1-3[25].

With the procedure as described above, it is possible to determine the shear buckling strength of ComFlor 210. The required dimensions of the webs are shown in Figure A.2 and Figure A.3. These figures correspond to the finite element model of this thesis.

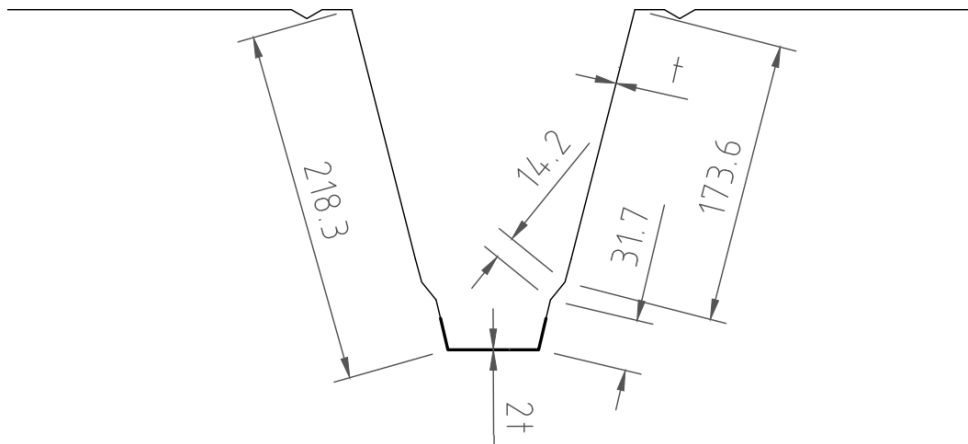


Figure A.2 - Dimensions of ComFlor 210 as applied in the FEA (unit: mm)

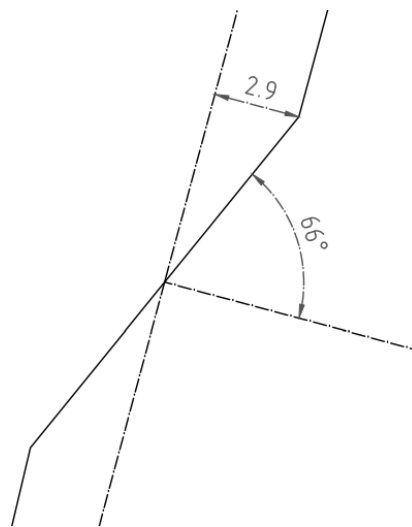


Figure A.3 - Stiffener (web, unit: mm)

The calculation of f_{bv} for ComFlor 210 is shown below, with $f_y = 409$ MPa and $E = 210000$ MPa.

$$s_{eff,1} = 0.76t\sqrt{E/(\gamma_{M0}\sigma_{com,Ed})} = 0.76 \cdot 0.96 \cdot \sqrt{\frac{210000}{409}} = 16.5 \text{ mm}$$

$$I_s = \frac{14.2 \cdot 0.96}{12} (14.2^2 \cos^2 66^\circ + 0.96^2 \sin^2 66^\circ) + 2 \cdot 16.5 \cdot 0.96 \cdot 2.9^2 = 305.19 \text{ mm}^4$$

$$k_\tau = 5.34 + \frac{2.10}{0.96} \left(\frac{305.19}{31.7+14.2+173.6} \right)^{\frac{1}{3}} = 7.78$$

$$\lambda_w = 0.346 \cdot \frac{31.7+14.2+173.6}{0.96} \cdot \sqrt{\frac{5.34}{7.78} \cdot \frac{409}{210000}} = 2.89 > \lambda_w = 0.346 \cdot \frac{173.6}{0.96} \cdot \sqrt{\frac{409}{210000}} = 2.76$$

$$f_{bv} = 0.67 \cdot \frac{409}{2.89^2} = 32.8 \text{ MPa}$$

Appendix B

Calculation of the overhang L_o as used in the FEA

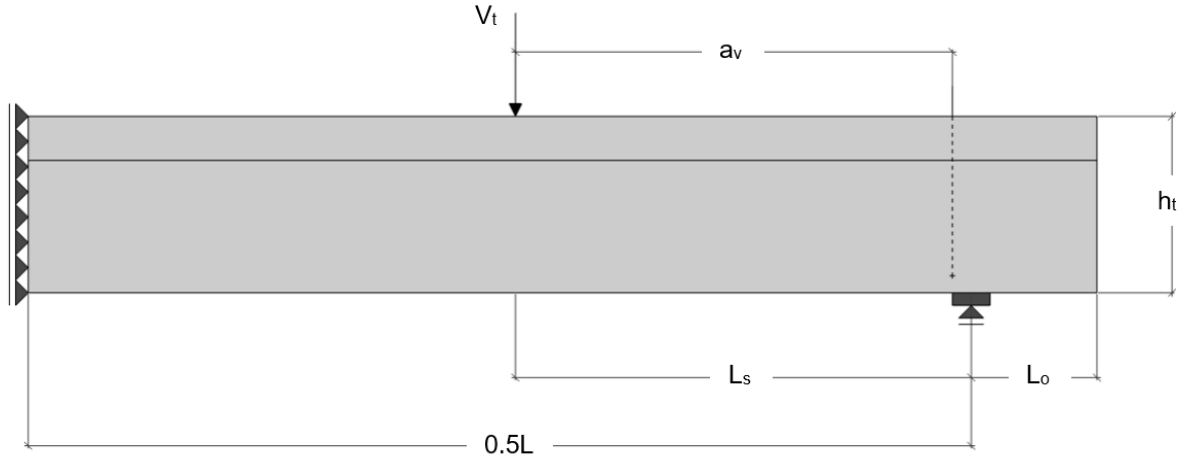


Figure B.1 – Test setup of the FEA (side view)

It has been chosen to include an overhang length L_o which is bigger than $l_{bd} + d$. The value for l_{bd} can be determined by using clause 8.4.3 and 8.4.4 of EN 1992-1-1[24]:

$$l_{bd} = \alpha_1 \alpha_2 \alpha_3 \alpha_4 \alpha_5 l_{b,rqd} \geq l_{b,min} \quad \text{B.1}$$

$$l_{b,rqd} = \frac{\sigma_{sd}}{4 f_{bd}} \quad \text{B.2}$$

$$l_{b,min} = \max\{0.3l_{b,rqd}; 10\phi; 100\text{mm}\} \quad \text{B.3}$$

From equation B.2 it can be seen that $l_{b,rqd}$ is dependent on the stress level in the reinforcement σ_{sd} at the section from where the anchorage length is considered. If we consider the anchorage length from the support, it may be established that σ_{sd} is equal to zero, since the bending moment and normal force are also equal to zero at this location. This makes that $l_{b,rqd}$ is also equal to zero, meaning that the value for l_{bd} (equation B.1) is equal to $l_{b,min}$ (equation B.3). Using a diameter of 12 mm gives $l_{b,min} = 120$ mm and $l_{bd} \geq 120$ mm. Consequently, the summation of l_{bd} and d is equal to $120 + (280 - 40 - 6) = 354$ mm. Therefore, a value of 355.0 mm has been applied for L_o . This value is kept constant throughout the whole thesis.

Appendix C

Determination of the bond-slip behaviour for the FEA of ComFlor 210

As explained at the end of section 3.3.1, the bond-slip behaviour of the interface in longitudinal direction contains 3 different linear branches. The diagram as applied in the FEA is given in Figure C.1. Derivation of the corresponding values of the diagram is given below.

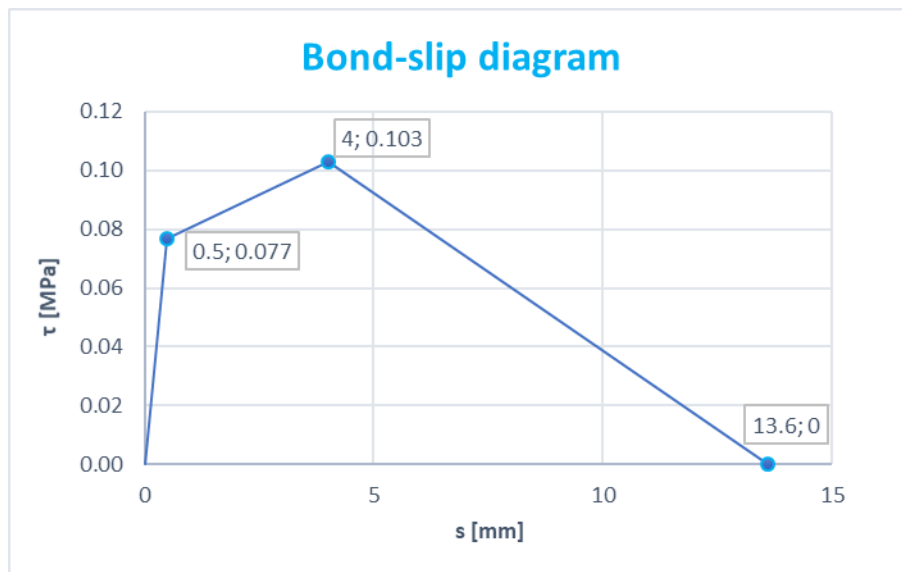


Figure C.1 - Bond-slip behaviour for local x-direction of interface elements

In section 2.4, it has been mentioned that Van Erp[16] found an average value of 0.103 MPa for the bond strength of the interface based on his experiments on ComFlor 210. Although this thesis doesn't follow his recommendation on using an effectiveness of 12.5% for the embossments (thickness reduction), this ultimate strength value of 0.103 MPa for the interface has still been used. Figure C.2 shows 3 typical load-displacement curves of experiments by Van Erp[16], with corresponding slip diagrams in Figure C.3. From these slip diagrams, it can be estimated that failure occurs at a slip value of approx. 4 mm. This value has been determined by averaging the slip that occurs from starting point to failure (most right vertical red lines in Figure C.3), for all measure points in every specimen. From the load-displacement curves in Figure C.2, it can be established that large non-linear behaviour starts at approx. 75% of the ultimate failure load. The final value of the first linear branch in Figure C.1 is therefore estimated at $0.75 \cdot 0.103 = 0.077$ MPa. The corresponding slip value is again determined from the diagrams in Figure C.3: the average value of slip, from starting point up till the most left red vertical lines, is estimated at 0.5 mm. The descending part of Figure C.1 is the least important for the FEA, since it is not demanded to simulate longitudinal shear failure. The recommendations by Ríos et al.[35] have been followed to describe this part of the bond-slip diagram.

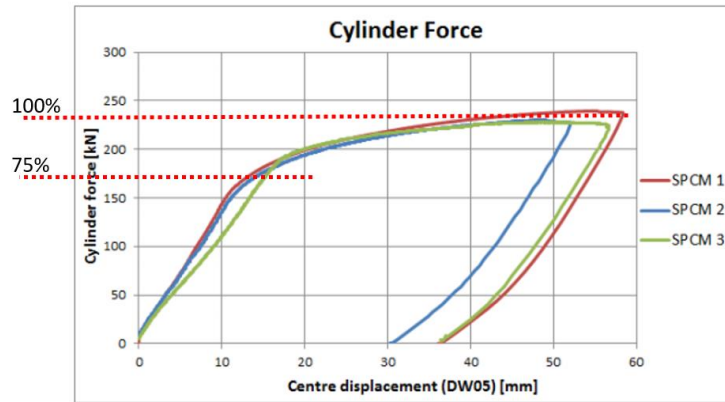
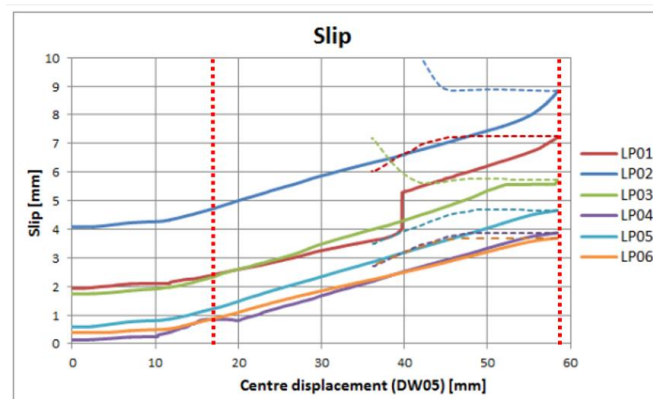
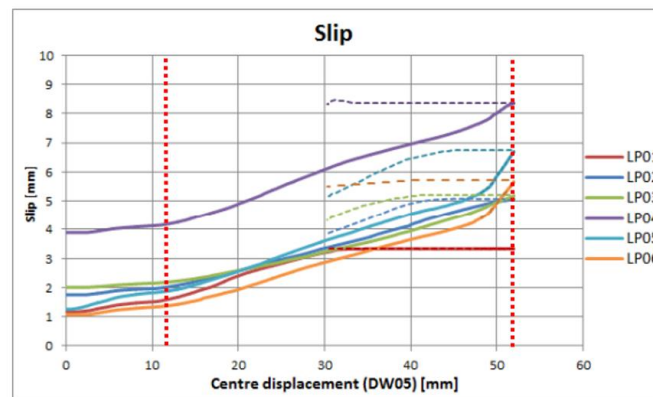


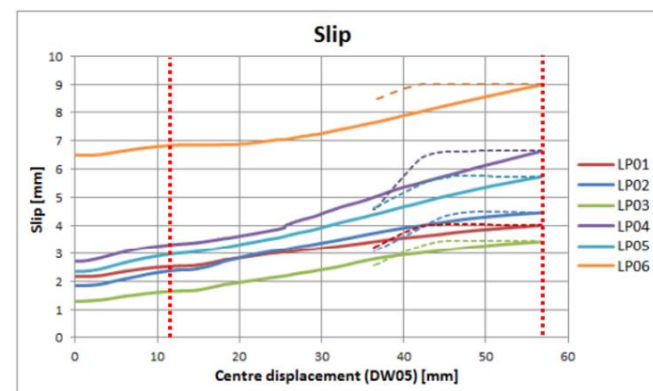
Figure C.2 – Typical load-displacement curves of experiments by Van Erp[16]



SPCM 1



SPCM 2



SPCM 3

Figure C.3 – Slip diagrams for the 3 different specimens (6 measure points per specimen)[16]

Appendix D

Transverse shear capacity of composite slabs according Eurocode 4 and literature

In this appendix, the calculations for the transverse shear capacity according to 4 different models will be given: Eurocode 4, Stark[18], Pereira et al.[17] and Hartmeyer & Kurz[27] (see chapter 2). Most calculations have been done in an Excel spreadsheet.

Eurocode 4

Input				Notes
$C_{Rm,c}$	0.15			Empirical coefficient
h_t	280 mm			Overall thickness of test specimen
e	46 mm			Distance centroidal axis rib reinforcement relative to the bottom
\varnothing	24 mm			Diameter rib reinforcement
b_w	56 mm			Smallest width of the cross-section in the tensile area
f_{cm}	41.8 MPa			Mean concrete compressive strength
Output				Notes
A_{sl}	452.3893 mm ²			Total area of the tensile reinforcement
d	234 mm			Effective depth of the slab
k	1.9245	<2.0	1.9245	Size factor = $\min(1 + \sqrt{200/d} ; 2.0)$
ρ_l	0.034523	<0.02	0.02	Longitudinal reinforcement ratio = $\min(A_{sl}/(b_w*d) ; 0.02)$
$V_{Rm,c}$	16.5405 kN	>	7.91657 kN	Transverse shear resistance composite slab per rib (green cel is governing)

The transverse shear resistance according to the Eurocode 4 is equal to 16.54 kN per concrete rib.

Stark

Input				Notes
$C_{Rm,c}$	0.15			Empirical coefficient
h_t	280 mm			Overall thickness of test specimen
e	46 mm			Distance centroidal axis rib reinforcement relative to the bottom
\varnothing	24 mm			Diameter rib reinforcement
t	0.96 mm			Design sheet thickness (excluding coatings)
b_o	115.5 mm			Mean width of the concrete rib
f_{cm}	41.8 MPa			Mean concrete compressive strength
h_L	208.7 mm			Height of the web, specified as the distance between the radii to the flanges
f_y	409 MPa			Yield strength steel
α	0.261799 rad			Angle of the web relative to the vertical axis
Output				Notes
A_{sl}	452.3893 mm ²			Total area of the tensile reinforcement
d	234 mm			Effective depth of the slab (centroidal axis rebar to top fibre slab)
k	1.9245	<2.0	1.9245	Size factor = $\min(1 + \sqrt{200/d} ; 2.0)$
ρ_l	0.016738	<0.02	0.016738	Longitudinal reinforcement ratio = $\min(A_{sl}/(b_o*d) ; 0.02)$
$V_{Rm,c}$	32.14924 kN	>	16.32793 kN	Transverse shear resistance concrete rib (green cel is governing)
$V_{Rm,p}$	91.39662 kN			Transverse shear resistance steel deck per "rib"
$V_{t,Rm}$	123.5459 kN			Total transverse shear resistance composite slab per rib

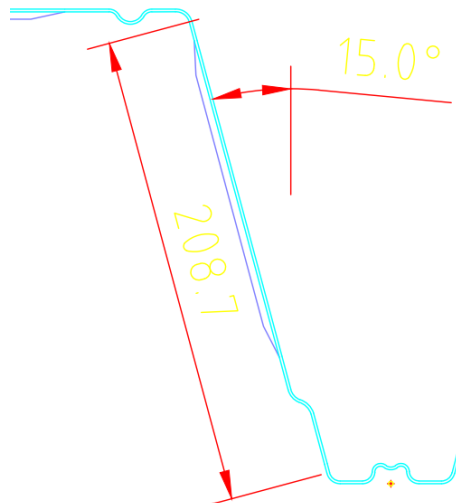


Figure D.1 – Parameters h_L and α for ComFlor 210

The transverse shear resistance according to Stark[18] is equal to 123.55 kN per concrete rib of the composite slab. The values for h_L and α are shown in Figure D.1. The original yield strength of the steel plate (409 MPa) has been used in calculation.

[Pereira et al.](#)

Input				Notes
$C_{Rm,c}$	0.15			Empirical coefficient
h_t	280 mm			Overall thickness of test specimen
e	46 mm			Distance centroidal axis rib reinforcement relative to the bottom
\varnothing	24 mm			Diameter rib reinforcement
t	0.96 mm			Design sheet thickness (excluding coatings)
b_0	115.5 mm			Mean width of the concrete rib
f_{cm}	41.8 MPa			Characteristic concrete compressive strength
h_w	208.5 mm			Height of the web between the centrelines of the flanges
f_{bv}	32.8 MPa			Shear strength considering buckling
φ	1.308997 rad			Angle of the web relative to the horizontal axis
Output				Notes
A_{sI}	452.3893 mm ²			Total area of the tensile reinforcement
d	234 mm			Effective depth of the slab (centroidal axis rebar to top fibre slab)
k	1.9245	<2.0	1.9245	Size factor = $\min(1 + \sqrt{200/d}; 2.0)$
ρ_l	0.016738	<0.02	0.016738	Longitudinal reinforcement ratio = $\min(A_{sI}/(b_0*d); 0.02)$
$V_{Rm,c}$	32.14924 kN	>	16.32793 kN	Transverse shear resistance concrete rib (green cel is governing)
$V_{b,Rm}$	13.59369 kN			Transverse shear resistance steel deck per "rib"
$V_{t,Rm}$	45.74293 kN			Total transverse shear resistance composite slab per rib

The transverse shear resistance according to Pereira et al.[17] is equal to 45.74 kN for one rib.

Hartmeyer & Kurz

In the method of Hartmeyer & Kurz[27], it is mentioned that eq. 2.14 may be used to calculate the height of the compressive zone in the concrete. Instead of this, the height of this compressive zone has been estimated from the FEA. In Figure D.2, the normal stress in the concrete is plotted over the height of the composite slab. The compressive zone at the top is relatively small and its height is approx. equal to 20 mm. The given distribution of normal stresses is taken from the analysis of ComFlor 210 as discussed in section 3.4. The calculation of the transverse shear capacity of the composite slab is shown below. For the partial resistance of the steel deck $V_{p,Rm}$, a value of 44.98 N/mm has been used as mentioned in the report of Tuls[22]. This value is based on real tests.

$$V_{t,0,Rm} = V_{p,Rm} + \frac{2}{3} \cdot x_m \cdot b_c \cdot f_{ctm} = 44.98 \cdot 600 + \frac{2}{3} \cdot 20 \cdot 600 \cdot 3.1 = 26988 + 24800 = 51788 \text{ N}$$

$$V_{t,0,Rm} = 51.79 \text{ kN}$$

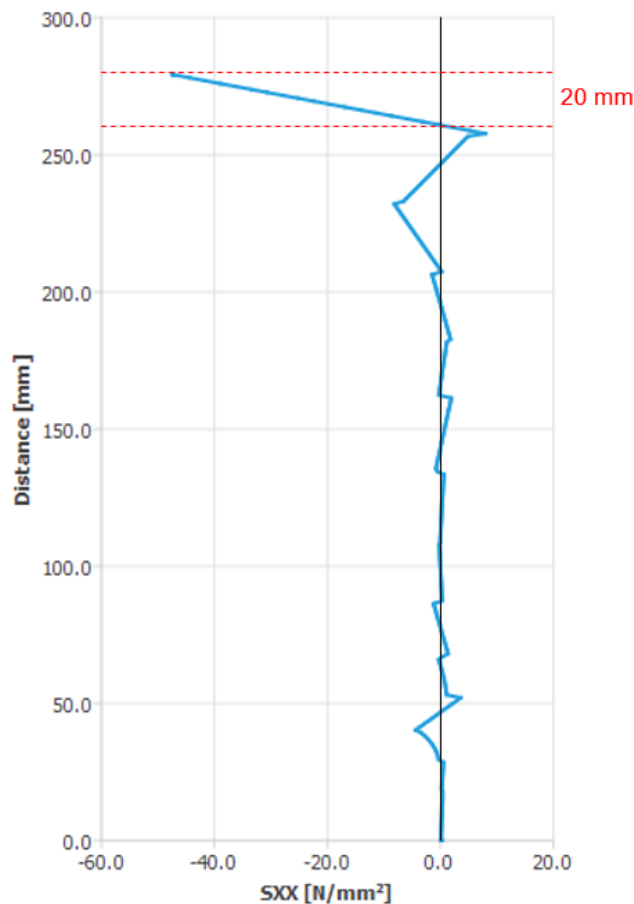


Figure D.2 – Distribution of normal stress in the concrete over the height of the slab at maximum load (in the middle of the rib at the location of the applied load V_t)